POLITECNICO DI TORINO

Collegio di Ingegneria Chimica e dei Materiali

Corso di Laurea Magistrale
in Ingegneria Chimica e dei Processi Sostenibili

Tesi di Laurea Magistrale

Synthesis and characterization of Carbon Dots as platforms for DADs loading

Relatore

prof. Alberto Tagliaferro

Corelatore

Dr. Mattia Bartoli

Candidata

Elena Marras

Marzo 2021

Riassunto in italiano per tesi in inglese

Questo lavoro mira a combinare i Diallile Disolfuri con *Carbon Dots* per integrare la capacità diagnostica dei *Carbon Dots* con l'attività terapeutica di questi analoghi dell'Allicina.

Per raggiungere il suo scopo, questa tesi parte dalla sintesi e caratterizzazione di *Carbon Dots* adatti. Il precursore è l'Acido Citrico (CA) e l'agente amino-passivante è l'Urea (U), che è stato scelto come fonte di azoto non solo per il suo basso costo e abbondanza ma anche perché particolarmente adatto al tipo di trattamento termico che viene impiegato. Il PEG ha un ruolo importante sia nel potenziamento della fotoluminescenza dei CDs, sia nella struttura stessa poiché potrebbe essere utilizzato come mezzo per assistere la sintesi. In questo lavoro, la quantità di acido citrico e urea è sempre in rapporto 1/10, mentre la quantità di PEG viene variata per indagare con precisione il suo ruolo. Le variabili di sintesi sono la temperatura e il tempo di reazione. Dopo le sintesi, la caratterizzazione fornisce le informazioni per scegliere correttamente il *Carbon Dot* adatto al secondo processo: il caricamento DAAD. Tre diversi tipi di DAAD (molecole X, A, B in fig (2)) sono caricati mediante un processo di adsorbimento in soluzione di etere di petrolio con un rapporto di più di uno a uno. Infine, un'analisi termogravimetrica finale indica quanto DAAD è adsorbito.

L'analisi del processo di *loading* unitamente all'ampia caratterizzazione hanno permesso la simulazione strutturale del *Carbon Dot* caricato mediante metodi di meccanica molecolare.

I *Carbon Dots* (CDs) sono materiali carboniosi con dimensioni che variano nell'ordine del nanometro, comunemente definiti come materiali a zero dimensioni. La maggior parte dei *Carbon Dots* sono costituiti da carboni sp2 ed altri eteroatomi come ossigeno e azoto. I *Carbon Dots* sono l'alternativa "*green*" dei predecessori *Carbon Quantum Dots* e sono stati scoperti all'inizio degli anni 2000 dal gruppo Carlson durante la purificazione dei nanotubi di carbonio come preparazione per l'elettroforesi. Da tale scoperta sono stati sviluppati diversi metodi di sintesi, nonché un numero considerevole di precursori, portando ad una diversificazione nei prodotti ottenuti.

Le procedure sintetiche per la produzione di Carbon Dot sono raggruppate in due classi: *bottom-up* e *top-down*. I metodi *top-down* richiedono precursori di carbonio che devono essere ridotti su scala nanometrica, un esempio di questi materiali di carbonio è il grafene. I metodi *bottom-up* invece coinvolgono, come precursori, molecole organiche che devono essere polimerizzate e carbonizzate durante il processo. La richiesta energetica degli approcci è diversa: quello *top-down* richiede più energia a causa del processo fisico necessario a ridurre la dimensione della materia prima. I principali vantaggi della tecnica *top-down* sono l'abbondanza dei precursori e il fatto che i prodotti ottenuti siano fortemente funzionalizzati in superficie. La tecnica *bottom-up* utilizza, invece, reazioni chimiche come l'approccio idrotermale, a microonde o a ultrasuoni. I prodotti ottenuti con la tecnica *bottom-up* presentano meno difetti e le dimensioni possono essere controllate meglio. Recentemente le sintesi di CDs "eco-friendly" sono state studiate variando i precursori e i diversi percorsi sintetici. Le fonti di carbonio per questo tipo di sintesi possono essere delle biomasse, come organismi o materiali di scarto, mentre la domanda di energia può essere ridotta per seguire un percorso più sostenibile. Questa tesi procederà con un metodo di sintesi *bottom-up*.

L'eccellente biocompatibilità, la facilità della loro preparazione e il costo di produzione relativamente basso sono solo alcune delle proprietà dei CD. I gruppi carbossilici, idrossilici e amminici, che caratterizzano la superficie dei CD, consentono loro di essere solubili e stabili in acqua, consentendo in questo modo le applicazioni di imaging.

La fotoluminescenza (PL) è senza dubbio la proprietà più affascinante dei *Carbon Dots* ed è definita come segue: "La fotoluminescenza è un processo in cui una molecola assorbe un fotone nella regione visibile, eccitando uno dei suoi elettroni ad uno stato elettronico superiore, riemettendo poi un fotone ad energia più bassa durante il processo di rilassamento", ciò significa che la luce incidente verrà assorbita per essere quindi riemessa con un breve ritardo dell'ordine di 10^{-8} secondi, in altre lunghezze d'onda. Le nanoparticelle fluorescenti possono svolgere un ruolo come agente ottico nel campo dell'imaging cellulare grazie alla loro citotossicità. La funzione diagnostica degli agenti ottici consiste nel fornire informazioni sulla posizione di alcune cellule. Un esempio che si può fare è quello delle cellule tumorali; la funzione diagnostica, in questo caso, fornirebbe informazioni sulle dimensioni e sulla tipologia: è evidente come questo possa essere rivoluzionario nella diagnosi dei tumori.

L'allicina è un derivato dagli olii essenziali dell'aglio. È stato isolato per la prima volta nel 1944 e da allora è stato ampiamente studiato. L'aglio era noto da anni per le sue potenzialità antitumorali, antidiabetiche, antimutagene e antinfiammatorie. Inoltre, Donma et al. hanno studiato l'applicazione dell'aglio nell'indurre l'immunità nel trattamento dell'infezione da COVID-19. La molecola più bioattiva dell'aglio è l'Allicina. Il composto di Allicina si ottiene metabolizzando l'Alliina in Allicina. L'aglio deve essere disidratato, schiacciato, tagliato o esposto all'acqua per attivare l'enzima alliinasi e indurre la metabolizzazione.

Le molecole di Diallile Disolfuro (DADS) sono analoghi dell'Allicina, presentano una maggiore stabilità rispetto a quest'ultimo composto e hanno connotazioni farmacologiche differenti. I DADS possono inibire la proliferazione cellulare e indurre l'arresto del ciclo cellulare. Sulla base dello studio di Olivito et al. le configurazioni in fig(6) sono state scelte come composti di carico per questo lavoro. La molecola X è simmetrica, insatura e con doppi legami esterni che ne determinano la reattività. Le molecole A e B, prodotte con una reazione multi-step, sono simmetriche, con la stessa lunghezza della catena di carbonio ma con diverse posizioni di doppio legame. La posizione del doppio legame gioca un ruolo nella reattività dei composti e nella loro attività antiossidante. Gli antiossidanti possono inibire l'inizio o la propagazione di reazioni a catena ossidativa in ambienti biologici, riducendo la concentrazione di specie reattive dell'ossigeno. Questi fenomeni, che sono alla base degli eventi infiammatori, con la produzione di specie reattive dell'ossigeno, potrebbero indurre nel peggiore dei casi la morte delle cellule. Le configurazioni A e B, in fig(6), differiscono dalla posizione del doppio legame: la molecola A è più reattiva, il doppio legame esterno consente la possibilità di legarsi immediatamente con i radicali liberi, mentre il composto B è più stabile.

Il lavoro sperimentale di questa tesi comincia con la preparazione dei precursori per la sintesi termica. Tutti i precursori sono caratterizzati da una composizione di 1 g di acido citrico e 10 g di urea; la differenza risiede nella quantità di PEG: il primo ha zero PEG, il secondo tipo di precursore ha 0,1 g di PEG e il terzo 1 g di PEG; mentre, come si è detto in precedenza, il rapporto AC/U = 1/10 è stato mantenuto costante in tutte le preparazioni. Dopo la macinazione, per ottenere una polvere omogenea, i precursori vengono posti in 25 mL di soluzione acquosa. Per vedere come il processo di agitazione influisce sul prodotto finale, si è scelto di procedere con due diversi tipi di processi, partendo dalle stesse preparazioni (quelle che differiscono per quantità di PEG: 0 g PEG, 0,1 g PEG e 1 g PEG) in entrambi i casi. Una preparazione per tipo viene messa in agitazione meccanica durante la notte e allo stesso modo, una preparazione per tipo subisce un processo di sonicazione per 30 minuti con 5 secondi di pausa ogni 30 secondi.

L'essiccazione della soluzione, al fine di ottenere una matrice solida, viene effettuata in forno sotto i 100 ° C. La sintesi avviene in un reattore tubolare riempito con atmosfera inerte di Argon, a differenti temperature, in un range da 250 ° C a 550 ° C, con tempi di reazione che vanno da

5 minuti a 15 minuti. Un'analisi spettroscopica a infrarossi viene quindi utilizzata per analizzare i risultati. Ogni sostanza viene pesata prima e dopo la reazione per valutare le perdite di massa durante il processo termico. I set di sintesi svolte e relativi nomi sono riportati nelle tabelle dalla [1] alla [5].

Lo scopo della purificazione è quello di separare i componenti solubili da quelli insolubili. Il prodotto ottenuto dalla reazione viene solubilizzato in 5 mL di acqua, quindi viene agitato e, infine, il sonicatore viene utilizzato per precipitare la parte insolubile. Il sonicatore è impostato in modalità "sweep" per 15 min con una temperatura massima di 35 ° C. La modalità sweep evita l'innalzamento della temperatura impedendo l'ebollizione della soluzione ed inoltre aiuta a migliorarne l'omogeneizzazione. Grazie a questo processo è possibile prelevare la parte liquida solubile più pura con una pipetta Pasteur. Per realizzare una migliore separazione, la parte liquida prelevata nella fase precedente viene centrifugata. Successivamente, un'operazione di essiccazione permette di estrarre la parte solida solubile: il risultato finale.

La caratterizzazione viene eseguita mediante l'uso della Spettroscopia a Infrarossi (IR), dell'analisi Termogravimetrica (TGA), della Spettroscopia fotoelettronica a Raggi-X e infine della Spettroscopia Raman. L' IR esplora l'evoluzione dei composti durante la reazione termica e guida la scelta verso i prodotti più promettenti che verranno sottoposti alle successive caratterizzazioni e al processo di *loading*. La TGA studia la stabilità termica del prodotto deducendo così informazioni sulla sua struttura. L' XPS analizza e determina la composizione elementare dei Carbon Dots e ci permette di studiare i prodotti perimetrali. Il Raman ci restituisce un'idea, invece, strutturale del *core* del materiale.

Il processo di caricamento prevede quattro diversi carichi: tiofene, DAAD tipo X, A e B. Le soluzioni per il processo di adsorbimento sono realizzate nel modo seguente: la prima soluzione è composta da 50 mL di etere di petrolio con 50 mg di tiofene, mentre le altre soluzioni sono composte da 50 mL di etere di petrolio e 50 mg di ogni tipo di DAAD (X,A,B). I *Carbon Dots* vengono quindi pesati e un campione da 50 mg viene posto in una soluzione da 5 mL per tipo - quelli la cui composizione è descritta sopra - per poi subire un'agitazione meccanica durante la notte. Successivamente, vengono filtrati sottovuoto utilizzando un *Buckner* e un filtro di carta. Il materiale ottenuto successivamente all'adsorbimento e alla filtrazione viene analizzato tramite TGA in un range da 35 ° C a 120 ° C.

Basato sul lavoro di Keenan et al. è possibile analizzare gli stadi di reazione coinvolti nelle prime fasi della sintesi e ipotizzare la struttura dei CD e, quindi, successivamente, anche simularla. I CDs mostrano percorsi di reazione vari e complessi, come riportato in fig(11). Poiché la reazione termica è portata avanti a temperature elevate, ci aspettiamo la presenza simultanea dei composti da tutti e tre i percorsi. Questi composti possono evolversi in composti ciclici che si combinano in strutture 3-D e creano gli strati delle strutture. Il nucleo sarà simile al grafene ossido (GO), con gli atomi di carbonio disposti ciclicamente e legati in modo covalente in strutture sp^2, mentre gli strati interagiscono con forze deboli tra di loro. Le strutture, N-dopate, saranno esterne, riorganizzate in triazine. I gruppi funzionali contenenti ossigeno, come carbossilici e idrossilici, saranno perimetrali alla struttura. Con i meccanismi di formazione mostrati in fig(11), è possibile creare un modello della struttura ipotizzata, che avrà un nucleo grafitico e gruppi funzionali perimetrali.

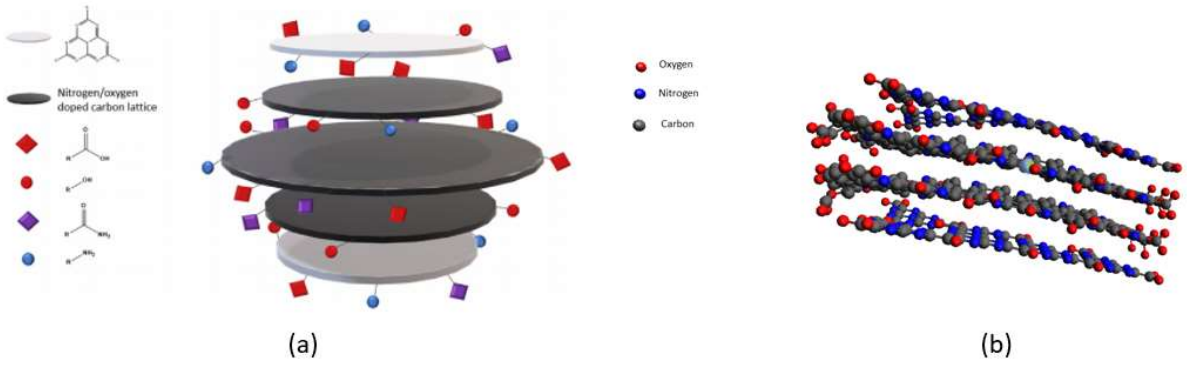

Figura I (a) Ipotesi strutturale del Carbon Dot (b) Struttura ottimizzata con software HyperChem.

La presenza di PEG cambia la dinamica della reazione descritta precedentemente. L'aggiunta di PEG favorisce la formazione di una fase micellare, l'ambiente interno delle pseudo-micelle è meno polare della fase acquosa pura di conseguenza i composti aromatici, attraverso processi di ciclizzazione e condensazione, arricchiscono la parte interna delle micelle, pertanto tali strutture andranno incontro ad ulteriori processi di aromatizzazione attraverso percorsi di condensazione intermolecolari. Questi fenomeni sono responsabili dell'incremento del C=C stretching nell'IR dei prodotti contenenti PEG.

La caratterizzazione è stata effettuata mediante analisi con spettroscopia a infrarossi, analisi termogravimetrica, spettroscopia fotoelettronica a raggi X e spettroscopia Raman.

La spettroscopia IR è stata realizzata su tutti i composti tabulati dalla tab[1] alla [5]. Vengono qui di seguito riportati i più rilevanti ai fini del sommario. Gli spettri dei precursori della sintesi, in fig(II), vengono interpretati confrontandoli con gli spettri dei reagenti Acido Citrico, Urea e PEG.

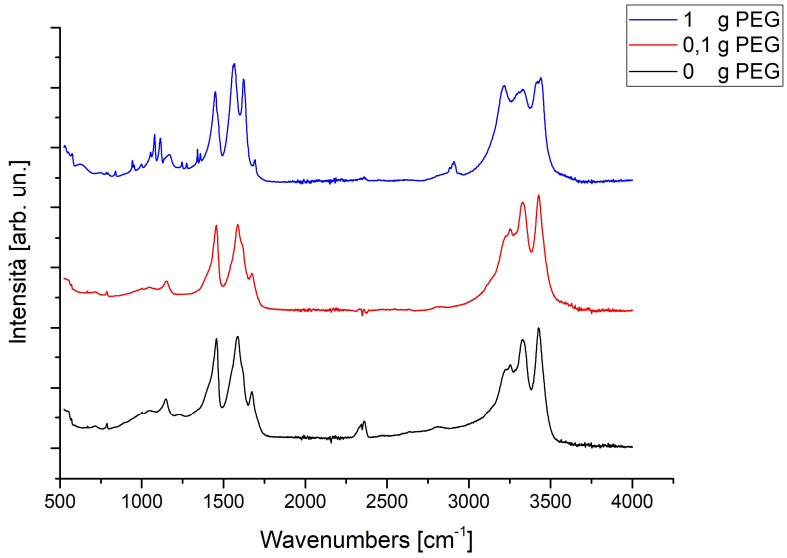

Figura II Spettri Precursori ottenuti mediante agitazione meccanica a diverse concentrazioni di PEG.

Mentre il metodo di preparazione dei precursori, sonicazione o agitazione meccanica, non ha mostrato significative differenze, la presenza di PEG può invece essere osservata mediante il picco a 2900 cm^{-1} dei carboni saturi tipici della catena di PEG. Osserviamo inoltre il crescere dei picchi a 1750 cm^{-1} e a 3200 cm^{-1} relativi rispettivamente ai carbossili liberi ed ai carboni insaturi. Osservando meglio lo spettro del precursore privo di PEG, si possono notare i due picchi delle ammidi nella regione intorno ai 3500 cm^{-1}, che ritroviamo nello spettro dell'Urea. Inoltre, possiamo notare l'assenza del picco relativo ai carbossili che dovrebbe, invece, essere adiacente a questa regione. L'assenza del picco carbossilico nella regione di 3000 cm^{-1}, combinata con la comparsa del picco a 1650 cm^{-1}, indica che il precursore ha reagito.

Gli spettri IR dei prodotti di reazione senza PEG a diverse temperature in fig(III)(a) e a diversi tempi di reazione in fig(III)(b).

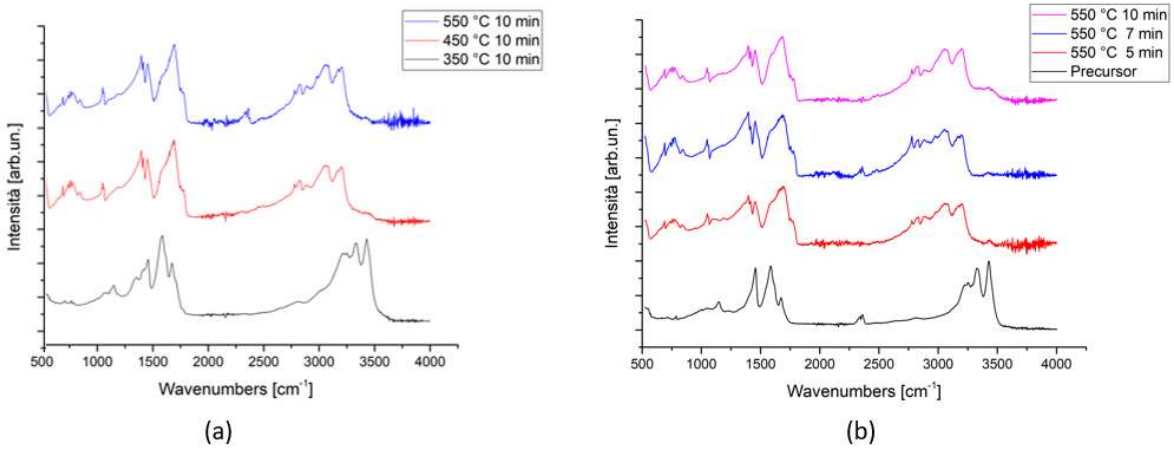

Figura III Spettri IR di (a) C-Dots prodotti dalle sintesi a diverse temperature da precursori privi di PEG, (b) C-Dots prodotti dalle

È possibile subito notare come la temperatura sia un parametro molto più influente rispetto al tempo di reazione, infatti, nel passaggio da 350 °C a 550 °C gli spettri sono molto diversi: spariscono i picchi delle ammine a 3500 cm^{-1} ma cresce il picco relativo alle triazine così come troviamo, alle temperature più alte, i picchi relativi a carboni saturi e insaturi tra 2750 cm^{-1} e 3200 cm^{-1} indicativi dell'avvenuta condensazione dei composti eterociclici che ipotizzavamo prima. A parità di temperatura non si notano importanti differenze negli spettri superati i 5 min.

Per interpretare meglio il ruolo del PEG si fa riferimento alle fig(25)(26) all'interno della tesi dove sono riportati gli spettri dei prodotti di reazione a 550 °C con la quantità di PEG in rapporto 1/1 con l'acido citrico. Negli spettri si nota come il picco delle ammidi scompare completamente ma, contrariamente a quanto visto prima, non c'è l'innalzamento del picco della triazina a 1571 cm^{-1}. Questo comportamento può essere spiegato ipotizzando che il PEG prevenga la formazione di gruppi perimetrici, come quelli carbossilici, mentre promuova il processo di aromatizzazione nel nucleo dei CDs. Il picco che si forma a 2800 cm^{-1} è assegnato allo stretching C-H, mentre il picco intorno a 1000 cm^{-1} è assegnato a C-O. Entrambi questi composti provengono dalla struttura PEG. Anche la regione del C-H *stretching* cambia nell'intervallo tra 1300 cm^{-1} e 1450 cm^{-1}. I picchi rimanenti intorno ai 3000 cm^{-1} indicano il processo di aromatizzazione in corso.

Sulla base dell'analisi degli spettri IR raccolti sono stati scelti i *C-Dots* più promettenti. I prodotti privi di PEG scelti sono quelli sintetizzati a 550 ° C per sette minuti e a 450 ° C per sette minuti. Tra i campioni contenenti 0,1 g di PEG e contenenti 1 g di PEG, sono stati scelti quelli a 550 ° C con un tempo di reazione di dieci minuti. La resa delle sintesi per questi

composti è riportata nella scheda (6). I prodotti più promettenti sono stati sottoposti ad un'analisi termogravimetrica e a spettroscopia XPS e Raman.

Viene utilizzata l'analisi termogravimetrica per indagare la stabilità termica dei composti al fine di dedurre informazioni sulla struttura del *Dot* e ottenere conferme sulla struttura ipotizzata dagli spettri IR.

In fig(27) del lavoro di tesi è riportato il prodotto privo di PEG sintetizzato a 550 ° C per 10 minuti. Nella prima parte dello spettro, alle basse temperature, si osserva un primo andamento decrescente causato dall'evaporazione dei carbossili liberi nel campione, comune a tutti gli spettri TGA analizzati in questo step. Tra i 200 ° C ei 400 ° C si osserva un andamento decrescente della curva che viene assegnata alla perdita in peso che corrisponde al 5%, questo punto indica il punto di partenza del processo di degradazione. La pendenza dopo 400 ° C è assegnata alla degradazione del nucleo grafitico N-dopato, che richiede temperature più elevate per degradarsi. Lo spettro TGA del prodotto a 450 °C, invece, mostra un andamento diverso: mostra la struttura di un processo non completamente terminato con minori quantità di composti aromatici. Viene ipotizzato, in questo caso, la non completa formazione dei *Carbon Dots*.

L'analisi degli spettri TGA dei composti contenenti PEG è stata fatta facendo riferimento alla TGA del PEG puro per vedere a quale temperatura degrada così da separare le informazioni relative al picco del PEG dalle altre informazioni che fornisce l'analisi. Facendo riferimento alla fig(31), relativa all'analisi TGA del prodotto con il PEG in rapporto 1/1 con l'acido citrico, si procede con alcune considerazioni. Si osserva a 335 ° C l'inizio della degradazione dei gruppi perimetrali e a 400 ° C, con la degradazione del PEG, anche la degradazione di tutte le altre strutture: prima le frazioni legate semplicemente e poi i composti aromatici che costituiscono il nucleo grafitico del Carbon Dot. Allo stesso modo in cui il PEG promuove il processo di aromatizzazione, i composti aromatici si degradano con il PEG a 400 ° C.

La caratterizzazione dei *Carbon Dots* prodotti continua con l'analisi spettroscopica XPS per determinare gli elementi presenti sulla superficie del *Dot*: carbonio, azoto e ossigeno. Gli spettri sono stati processati con OriginPro per elaborare le informazioni provenienti dall'analisi XPS: è stata studiata l'area sotto ogni curva, e il rapporto con il valore totale delle aree è stato utilizzato per calcolare la percentuale dei composti presenti. Gli spettri relativi al Carbonio sono quelli da cui si estrapolano più informazioni.

Lo spettro del Carbonio per il prodotto sintetizzato a 550 °C privo di PEG, riportato nel testo in fig(32), mostra che il carbonio ibridizzato sp^2 è presente per il 27% del totale, le frazioni C-X (X = O, N) sono solo il 14%. In questa fase, la differenziazione tra C-O o C-N non può essere fatta poiché questi componenti raggiungono il picco a valori simili. Mentre, il 59 % del Carbonio è sottoforma di composti carbossilici che si trovano sul perimetro della struttura. Questa analisi trova corrispondenza con l'IR esaminato in precedenza. Meno informazioni provengono invece dallo spettro relativo all'azoto, dove possiamo vedere solo la massiccia presenza dell'azoto grafenico nelle frazioni aromatiche presente per il 93%, mentre solo il 7% dell'azoto è presente come pirrolico.

Il componente con il PEG in rapporto 1/10 con l'acido citrico mostra, mediante gli spettri XPS, riportati in fig(34), un diverso comportamento. Le curve relative al Carbonio permettono di calcolare la percentuale di carboni insaturi che in questo campione sono presenti per il 36% di quelle totali, i carbossili invece sono solo il 4%. La percentuale di carbonili è, invece, rilevante essendo presente per il 36 % del carbonio. Infine, la restante parte è relativa al C-X(X=O, N). Lo spettro dell'azoto mostra un solo picco: tutto l'azoto presente è pirrolico. La dinamica precedentemente ipotizzata ha un'ulteriore conferma: la presenza del PEG favorisce il processo di aromatizzazione e un diverso riassetto dei componenti. Per comprendere meglio il ruolo del

PEG è necessario analizzare gli spettri del prodotto con il rapporto di PEG 1/1 con l'acido citrico.

Il composto con il rapporto di PEG più alto presenta ancora diverse percentuali di composti carboniosi: il carbonio insaturo è presente per solo il 19 % mentre quello saturo per il 47 %, la restante parte è C-X(X=O, N) dove i carbonili avranno un ruolo più centrale rispetto ai precedenti prodotti poiché il legame C-O è caratterizzante delle catene del polimero. Gli spettri XPS di questo prodotto sono riportati in fig(35). Poiché la presenza di PEG in questo prodotto è considerevole, le dinamiche sono cambiate, come si può osservare: procede l'aromatizzazione e diminuisce la percentuale dei gruppi carbossilici, indicando che è possibile che il PEG si sostituisca alle funzioni dell'idrossile che sono legate alle strutture aromatiche. Lo spettro di questo prodotto relativo all'ossigeno conferma questa ipotesi mostrando come quasi metà dell'ossigeno sia presente come gruppo carbossilico e più della metà come carbonilico.

La spettroscopia Raman viene utilizzata al fine di studiare l'ordine dei materiali ottenendo informazioni sulla struttura del materiale analizzato. Gli spettri derivanti dalla spettroscopia Raman mostrano un determinato fenomeno che può essere osservato in fig(IV). A causa dell'elevata fluorescenza dei CDs derivante dall'alta funzionalizzazione, lo spettro è dominato dalla deriva della fluorescenza e, di conseguenza, non possono essere osservati i picchi tipici di uno spettro Raman.

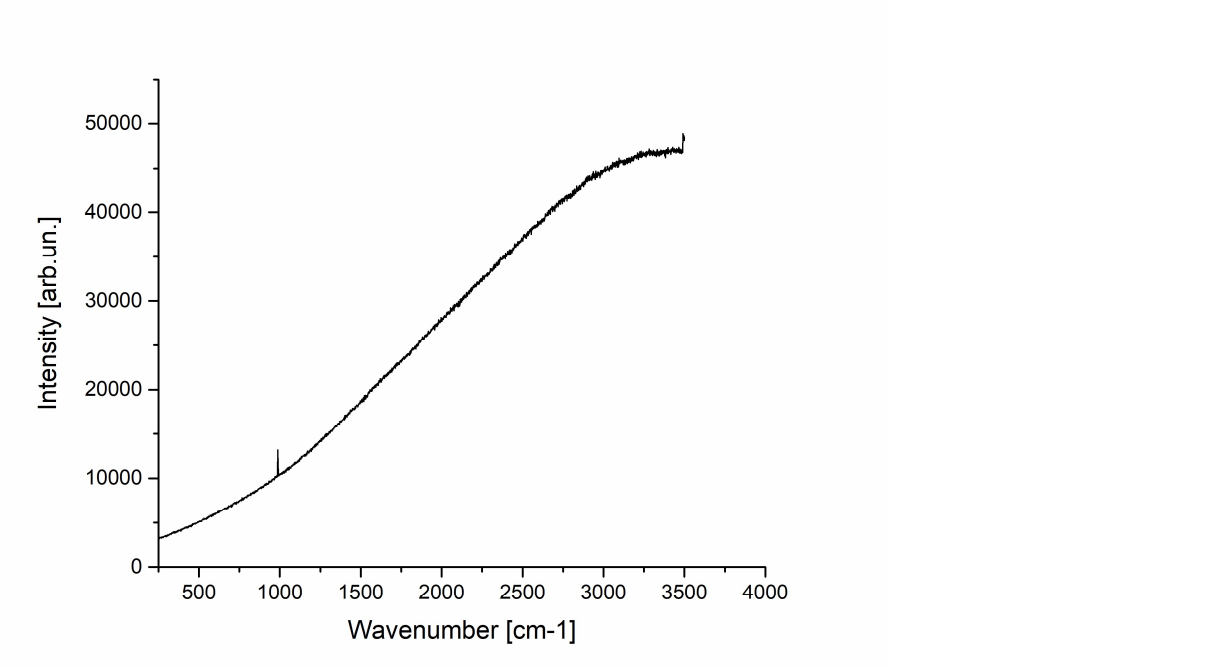

Figure IV Spettro Raman di Carbon Dots sintetizzati a 550 °C con un tempo di reazione di 10 minuti.

L'analisi termogravimetrica (TGA) aiuta a valutare la resa del processo di *loading*. Il calcolo può essere fatto conoscendo la temperatura di evaporazione dei composti DAAD, così da calcolare la percentuale di perdita in peso relativa ai composti caricati. Successivamente viene calcolato il rendimento per ogni carico e riportato nella tab(7).

La resa, come riportato in tab (7), è sempre inferiore allo 0,2%, il che significa che circa una molecola DAAD viene adsorbita su una struttura Carbon Dot, considerando il peso molecolare ipotizzato. Il limite computazionale del software di mille atomi ostacola la possibilità di simulare la struttura di *Carbon Dot* più grande. Pertanto, il *Carbon Dot* simulato avrà un peso molecolare di 8822 g/mol con almeno una molecola di DAAD adsorbito sulla superficie.

Le sintesi effettuate e la seguente caratterizzazione mirano a creare una libreria di composti per applicazioni biologiche. Quando si parla di ingegnerizzare materiali per applicazioni biologiche si possono intraprendere due diversi approcci: il primo consiste nel partire dallo studio del target e progettare un prodotto solo per tale target. Il secondo approccio consiste nel creare una libreria dalla quale è possibile scegliere la soluzione migliore per la situazione rilevante. Le variabili nella creazione di un materiale con finalità diagnostiche e terapeutiche sono molteplici, se non innumerevoli: bisogna trovare un equilibrio tra le migliori caratteristiche possibili del materiale. Il materiale perfetto ha un buon equilibrio nella sua polarità per raggiungere la cellula nel suo ambiente, un alto rendimento nella sua produzione e nel processo di caricamento e deve poter penetrare facilmente la barriera cellulare. Per soddisfare tutti questi criteri, diventa cruciale avere una libreria di composti. Questo lavoro e caratterizzazione intendono produrre diversi prodotti al fine di indirizzare le sintesi future.

Infine, la completa caratterizzazione del prodotto, riportata nella terza sezione di questo lavoro, fornisce le informazioni necessarie per comprendere la struttura del materiale nella sua interezza. Sulla base di questi dati è possibile simulare la struttura dei *Carbon Dots* prodotti ed i meccanismi coinvolti nel processo di caricamento. Il software HyperChem viene impiegato per simulare il minimo energetico mentre la struttura è stata disegnata con ChemSketch.

Come si può vedere in fig(I) il nucleo è grafitico e il perimetro presenta un'elevata funzionalizzazione. I *layers* uno e quattro sono costituiti da triazine e gruppi idrossilici. La distanza tra due diversi strati, ad esempio tre e quattro, è di circa 3,5 Å. La distanza del legame covalente nell'intera struttura varia da 1,29 a 1,47 Å. Nei cristalli di grafite il legame interatomico è di circa 1,42 Å, a seconda del tipo di grafite e la distanza tra gli strati varia da 3,3 Å a 3,7 Å. Il valore energetico di questa struttura è di 904,3 kcal/mol; questo dato, in particolare, sarà fondamentale durante lo studio della struttura caricata.

La fig(V) illustra la struttura ottimizzata di un Carbon Dot con l'aggiunta di catene PEG. In questo caso il valore energetico è di 862,2 kcal/mol. Durante l'ottimizzazione, le catene PEG mostrano due differenti comportamenti: possono interagire fra di loro o disporsi lungo i gruppi carbossilici perimetrali. Questi due tipi di tendenze possono essere osservate in fig(V) rispettivamente nel riquadro rosso e blu.

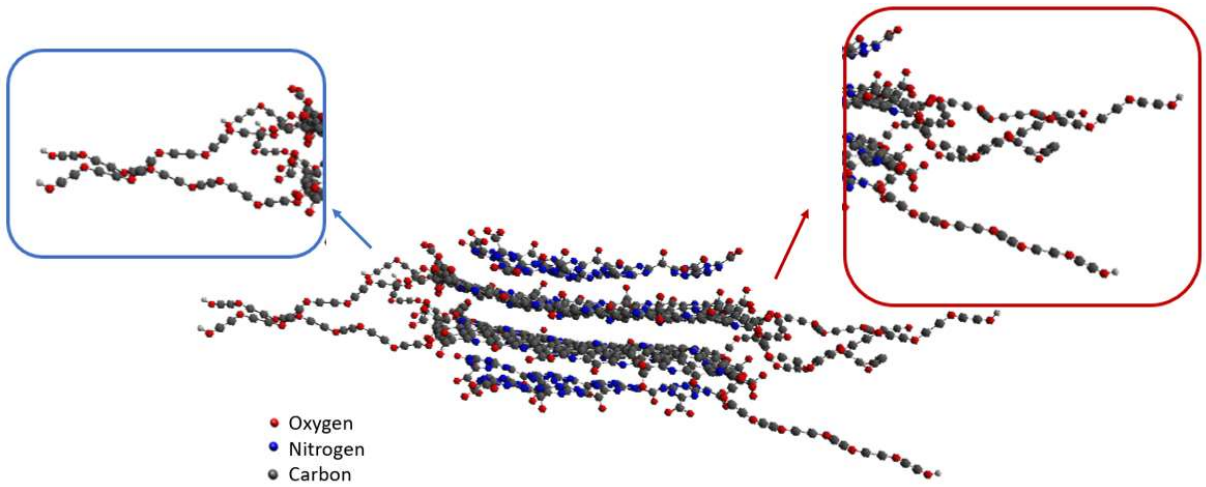

Figure V Struttura ottimizzata con metodi di meccanica molecolare di un Carbon Dot con l'aggiunta di PEG.

Il tiofene viene scelto come composto modello per il processo di *loading* prima di procedere al caricamento delle molecole di DAAD. Le sue caratteristiche strutturali ricordano quelle del diallil disolfuro. Questo composto eterociclico viene scelto tra vari composti insaturi a causa dell'impedimento sterico paragonabile a quello DAAD. Composti come solfoni e tioli non sono adatti per lo scopo della simulazione del modello. La fig(VI) mostra le possibili configurazioni del *carbon dot* caricato con una molecola di tiofene. La tendenza della molecola è di legarsi alla struttura con legami π.

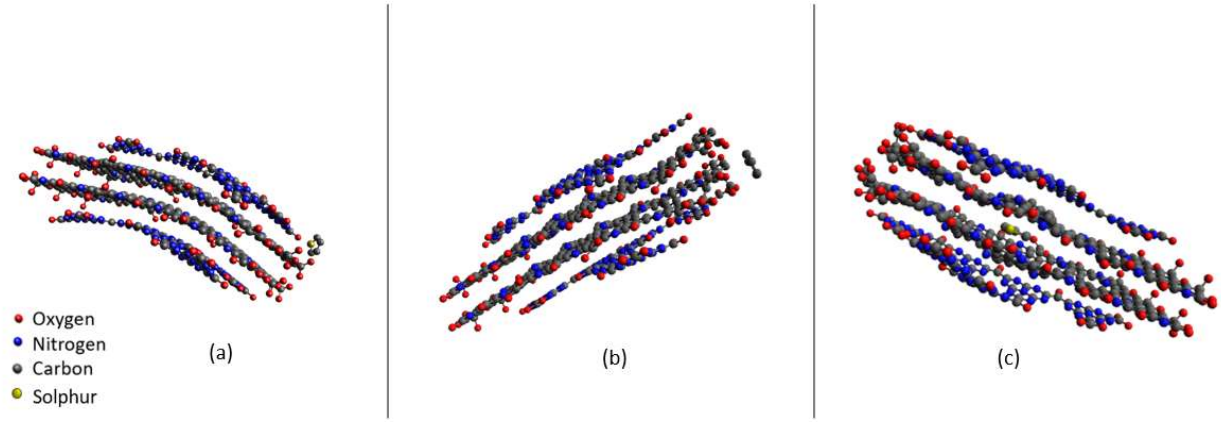

Figure VI Possibili configurazioni strutturali del Carbon Dot caricato con una molecola di tiofene.

Il tiofene si allinea con i gruppi funzionali perimetrali del *layer* triazinico in fig(VI)(a). L'atomo di zolfo, che è più ingombrante stericamente rispetto agli atomi di carbonio, si trova nella direzione opposta alla struttura *Carbon Dots*. La posizione degli atomi di carbonio, invece, è ortogonale ai *layers* e mostra la tendenza al legame π sopra descritta. La struttura carica della molecola di tiofene ha un valore energetico di 990,5 kcal/mol e conoscendo la struttura di base e l'energia della molecola semplice del tiofene è possibile stimare la forza di legame: 70,8 kcal/mol. Il legame π tra due atomi è solitamente compreso tra 30 e 65 kcal/mol, mentre, ad esempio, il legame idrogeno è molto più alto (più di 100 kcal/mol). Di conseguenza, le interazioni dei *Carbon Dots* col tiofene possono essere attribuite a interazioni deboli. La lunghezza dell'interazione tra il layer più vicino e la molecola è calcolata essere di 3,5 Å, coerentemente con i valori attesi.

Una diversa configurazione possibile è mostrata in fig(VI)(b). La figura presenta una diversa disposizione spaziale dei gruppi funzionali idrossilici. I gruppi perimetrali allineano gli -OH per esporre gli atomi di carbonio a quelli della molecola di tiofene. Questo comportamento conferma la tendenza osservata in fig(VI)(a). In questo caso, la lunghezza del legame è di 4,9 Å mentre l'energia ha una natura diversa. Il valore energetico finale è -5,9 kcal/mol che indica la maggior stabilità della struttura.

Un'ulteriore configurazione è riportata in fig(VI)(c). Questa configurazione è difficile che si presenti a causa dell'inaccessibilità della struttura e dell'elevata energia richiesta per raggiungere il nucleo interno del Carbon Dot. L'energia corrispondente è 968,3 kcal/mol che consente il calcolo della forza di legame: 48,6 kcal/mol. Pertanto, il legame è debole anche in questa configurazione finale. Il tiofene presente come composto di intercalazione tra gli strati del *Carbon Dot* deforma i *layers* creando una "tasca". L'elevata energia richiesta per questa configurazione rappresenta uno svantaggio per l'adsorbimento in questo preciso sito.

La situazione configurazionale cambia nel caso siano presenti catene di PEG come mostrato in fig(VII).

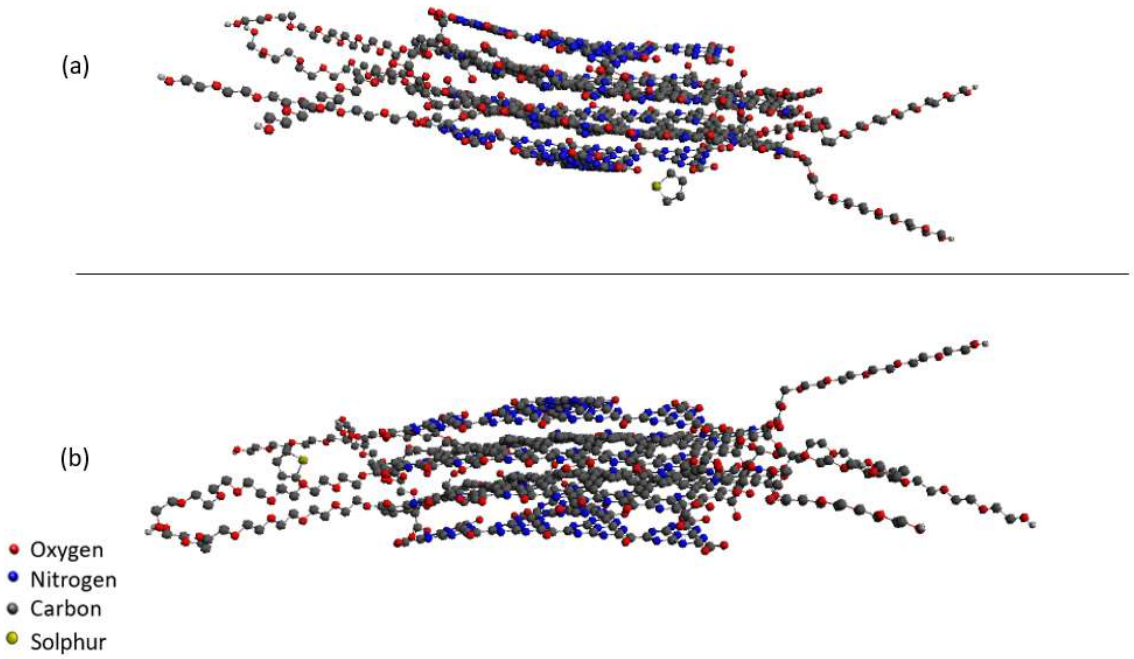

Figure VII Possibili configurazioni strutturali del Carbon Dot contenente PEG caricato con una molecola di tiofene.

Le configurazioni strutturali illustrate in figura mostrano come il tiofene abbia la tendenza a formare legami π con la struttura del Carbon Dot anche in presenza delle catene di PEG. Nel primo caso in fig(VII)(a) il tiofene interagisce col piano triazinico deformandolo. Mentre in fig(VII)(b) vediamo un'altra possibilità: il tiofene interagisce con la struttura, venendo, però, orientata dalla diversa polarità delle catene di PEG.

Le simulazioni con le molecole di DAAD tipo A, B e X seguono le considerazioni fatte per il composto modello.

Il composto insaturo con i doppi legami esterni e la catena carboniosa più lunga (il DAAD tipo A) ha la tendenza, come il composto modello, a formare interazioni π con la struttura. Come riportato in precedenza, la tendenza dei composti insaturi ad interagire tramite interazioni π diventa più apprezzabile nelle simulazioni con DAAD. Questi, infatti, consentono la disposizione spaziale della molecola parallelamente al legame C = O dei gruppi carbossilici di confine. Inoltre, quando la molecola di DAAD è presente come composto di intercalazione, la deformazione dei *layers* sarà più marcata rispetto al caso del tiofene. Inoltre, l'interazione con la struttura del *Carbon Dot* induce un'alterazione della lunghezza del legame tra gli atomi di zolfo del composto. La forza di legame dei solfuri è più debole di quella C-C (rispettivamente 63 kcal/mol e 83 kcal/mol) e per questo motivo il legame S-S è quello che viene maggiormente deformato durante il processo di adsorbimento.

La molecola DAAD di tipo B non ha il doppio legame esterno ma presenta un comportamento simile al precedente DAAD tipo A. La diversa posizione del legame insaturo consente la possibilità di una disposizione spaziale diversa della molecola con la struttura del *Dot*. Inoltre,

la lunghezza del legame degli atomi di zolfo cambia da 2,04 Å a 2,16 Å nelle diverse configurazioni riportate in fig(46).

La configurazione “a tasca” con la molecola di DAAD tipo B come composto di intercalazione mostra un diverso comportamento dalle configurazioni precedenti sebbene, a causa dell'impedimento sterico, questa disposizione sia ancora improbabile. Il doppio legame interno carbonio-carbonio blocca la struttura riducendo la mobilità delle catene alchiliche. Ciò consente la minimizzazione della deformazione interplanare di questo composto. Lo stereoisomero in questione modificherà la struttura più a lungo raggio.

Il composto naturale Diallil disolfuro tipo X è più corto del tipo A e B. Ha solo sei atomi di carbonio nella sua struttura e il legame insaturo è esterno.

Nella fig(48)(A) la molecola DAAD X confina con i gruppi carbossilici, cercando di formare interazioni π con la struttura. Nel caso di interazione con i piani triazinici e nel caso in cui la molecola risulti come prodotto di intercalazione all’interno della struttura, la molecola X, avendo la catena carboniosa più corta, non modifica in maniera massiccia la conformazione geometrica degli strati interni.

Le simulazioni del *Carbon Dot* contenente PEG e caricato con le molecole di DAAD riportano un comportamento molto simile al tiofene (il composto modello). La fig(50) nel testo mostra come ogni molecola di diallile abbia la tendenza a deformare lo strato di triazina interagendo con interazioni π con la struttura. Le configurazioni non riportano evidenti differenze tra il comportamento dei vari composti.

Concludendo, questo lavoro mirava a sintetizzare una classe specifica di *Carbon Dots* mediante sintesi termiche eseguite in condizioni diverse. Una conseguente completa caratterizzazione dei prodotti fornisce le informazioni per scegliere correttamente i *Carbon Dots* adatti al processo di *loading* dei DAAD. Successivamente, uno studio strutturale eseguito tramite il software HyperChem fornisce una panoramica della loro struttura e delle possibili configurazioni.

La procedura sperimentale inizia con la preparazione dei precursori per le sintesi termiche. Tutti i precursori sono preparati con Acido Citrico e Urea in rapporto 1/10, mentre la quantità di Polietilenglicole (PEG) viene variata per indagare con precisione il suo ruolo nell'assistere la sintesi e nel potenziarne la fotoluminescenza. I precursori vengono preparati con agitazione meccanica o con ultrasuoni. I parametri di sintesi sono la temperatura, che varia da 250 ° C a 550 ° C, e il tempo di reazione, che va da 5 minuti a 15 minuti. Infine, il processo di purificazione viene condotto in acqua con ultrasuoni e successiva centrifugazione. Vengono quindi caratterizzati i Carbon Dots così prodotti e purificati. La caratterizzazione prevede un’analisi con spettroscopia a infrarossi, un’analisi termogravimetrica, spettroscopia fotoelettronica a raggi X e spettroscopia Raman. La spettroscopia IR indaga l'evoluzione dei composti durante la sintesi e guida la scelta dei *Carbon Dots* più promettenti per il processo di *Loading*. Gli spettri IR dei precursori mostrano il ruolo del processo di agitazione nel migliorare l'inizio della reazione. Nel frattempo, gli spettri IR dei prodotti purificati dimostrano come le successive sintesi promuovano la formazione di frazioni triaziniche e dei processi di aromatizzazione. La formazione di composti aromatici è più estesa nei *Carbon Dots* contenenti PEG poiché il polimero promuove l'aromatizzazione mentre ostacola la formazione di gruppi perimetrali. In base ai dati IR i *Carbon Dots* scelti sono quelli prodotti a 550 ° C per sette e dieci minuti con differenti concentrazioni di PEG. Tuttavia, un composto sintetizzato a 450 ° C viene scelto tra quelli privi di PEG. Quindi, un'ulteriore caratterizzazione completa segue il set di prodotti scelto per il processo di caricamento. L'analisi termogravimetrica indaga la stabilità termica dei composti per dedurre informazioni sulla struttura del *Dot* mentre l'analisi spettroscopica fotoelettronica a raggi X determina la composizione elementare sulla superficie

del prodotto. I risultati della successiva caratterizzazione confermano la scomparsa delle ammine con formazione di triazine e gruppi carbossilici perimetrali. La spettroscopia Raman fornisce dati sulla struttura del materiale. Il processo di caricamento viene eseguito sulla set scelto di *Carbon Dots* completamente caratterizzati che hanno il ruolo di piattaforme per il caricamento di Dyallil Disulfide. Il processo di caricamento coinvolge quattro diversi carichi: tiofene, DAAD tipo X, A e B dove i composti variano la lunghezza della catena di carbonio e la posizione del doppio legame. Questo lavoro mira a combinare questi disolfuri e le loro proprietà con i *Carbon Dots* per integrare la capacità diagnostica di quest'ultimi con l'attività terapeutica di questi specifici analoghi dell'allicina. Le soluzioni per il processo di adsorbimento vengono preparate in etere di petrolio e quindi sottoposte ad agitazione meccanica durante la notte. Successivamente, vengono filtrati sottovuoto utilizzando un Buckner e un filtro di carta. Il materiale ottenuto successivamente dall'assorbimento e dalla filtrazione viene analizzato tramite TGA in un range da 35 ° C a 120 ° C. Questa analisi permette di calcolare la resa di adsorbimento.

La resa è per tutti i *Carbon Dots* e per tutte le molecole di DAAD inferiore allo 0,2%, il che significa che circa una molecola DAAD viene adsorbita su ogni *Carbon Dot*, considerando il peso molecolare ipotizzato sulla base di ricerche precedenti.

La completa caratterizzazione del prodotto fornisce le informazioni necessarie per comprendere la struttura del materiale nella sua interezza ed, sulla base di questi dati, è possibile simulare la struttura *Carbon Dots* ed i meccanismi coinvolti nel processo di caricamento. Il software HyperChem viene utilizzato per simulare il minimo energetico mentre la struttura è disegnata con ChemSketch. Le simulazioni mostra la tendenza, ricorrente in tutti i composti insaturi, a disporsi perimetralmente alla struttura del *Carbon Dot* per formare interazioni *p* con i gruppi perimetrali, ad esempio con i gruppi carbossilici. I Carbon Dots contenenti PEG presentano una diversa configurazione poichè la polarità delle catene di PEG e l'apolarità della struttura orientano la molecola adsorbita.

Questo lavoro e caratterizzazione intendono produrre diversi prodotti al fine di indirizzare sintesi future in cui il ruolo centrale dei *Carbon Dots* nelle applicazioni diagnostiche può essere accoppiato in modo efficiente con molecole bioattive e i loro effetti terapeutici come, ad esempio, gli analoghi dell'allicina, come indagato in questa tesi.

Contents

1. Introduction

1.1 Carbon Dots

CDs are carbonaceous materials with dimensions ranging in the order of the nanometer: CDs are defined as zero-dimension materials.[1]

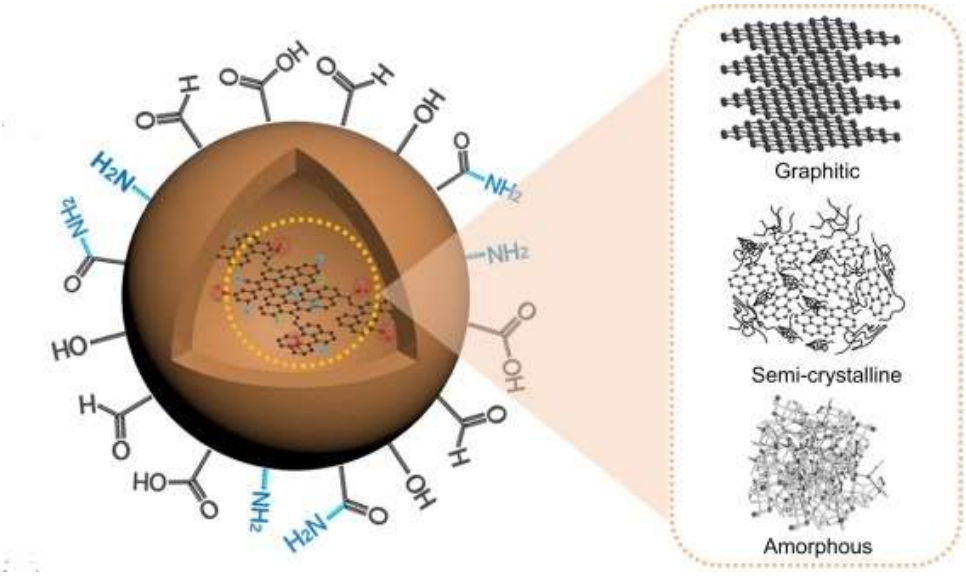

Figure 1 Carbon Dot representation.[2]

Carbon Dots' properties and applications brought great interest in the nanotechnology field. The majority of Carbon Dots are constituted of carbons sp2 and other heteroatoms as oxygen and nitrogen. The key property of these materials is photoluminescence and is determined by the superficial structure. Carbon Dots are the "green" alternative of the predecessors quantum dots, they've been discovered in the early 2000s from the Carlson group during the carbon nanotubes purification as preparation for electrophoresis.[3] Since their discovery, several synthesis methods, as well as a considerable number of precursors have been explored, bringing diversification in the products obtained.

The first classification of CDs has been carried out from Valcárcel[4] research group, depending on Carbon Dots' nature, crystalline structure, and quantum confinement, which is a parameter in the luminescent class of materials. According to this classification, Carbon Nanodots (CNDs) are amorphous, semi-spherical, and do not present quantum confinement, Carbon Quantum Dots (CQDs) have a full spherical structure with quantum confinement, and Graphene quantum dots (GQDs) with shapes usually circular or elliptical depending on the synthesis.[4]

Regarding this work, we dwell on GQDs and their alternative Graphene Oxide (GO). Graphene oxide is a single monomolecular layer of graphene, with a thickness up to 1 nm and a length in the micrometer scale, it has functional groups oxygen-containing like carboxylic, hydroxylic, or carbonylic. Graphene quantum dots are nanoparticles whose dimensions are generally below 20 nm and whose graphene sheets are single or multi-layered.[5] . Both GQDs and GO are highly dependent on their synthesis methods and they differ on their physicochemical properties for the variety of the precursor, defects, and functional groups.[6]

The synthetic procedures for Carbon Dot production are regrouped into two classes: bottom-up and top-down.[7]

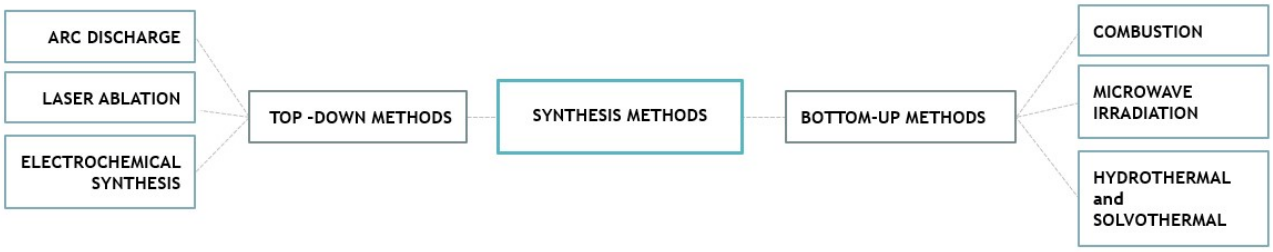

Figure 2 Synthetic routes for carbon dots production

Top-down methods need bulk carbon precursors which have to be cut down in the nanoscale, an example of bulk carbon materials is graphene. The bottom-up methods, instead, involve, as a precursor, organic molecules which have to be polymerized and carbonized during the process. The energetic request by the approaches differs: the top-down one demands more energy due to the physical process necessary to reduce the dimension of the raw material. The top-down technique's principal advantages are the precursors' abundance and the fact that the products obtained are strongly functionalized on the surface. The bottom-up technique uses chemical reactions such as hydrothermal approach, microwave, or ultrasonication. The products obtained with the bottom-up technique present fewer flaws and the dimensions can be controlled better. Recently, "environmental friendly"'s CDs syntheses are investigated by varying the precursors and studying different synthetic routes. The carbon's sources can be biomasses like organisms or waste materials while the energy demand can be decreased to follow a more sustainable path. This thesis will proceed with a bottom-up synthesis method.[7]

1.1.1 Properties of Carbon Dots

An objective differentiation could be done based on the precursor for the synthesis of CDs and their chemical properties.[8]

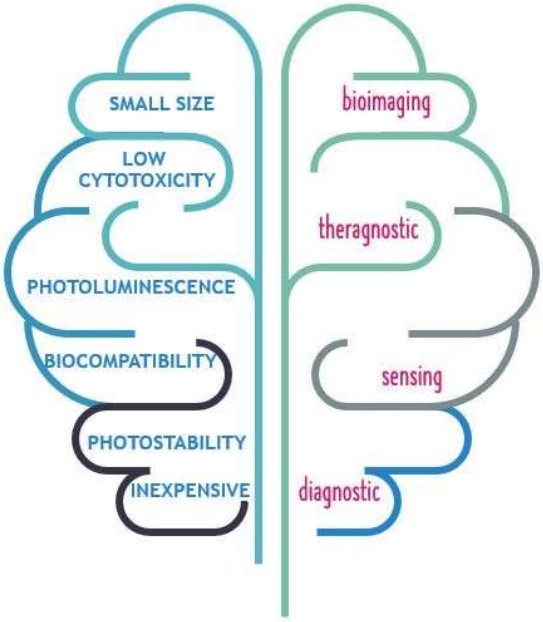

Figure 3 On the left are displayed Carbon Dots' properties, on the right Carbon Dots' field of applications.

The Carbon-based nanoparticles class can be furtherly divided into two major groups: Fullerenes and carbon nanotubes. Both groups have interesting characteristics such as electrical conductivity, strength, and electron affinity which find space in the market as, for example, fillers or as a support medium. The structure resembles a graphitic sheet and this brings to another differentiation: the rolled sheet can be single, double or multi-walled.

The complexity of the properties that CDs exhibit depends on their chemical structure and crystallinity degree. The UV-visible absorption is a property that is common to most CDs, even if obtained with different precursor and synthesis routes but the absorption peaks are going to change with the aforementioned variables.[9]

Hydrophilicity and dispersibility are properties that depend on the functional groups that tailor the perimeter of the dot, like carboxylic groups, and they are key-properties for various applications. Pan et al.[10] studied how turning hydrophilic CDs in hydrophobic using dodecylamine. Hydrophilic CDs have imaging applications while hydrophobic ones can be used as catalysts.[11]

The excellent biocompatibility, the ease of preparation, and the relatively low production cost are just some of CDs properties. The carboxylic, hydroxylic and aminic groups, that characterize the surface of CDs allow them to be soluble and stable in water enabling, in this way, the imaging applications.[12]

The photoluminescence (PL) is without a doubt the most compelling property of Carbon Dots and it is defined as it follows: "Photoluminescence is a process in which a molecule absorbs a photon in the visible region, exciting one of its electrons to a higher electronic excited state, and then radiates a photon as the electron returns to a lower energy state"[13], this means that

the incident light will be absorbed to, then, be re-emitted with a brief delay in the order of 10-8 second, in other wavelengths.[14]

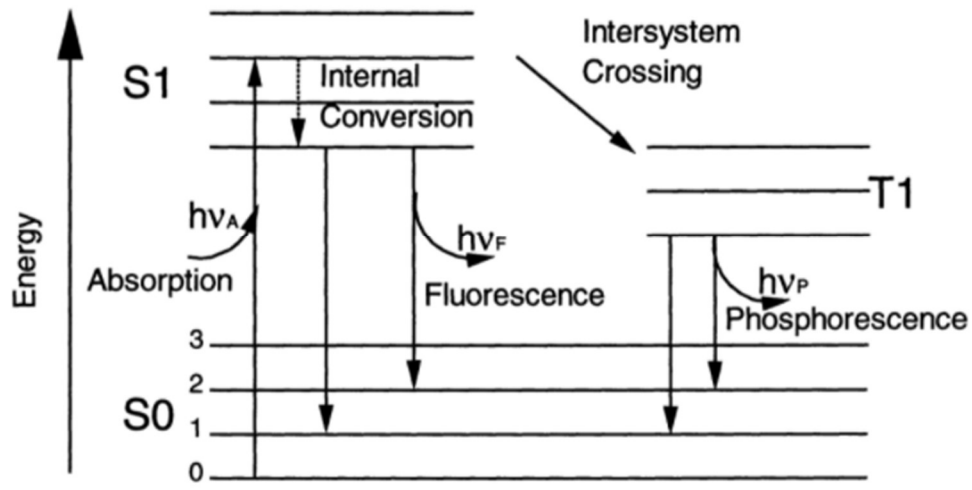

Figure 4 Photoluminescence mechanism scheme.

Metal-based nanoparticles have as precursors noble metals such as copper, silver, or gold. Their optical properties allow applications in the spectroscopy's technologies field.

On the contrary, Ceramic-NPs are inorganic and non-metallic.

There are, then, some nanoparticles that possess properties of both metallic and non-metallic materials, they are semiconductors and therefore they have several fascinating applications in photocatalysis and electronics.

A further class of CDs is the lipid-based NPs, their core is constituted of lipid and, on their surface, there are lipophilic molecules. Since, thanks to these characteristics, they can be employed as a drug carrier, the lipid-based NPs are heavily utilized in the Biomedical field. [8, 15]

Finally, there are the Polymer carbon dots (PCDs), a new structure of nonconjugated groups and metal-free products. The presence of high luminescence and the great interaction between its molecules render PCDs properties unique.[16]

In 2004 Xu et al. prepared CDs starting from single-walled nanotubes. In 2006 Zhongke et al. used laser ablation and a boron/carbon target producing c-dots with enhanced luminescence emissions due to surface passivation.

Ionic liquids are solvents already used in chemical synthesis and extractions, but researches shown new applications for ionic liquids in bio-applications and as precursors for nanomaterials.[17] For example, Jiang et al. reported how to produce carbon dots starting from amino acids in acid or alkali medium. What makes ionic liquids good precursors for the synthesis of CDs with luminescent activity are the nitrogen-functionalized bulk.[17]

According to whether it is the synthetic route chosen we will have different CDs, different defects, and properties. The characterization that follows the synthesis is done with the X-ray diffraction, the transmission electronic microscopy, UV-vis, and the Fourier transform infrared spectroscopy.

1.1.2 Theragnostic applications

What started as a research on an alternative on the older zinc or cadmium-doped quantum dots brought to the acknowledgment of the property of CDs surface-passivated with organic biomolecules. Carbon Dots become fluorescent in the visible regions and once functionalized they are both physiochemically stable and photochemically stable, enabling the possibility of cellular imaging.[18]

Fluorescent nanoparticles can play a role as an optical agent in the cellular imaging field due to both their cytotoxicity and Vivo toxicity. The diagnostic function of the optical agents consists in providing information on the position of certain cells. An example that can be made is the one of tumoral cells, the diagnostic function, in this case, would provide information on the dimensions and type. It is evident how this could be ground-breaking on the diagnosis of tumours.[19]

To further understand how the diagnostic with bioimaging functions it is worth exploring the cell.

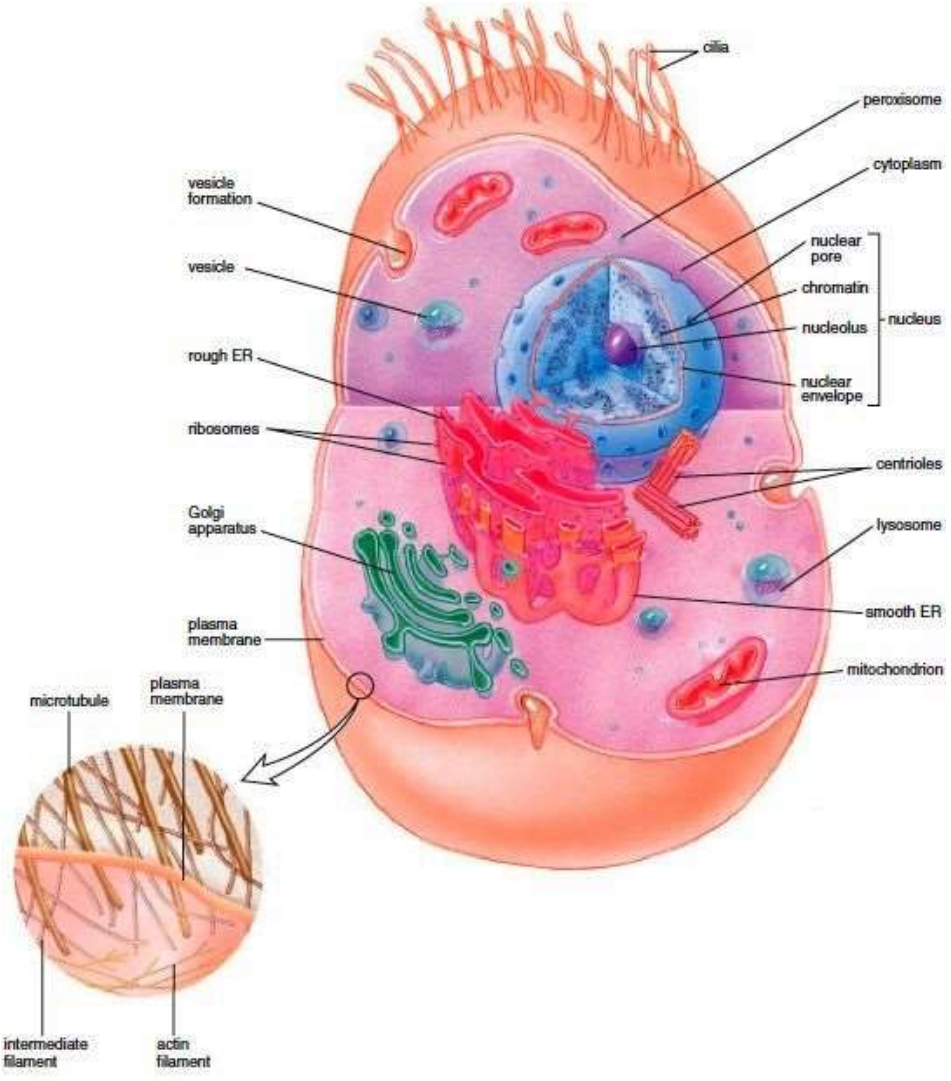

Figure 5 Human cell structure.

The cell membrane is defined as "a double layer of lipids and proteins that surround a cell" sheltering the cytoplasm, which is the internal part; the proteins constituting the membrane

allow the differentiation of cells per type. These biomarkers, using receptors linked to our CDs, become essential in this kind of investigation.[20]

Carbonaceous materials are non-toxic and In vivo investigation discovered the biocompatibility of these materials and the prospect of using them as a contrast agent raised further interest. Yang et al. reported in their studies the competitive performance for the imaging applications of CDs. [21]

Eskalen et al. synthesized carbon quantum dots with a hydrothermal approach paired with a microwave process employing cotton linter as precursor; this method provided for both a cheaper and easier approach to the synthesis of this product and also more efficient CDs for cancer-imaging applications.

After the characterization with the technologies afore listed, the cell viability and the proliferation were analysed. The results suggested that, depending on the dose, CDs were cytotoxic against the cell, inhibiting also cellular growth. [22]

Ding et al. synthesized nitrogen and sulphur carbon dots (N/S-CDs), once characterized, the team analysed the wavelength and emissions. The thus produced dots were employed for the detection of MnO4- and Cr2O7-2. Furthermore, N/S-CDs, for their biocompatibility, have proved to be a proper choice for their cellular imaging application. [23]

Theragnostic is a nanotechnology strategy that integrates a diagnostic approach with a therapeutic one; it allows to monitor the real-time response to the therapy. Thanks to the nanoparticles' functional groups situated on their surface it is possible to bond biomolecules to achieve a multi-functionalization that can, in turn, lead to the targeting of the ligand cells, drugs for cancer therapy, and genes. Theragnostic nanoparticles are made of some fundamental components: a signal emitter, which performs the imaging, a therapeutic load, that can be a chemotherapeutic medication or nucleic acids, and a carrier, usually a polymeric material.[24]

Drug delivery faces hard challenges since the blood-brain-barrier (BBB) hinders the entering of drugs in the central nervous system, this causes reduced treatment options for diseases like brain cancer and Alzheimer's.[25] CDs, although, find an application in this sense thanks to their outstanding properties and dimensions.

Keenan et al. used EDA (1,2-ethylenediamine) and urea during the synthesis of CDs and they have shown how the CD-EDA could penetrate the BBB. In the case of an intracranial hemorrhage, due to the damages in the membrane, CDs may be used for the evaluation of the damage and even to administer a therapy; for example, they can be used to carry a thrombolytic agent. [26]

CDs can carry simultaneously more than one therapeutic agent on their surface by reason of the covalent bonds of the functional groups, like the carboxylic and hydroxylic ones. To combine optical properties and therapeutic performance, Vijay et al. passivated CDs with oxaliplatin. Oxaliplatin is a chemotherapeutic agent that can hinder the ordinary DNA life cycle. The Oxa-C-dots therefore produced, shows, during in vitro and in vivo studies, how the fluorescent tracking leads to the drug dosage distribution in the cells. [27]

Allicin is a derivate of garlic, it was first isolated in 1944 and it has been largely studied ever since. Garlic was known for years for its antitumoral, antidiabetic, antimutagenic and anti-inflammatory potentials.[28] Donma et al studied the garlic application in inducing immunity in the treatment of COVID-19 infection.[29]

The most bioactive molecule of garlic is Allicin. Allicin compound is obtained metabolizing alliin into allicin. Garlic has to be dehydrated, crushed, cut or exposed to water in order to activate the enzyme alliinase and induce metabolization.[30]

Diallyl Disulfide (DADS) molecules are the by-product of allicin, they present more stability than the precedent compound and have different pharmacological connotations. DADS can inhibit cell proliferation and induce the arrest of the cell cycle.

Olivito et al.[31] synthesized symmetrical disulfide compounds with different carbon chain lengths and different double bond positions to study how these factors vary the antitumor activity. The compounds X, A, B in fig(6) have demonstrated better performance in inhibiting the cell viability compared to other unsaturated molecules produced.

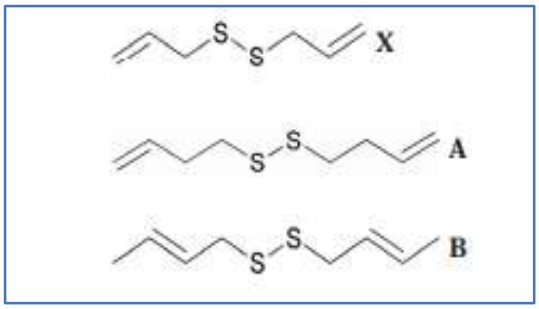

Figure 6 Diallyl disulphide molecules X, A and B.

The unsaturated configurations with a longer carbon chain were discarded by the author because of the loss of antitumoral activity, while the final double bond in compound A has proved a better cell inhibition viability.[31] Other studies like the one from Seki et al. [32] proved the better effectiveness of the unsaturated compounds compared to the saturated ones.

Based on the study by Olivito et al. [31] the configurations in fig(6) were chosen as the loading compounds for this work. The molecule X is the natural disulphide configuration: is symmetrical, unsaturated with external double bonds that determine its reactivity. Molecules A and B, which are produced with multi-step reaction, are symmetrical, with the same carbon chain length but with different double bond positions. The double bond position plays a role in the reactivity of the compounds[33] and in their antioxidant activity. Antioxidants can inhibit the initiation or propagation of oxidative chain reactions in biological environments depleting reactive oxygen species concentration.[34] These phenomena, that lay behind the inflammatory events, with the production of reactive oxygen species could induce in the worst case scenario the death of the cells.[35] The configurations A and B, in fig(6), differ from the position of the double bond: molecule A is more reactive, the external double bond enables the possibility to immediately bond with free radicals, while, compound B is more stable.[33]

This work aims to combine these resourceful disulphides with Carbon Dots to integrate the diagnostic capability of fluorescent carbon dots with the therapeutic activity of these specific allicin by-products.

1.2 Scope of the work

This work aims to combine the diagnostic properties of Carbon dots with the therapeutic effects of Diallyl Disulphide. To reach its scope, this thesis starts with the synthesis and characterization of a proper type of carbon dot. The precursor is Citric Acid (CA) and the amino passivating agent is Urea (U), which has been chosen as an N-source not only for its low cost and abundance but also for being particularly suitable for the type of thermic synthesis which will undergo. Similar work has been brought on by Liyanage et al.[26] Polyethylene glycol (PEG) is already used in various applications and recent studies, like the one from Sachdev et Al.[36], demonstrated its role in CDs for their surface passivation. PEG has an important role both in the enhancement of the photoluminescence of CDs, and in the structure itself since it could be used as a medium to assist the synthesis. In this work, the amount of Citric acid and Urea are always in the same ratio meanwhile, the amount of PEG is varied to investigate precisely its role. The synthesis variables are the temperature and the reaction time. After the syntheses, the characterization provides the information to properly choose the carbon dot suitable for the second process: the DAAD loading.

Three different types of DAAD (molecules X, A, B in fig(2)) are loaded with a ratio of more than one to one, and a final thermogravimetric analysis indicates how much DAAD is adsorbed.

2. Materials and methods

2.1 Materials

Citric Acid was acquired from Nortem Chem SA (Spain). Urea was procured by Sigma-Aldrich (99 - >100%) with ACS grade. PEG_{4000} was procured by Sigma-Aldrich. Petroleum Ether (40 °C – 60 °C) was purchased from CARLO ERBA reagents. DAAD were provided from the University of Calabria. The tubular reactor is made of PYREX glass in fig(3). A vacuum pump is used for the filtration process. The centrifuge used for the purification process is the Microcentrifuge MPW-55 from MPW MED. INSTRUMENT. The sonicator used for the precursor's preaparation is the Vibra Cell Sonicator purchased from Sonics. The sonicator used for the purification process is the S15H from Elmasonic.

Figure 7 Pyrex tubular reactor, Microcentrifuge MPW-55, Vibra Cell Sonicator.

2.2 Methods

2.2.1 Synthesis and Purification

All precursors are characterized by a composition of 1 g of citric acid and 10 g of urea, the difference lies in the quantity of PEG: the first one has zero PEG, the second type of precursor has 0.1 g of PEG, and the third one 1 g of PEG; while, as it has been stated before, the ratio AC/U=1/10 has been maintained constant in all the preparations. Postliminary the grinding procedure, to obtain a homogeneous powder, the precursors are placed in a 25 mL water solution. To see how the stirring process would affect the final product, it has been chosen to

proceed with two different types of stirring processes, starting with the same preparations (the ones that differ for PEG quantity: 0 g PEG, 0.1 g PEG, and 1 g PEG) in both cases. One preparation per type is put into mechanical agitation overnight and in the same way, one preparation per type undergoes a sonification process, for 30 minutes with 5 seconds pause every 30 seconds.

The drying of the solution, to obtain a solid matrix, is carried out in the oven below 100°C. The precursors produced have been labeled from EM-01 to EM-06.

Table 1 Precursors' ID and preparation.

	Weight [g]			Volume [mL]	
	AC	U	PEG	Water	stirring method
EM-01	1	10	0,0	25	Mechanical agitation
EM-02	1	10	0,1	25	Mechanical agitation
EM-03	1	10	1,0	25	Mechanical agitation
EM-04	1	10	0,0	25	Sonication
EM-05	1	10	0,1	25	Sonication
EM-06	1	10	1,0	25	Sonication

The synthesis took place in a tubular reactor filled with an Argon inert atmosphere, at different temperatures, in a range from 250 °C to 550 °C, with reaction times that span from 5 minutes to 15 minutes. An infrared spectroscopy analysis is then used to analyse the results. Every substance is weighed before and after the reaction to evaluate the mass losses during the thermal process.

The first set of analyses was performed at 550 °C on precursors: both the ones stirred with mechanical agitation and the ones sonicated, with reaction times of 5 minutes, 7 minutes and 10 minutes. This set was labelled from EM-07 to EM-26.

The EM-07 was put at 550°C for 5 minutes. With the aim to promptly see the difference with the afore mentioned sample, EM-08 undergoes an exceptional treatment: it is put at 250 °C for 5 minutes. The only other irregular sample is EM-19, in the course of its thermal treatment, we observed some leaks due to a massive release of volatile organic matter which over-pressurized the reactor. Accordingly, we did not use the solid recover after the reaction.

Table 2 Set of synthesis at 550°C with different precursors and reaction times.

Product	**Precursor**	**Temperature [°C]**	**Time [min]**	**Weight loss**
EM-07	EM-04	550	5	66%
EM-08	EM-04	250	5	0%
EM-09	EM-04	550	10	66%
EM-10	EM-04	550	7	73%
EM-11	EM-05	550	5	68%
EM-12	EM-05	550	10	73%
EM-13	EM-05	550	7	69%
EM-14	EM-06	550	5	63%
EM-15	EM-06	550	7	73%
EM-16	EM-06	550	10	77%

EM-17	EM-01	550	5	65%
EM-18	EM-01	550	7	79%
EM-20	EM-01	550	10	73%
EM-21	EM-02	550	5	59%
EM-22	EM-02	550	7	64%
EM-23	EM-02	550	10	71%
EM-24	EM-03	550	5	62%
EM-25	EM-03	550	7	71%
EM-26	EM-03	550	10	72%

Figure 8 Products EM-16 and EM-13 appearance after thermic treatment.

The second set of analysis is run at 250 °C for 10 minutes. This set is labelled from EM-27 to EM-31. Due to the lower temperature, there aren't any weight losses, thus, the lack of report on them. The only ones that have been observed are the ones caused by the recovery of the material from the reactor.

Table 3 Set of synthesis at 250 °C for 10 minutes with different precursors.

Product	**Precursor**	**Temperature [°C]**	**Time [min]**
EM-27	EM-03	250	10
EM-28	EM-01	250	10
EM-29	EM-02	250	10
EM-30	EM-05	250	10
EM-31	EM-06	250	10

The third and fourth set of analysis are performed at 350 °C and 450°C on the precursor named EM-04, the one void of PEG that underwent sonication. The reaction times are set on 5 minutes, 7 minutes, and 10 minutes. The resulted sets of reactions are named from EM-32 to EM-37.

Table 4 Set of synthesis on EM-04 at 350° and 450°C with different reaction times.

Product	**Precursor**	**Temperature [°C]**	**Time [min]**	**Weight loss**
EM-32	EM-04	350	5	13%
EM-33	EM-04	350	7	18%
EM-34	EM-04	350	10	53%
EM-35	EM-04	450	5	55%
EM-36	EM-04	450	7	65%
EM-37	EM-04	450	10	66%

The last set of thermal treatment is executed at 550 °C for 15 minutes only on the precursors that have undergone the mechanical agitation, namely precursors EM-01, EM-02 and EM-03 since the other precursors already faced punctual high temperatures during the sonication. This set was intended to lead the reaction to the limit and see whether the sample degrades.

Table 5 Set of synthesis at 550 °C for 15 minutes from different precursors.

Product	**Precursor**	**Temperature [°C]**	**Time [min]**	**Weight loss**
EM-38	EM-01	550	15	71%
EM-39	EM-02	550	15	78%
EM-40	EM-03	550	15	70%

A mild method was also evaluated: at 80 °C overnight in an oil bath. The precursors, in vials, were installed in a bath of oil brought to the 80 °C.

The purification aim is to separate the soluble from the insoluble components. The product of the reaction is solubilized in 5 mL of water, then it is stirred, and finally, the sonicator is used to precipitate the insoluble part. The sonicator is set in “sweep” mode for 15 min with a maximum temperature of 35 °C. The sweep mode avoids the temperature rising preventing the solution from boiling besides enhancing the homogenization. Thanks to this process, it is possible to draw the purest soluble liquid part with a Pasteur pipette. To realize a finer separation, the liquid part drawn in the previous step is centrifugated. Subsequently, A drying operation allows extracting the soluble solid part: the final result.

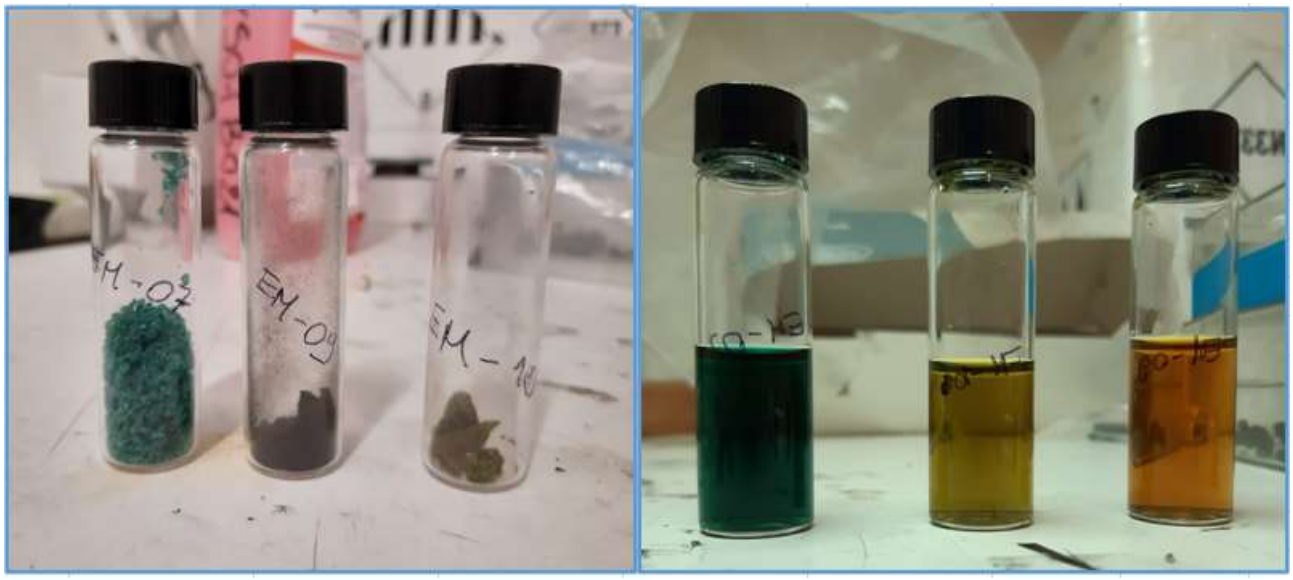

Figure 9 Products EM-07, EM-09, EM-10 before and after purification.

2.2.2 Characterization

Carbon dots are analysed through FT-IR (Nicolet 5700, Thermoscientific, Waltham, US) on attenuated total reflectance (ATR) mode (Smartorbit, Thermoscientific) in a range from 500 to 4000 cm−1.

Thermogravimetric analyses (TGA) are performed using a Pyris1TGA apparatus (Perkin Elmer, USA) (experimental error: ±0.5 wt%, ±1 °C). Samples (about 10 mg), instead, are placed in alumina pans and runs were carried out in a range from 50–900 °C, with a heating rate of 10 °C/min, and a N2 flux of up to 35 mL min-1.

Raman spectra are recorded using a Renishaw Inviah Spectrometer equipped with a 50x objective and with blue (457 nm), green (514.5 nm), and red (wavelength 785 nm) laser sources. Employing the green laser source, power is applied in a range from 10-100 mW, while the red laser line range from 50 to 500 mW and the blue laser line from 100 mW to 1 mW.

Carbon dots are studied through XPS. In order to carry out the XPS analysis, PHI 5000 Versa Probe instrument (Physical Electronics) equipped with an Al Kα radiation (1486.6 eV) X-ray is employed. was used to carry out the XPS analysis

Figure 10 Infrared Spectroscopy and RAMAN equipment.

2.2.3 Loading process

The loading process involves four different loads: thiophene, DAAD type X, A, and B.

The solutions for the adsorption process are made in the following way: the first solution is composed of 50 mL petroleum ether with 50 mg of thiophene, while, the other solutions are composed of 50 mL petroleum ether and 50 mg of every DAAD type (X, A, B). (In the introduction of this work the reader can find a proper description of the differences between the aforementioned DAAD types).

The carbon dots are then weighted, and a 50 mg sample is put in a 5 mL solution per type - the ones whose composition is described right above - to then undergo a mechanical agitation overnight. Afterward, they are filtered under vacuum by using a Buckner and a paper filter. Solid recovery are further analyzed.

The material obtained subsequently the absorption and filtration is analysed through TGA in a range from 35 °C to 120 °C.

3. Results discussion

3.1 Thermal reaction

3.1.1 Citric Acid and Urea

The samples' preparation, purification, and synthesis will be briefly reiterated in this section. Citric Acid and Urea, in a 1/10 ratio, are heated at different temperatures and with different reaction times to investigate the role of these variables. After the thermal treatment, the mixture is purified and dried.

Based on the work of Keenan et al.[37] it is possible to analyse the reaction pathways involved in the early stages and hypothesize the CDs structure and, therefore, also simulate it.

CDs exhibit various and complex reaction pathways, as reported by Keenan et al.[37] and sketched in fig(11).

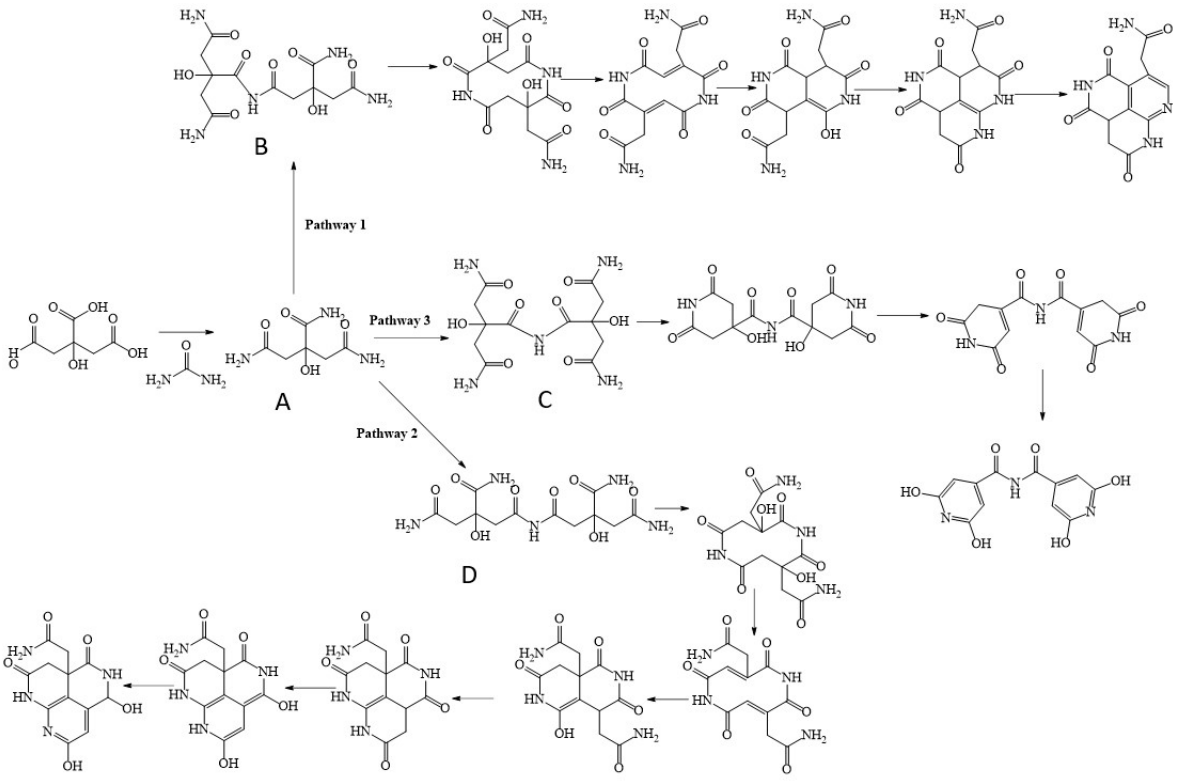

Figure 11 Chemical pathways during the thermal reaction of Citric Acid and Urea.

The reagents, Citric Acid and Urea, during the stirring processes, with both mechanical agitation and sonication, react, producing the dimeric intermediate (A). During the thermal reaction, a lot of mechanisms are involved, and the possible products are several depending on the connection between dimers. The possible pathways are defined by the possible configurations allowed by the citric acid structure: the three NH_2 groups are the sites of the

bonds between dimers (B) (C) (D) as shown in fig(11). The cyclization goes on with the mechanisms in fig(11) which shows the possible cyclic structures that the reaction involves. Since the thermal reaction is forced to high temperatures we expect the simultaneous presence of compounds from all three pathways. Even if pathway 3 originates from high steric hindered precursor C, cyclization compound could be also present due to the high temperature adopted for the synthesis.

These compounds can evolve into cyclic compounds that will combine in 3-D structures and creates the structures' layers. The core will be similar to graphene oxide, with the carbon atoms cyclic arranged and covalently bonded in sp^2 structures, while the layers interact with weak forces among them. The N-doped structures will be external, rearranging in triazines, oxygen-containing functional groups will be in the perimeter of the structure as well.

With the formation mechanisms displayed above, it is possible to create a model of the expected structure, which will have a graphitic core and functional groups tailoring on the surface perimeter. Comparing to fig(12) the structure has been simulated on Hyperchem, in order to see how it rearranges at the minimum energy value. The core structure is reported in fig(9).

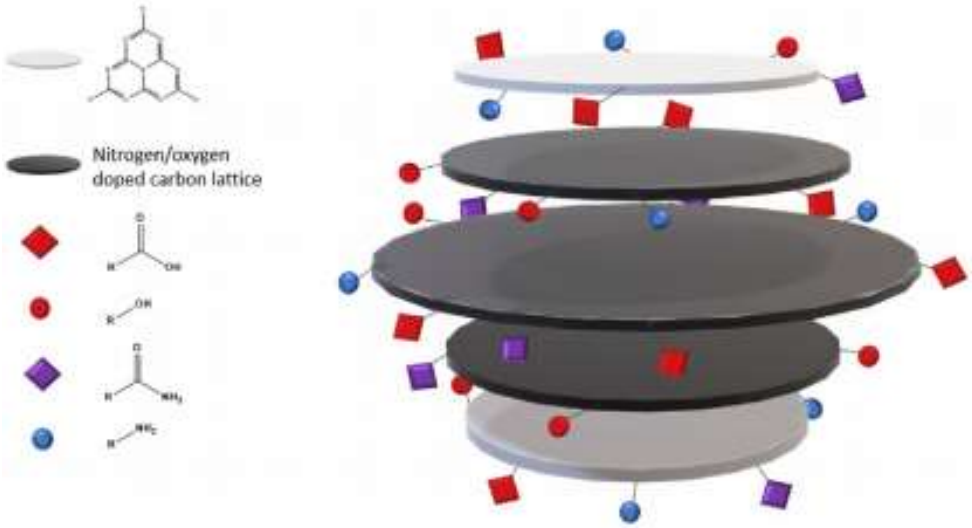

Figure 12 Hypothesis of the structural model of CD.[37]

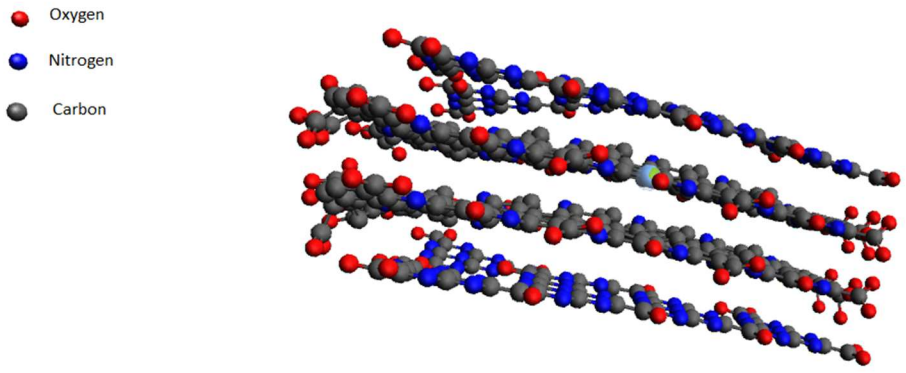

Figure 13 Model, Simulation and optimization of CD structure.

3.1.2 Citric Acid, Urea and PEG

The presence of PEG changes the reaction's dynamic described above, this section will describe how and which advantages this compound brings to the CDs formation mechanism.

The addition of PEG promotes the assembling of the micelles phase, the internal environment of pseudo-micelles could be assumed as less polar than the pure watery phase as shown in fig(14). Accordingly, aromatic compounds through cyclization and condensation processes enriched the internal part of the micelles therefore those structures underwent further aromatization process through intermolecular condensation routes. These phenomena are accountable for the increment of C=C stretching mode in the products' IR containing PEG as shown in the next sections.

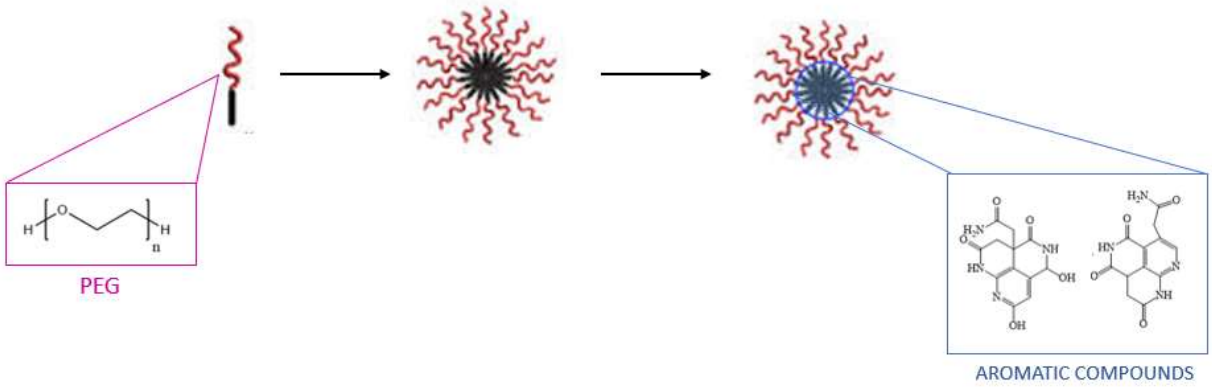

Figure 14 PEG reaction mechanism.

3.2 Characterization

The characterization provides for analysis with Infrared Spectroscopy, Thermogravimetric analysis, X-ray photoelectron spectroscopy, and Raman spectroscopy.

3.2.1 Infrared spectroscopy

The evolution of the compounds occurring during the synthesis, can be monitored with the IR spectroscopy analysis. The results of this analysis are reported in the following section.

In fig(15) the reagents spectra are reported.

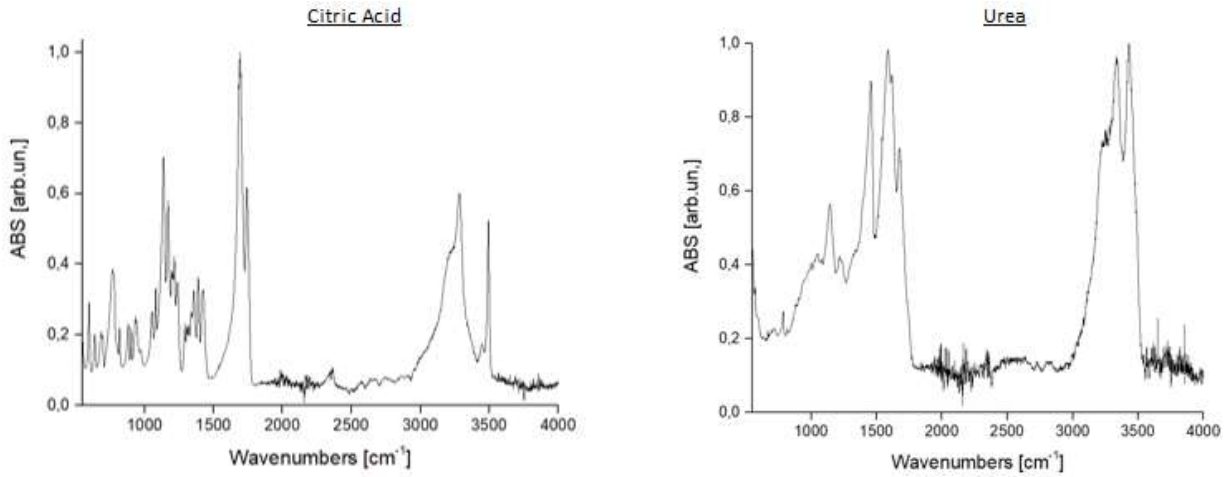

Figure 15 The IR spectra of the reagents Citric Acid and Urea.

The the citric acid IR spectrum (500 cm^{-1} - 4000 cm^{-1}) has a large band at 3500 cm^{-1} that due to -OH groups and the large band between 3220 and 3280 cm^{-1} can be assigned to the -OH stretching of carboxylic groups. The peak at 1700 cm^{-1} is assigned to the stretching of double bond C=O. [38] The urea IR spectrum shows two peaks between 3000 cm^{-1} and 3500 cm^{-1} which is assigned to the $-NH_2$ stretching. At 1600 cm^{-1} there is a sharp peak imputable to C=O stretching vibration.[39]

During the stirring processes, the reagents start to react, in different ways based on the mechanisms involved: EM-01 is the precursor obtained with mechanical agitation, EM-04 is the precursor obtained with sonication. We are going to compare the two different precursors devoid of PEG in fig(16).

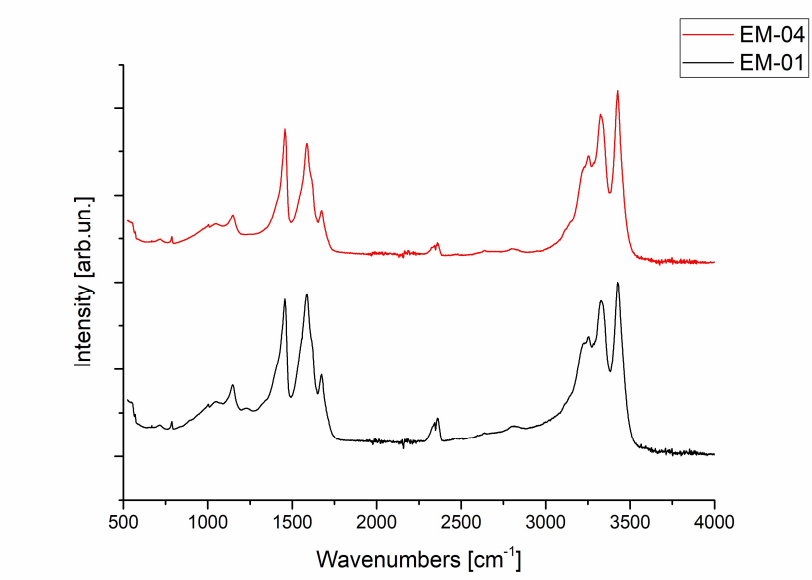

Figure 16 The IR spectra for the precursors EM-01, EM-04.

In the precursors, EM-01 and EM-04, spectra, it is immediately brought to attention the two amides peaks in the frequency region around 3500 cm^{-1}, which we find in the Urea spectrum. Furthermore we can notice the absence of the carboxylic peak that should, instead, be adjacent to this region.[40] The absence of the carboxylic peak in the 3000 cm^{-1} region, combined with

the appearance of the peak at 1650 indicates that the precursor reacted. It is possible, then, to assume that we are in the case of the species A fig(11), or, perhaps, already in the three pathways of the figure.[41] At this stage, There are not noteworthy detectable differences between the two precursors.

EM–36 underwent a synthesis at 250 °C for 10 minutes; it doesn't present peaks diversification from the EM-01 precursor, so it is possible to deduce that the evolution of the structure did not take place. The spectrum is not reported since it does not provide new information.

In fig(17) there are the spectra of the precursor EM-01 compared to the ones of EM-17, EM-18, and EM-20 which are the products of the synthesis conducted at 550 °C at different times.

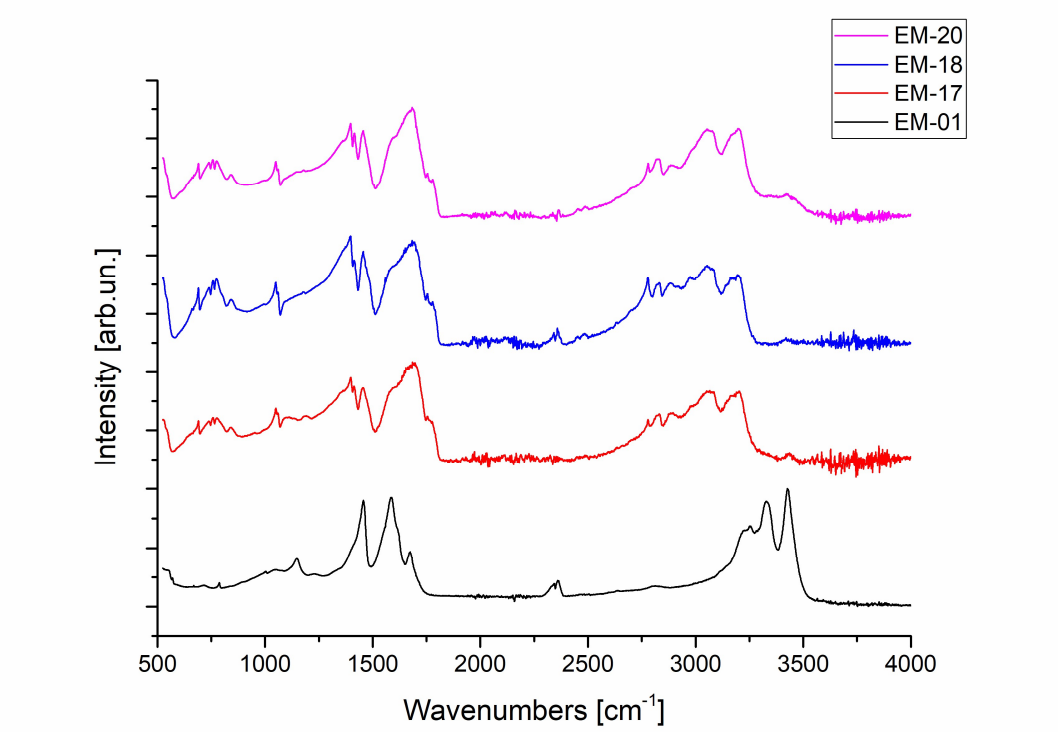

Figure 17 The IR spectra of the precursor EM-01 and the products: EM-17, EM-18, EM-20.

Fig(17) displays the IR spectra in order to show how they change during the synthesis with the reaction time increasing. First of all, it is important to notice the disappearance of the peak at 3500 cm^{-1} that is assigned to N-H stretching of the amides occurring at the same time as the relative rising of the peak at 1571 cm^{-1} assigned to the C=N stretching due to the formation of triazine moieties.[42] The peak around 3400 cm^{-1} – 3500 cm^{-1} is assigned to the -OH stretching.[43]

With the progressing of the reaction, we can see the rising of two peaks: one around 2700 – 2950 cm^{-1} region due to the C-H saturated stretching, one at 3200 cm^{-1} indicating the unsaturated C-H, due to the formation of the aromatic moieties.[44] The residual amides are identified with the peak at 1700 cm^{-1} and the residual carboxylic groups at 1650 cm^{-1}. The aromatization is monitored by the rising of the peak at 1600 cm^{-1}. [45]

The region between 1300 cm^{-1} - 1450 cm^{-1} is assigned to the bending of the C-O, C-N, C-C groups.[46]

Regarding the EM-04 precursor, the syntheses were run at different temperatures than the EM-01 precursor.

Fig(18) reports the time-independent reaction displaying the spectra of the products obtained with 10 minutes of reaction time at 350 °C, 450 °C, and 550 °C.

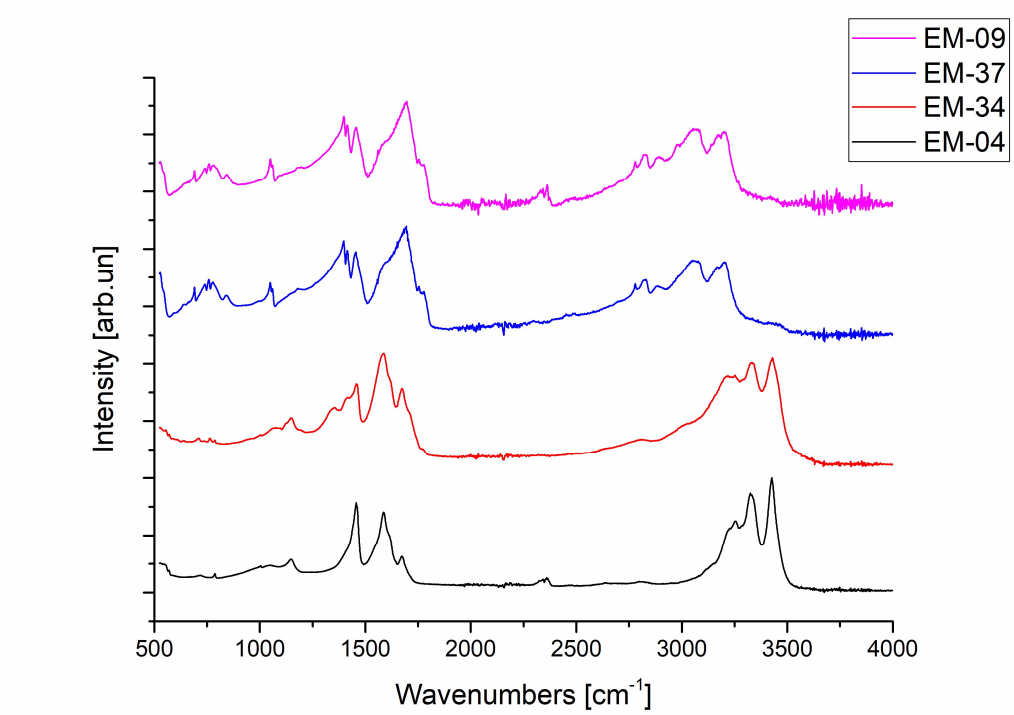

Figure 18 The IR spectra for the synthesis at 350 °C, 450 °C and 550 °C for ten minutes of the precursor EM-04.

EM-34 is the reaction performed at 350 °C and its spectrum shows how the reaction slowly started. The first difference from the precursor spectrum is the different peak shape in the carboxylic region (3000 - 3200 cm^{-1}), moreover, the peaks assigned to the bending of C-O, C-N, C-C around 1300 – 1400 cm^{-1} start to change. EM-37, which is synthesized at 450 °C, presents more differences, resembling more the disposition of the peaks we see in the 550 °C reactions.

In fig(19) are reported two syntheses ran for ten and fifteen minutes, respectively EM-20 and EM-38.

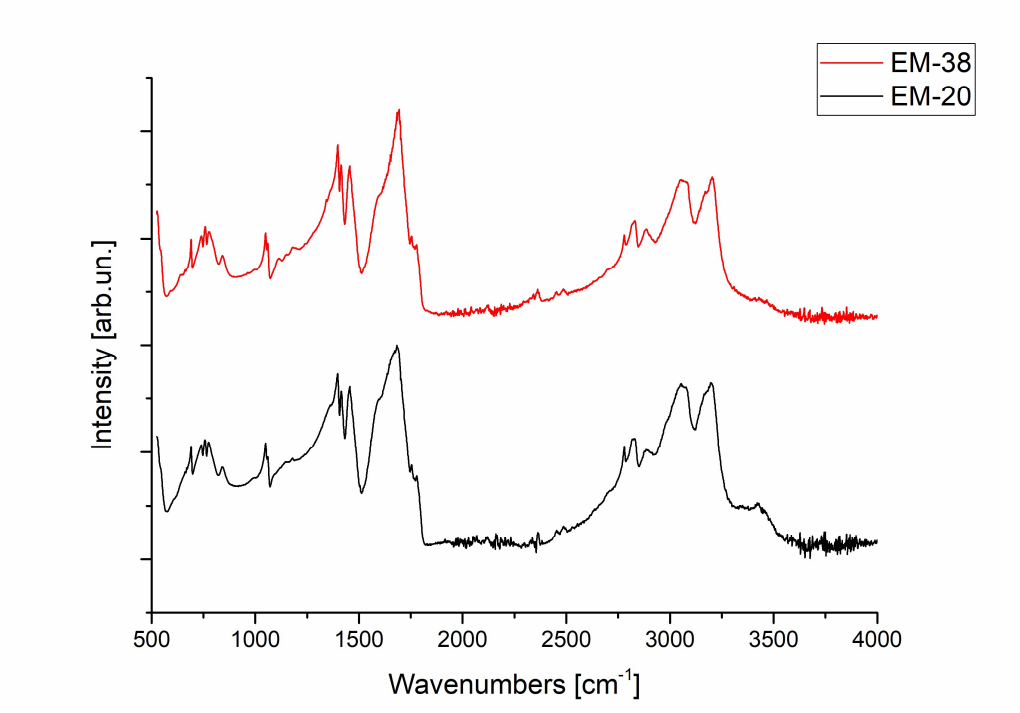

Figure 19 The IR spectra of the products EM-20 and EM-38 with 10 minutes and 15 minutes reaction times.

The comparison between the syntheses carried out at different reaction times, respectevely ten and fifteen minutes, is reported in fig(19). The differences in the spectra are minimal so it is fair to infer that the same result is still achieved with a, shorter, ten minutes reaction time.

The PEG spectrum is reported in fig(20) in order to analyse the typical peak of this material as a starting point for the PEG synthesized compound's IR spectroscopy analysis.

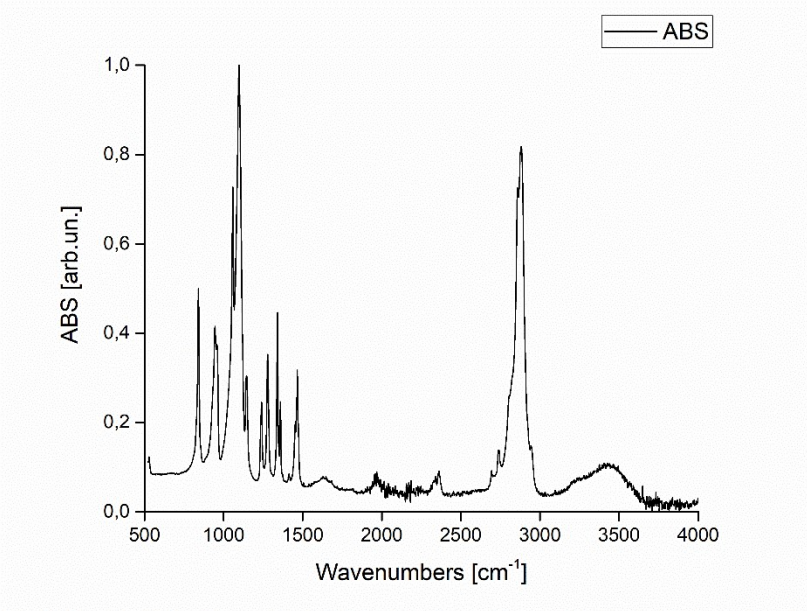

Figure 20 The IR spectrum for the reagent PEG.

The peak between 2700 cm^{-1} and 3500 cm^{-1} is assigned to C-H stretching and the peak at 3500 cm^{-1} is the terminal -OH. In the region with small wavenumbers, at high energy, there is another

important peak, the sharpest in the region, that is assigned to C-O stretching. Furthermore, in this region, there are the bending vibrations.[47]

The precursors EM-02 and EM-05 are obtained with 0.1 g of PEG and, respectively, with mechanical agitation and sonication for the stirring process. In fig(21) are reported their spectra.

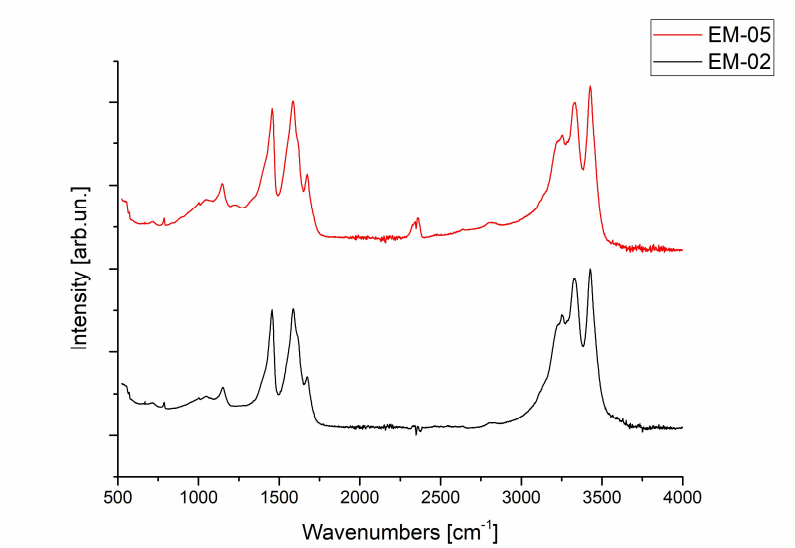

Figure 21 The IR spectra for the precursors EM-02, EM-05 with 0.1 PEG.

The precursors' spectra are very similar except for the small peak at 1250 cm^{-1}, assigned to C-O stretching. This peak is present only in the EM-05 spectrum, which leads to the conclusion that, during the sonication process, other phenomena occurred, leading to a more efficient reaction pathway. During sonication, we promote ultracavitation effect where the bubbles go from a spherical shape to an ellipsoidal one. This causes punctual rise of the temperature as a consequence of instantaneous volume reduction.[48] A similar effect is induced in the micelle-like phase formed through the addition of PEG. While at this stage there are no important differences, these might result later, during the stage of the thermal reaction. For these reasons the spectra of the synthesis at 550 °C at different reaction times for both precursors are reported in fig(22).

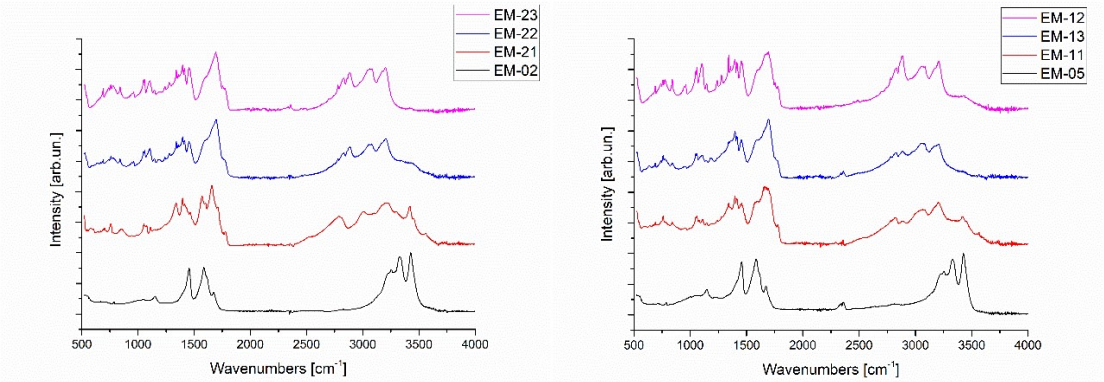

Figure 22 The IR spectra of the precursor EM-02 with its products at 550 °C on the left. The IR spectra of the precursor EM-05 with its products at 550 °C on the right.

It is clear that, at this stage, there are no important differences between the two processes. Considering both EM-21 and EM-11, it is, indeed, evident how at 550 °C after 5 minutes the

reaction is still halfway through. The amides peaks are still present; the peaks rising around 2700 – 3200 cm^{-1} are assigned to saturated C-H stretching and, relatively to the aromatization of the moieties, to the unsaturated C-H stretching. In EM-11 the trend of the amides peaks at 3500 cm^{-1} to disappear is more evident than in EM-21. After 10 minutes of reaction, there are only peaks relative to the aromatization. The residue of the amides and carboxylic groups are assigned to the rising peaks in every spectrum at 1600 cm^{-1}. The bending regions slightly change depending on the product.

Fig(23) illustrates the spectra of the precursor EM-05 and EM-30, which were synthesized at 250 °C for 10 minutes.

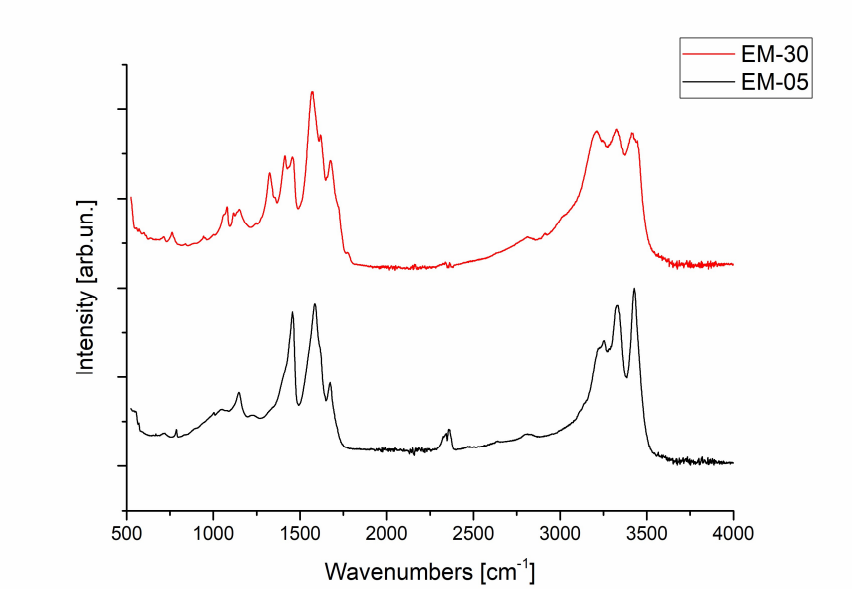

Figure 23 The IR spectra for the precursor EM-05 and the product EM-30.

EM-30 shows the disappearance of the N-H peaks at 3500 cm^{-1} followed by the rising of the peaks relative to the C-H stretching for the aromatization starting. The amides' peak combined with the information extrapolated from the region around 1570 cm^{-1} indicates the reaction that brings to the formation of the triazines.

The precursor EM-02 also has been synthesized for a reaction time of fifteen minutes to compare it to the ten minutes synthesis, but, as previously reported for precursor EM-01, there are not enough differences in the spectra to justify the more time needed.

The precursors EM-03 and EM-06 are obtained with 1 g of PEG and, respectively, with mechanical agitation and sonication as the stirring process. Putting in comparison these precursors' spectra we notice that are very similar, so the precursor EM-06 spectra will not be reported to avoid redundancy. Nevertheless, it is important to notice, as reported in fig(24), the differences between two different precursors, respectively with 0.1 g and 1 g of PEG.

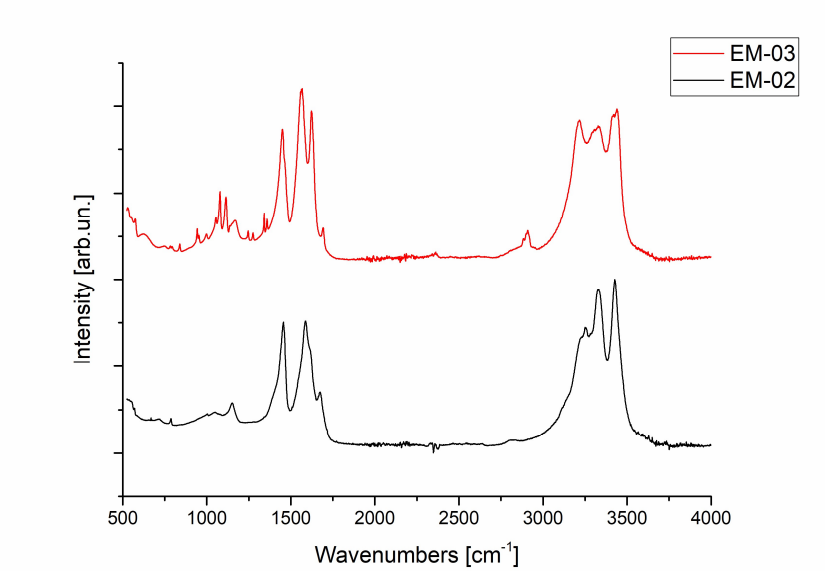

Figure 24 The IR spectra for the precursors EM-02, EM-03.

In fig(24) the precursors with different amounts of PEG are compared, respectively 0.1 g and 1 g and we can see how the peaks change in certain regions. At 3200 cm^{-1} the peak assigned to unsaturated C-H stretching is more evident in EM-03 suggesting that PEG promotes the aromatization process. The peak of the sature C-H at 2900 cm^{-1} stretching confirms this aromatization process' promotion. Considering the chemical structure of PEG, it is reasonable to attribute the peak at 1650 cm^{-1} to free carboxylic compounds, and the peak at 1700 cm^{-1} testifies the presence of free amides. The bending region indicates the different bonds that are established, due to the presence of PEG that enables the promotion.

In fig(25)(26) are reported the results from the precursor EM-03 and EM-06, the syntheses were conducted at 550 °C at different reaction times.

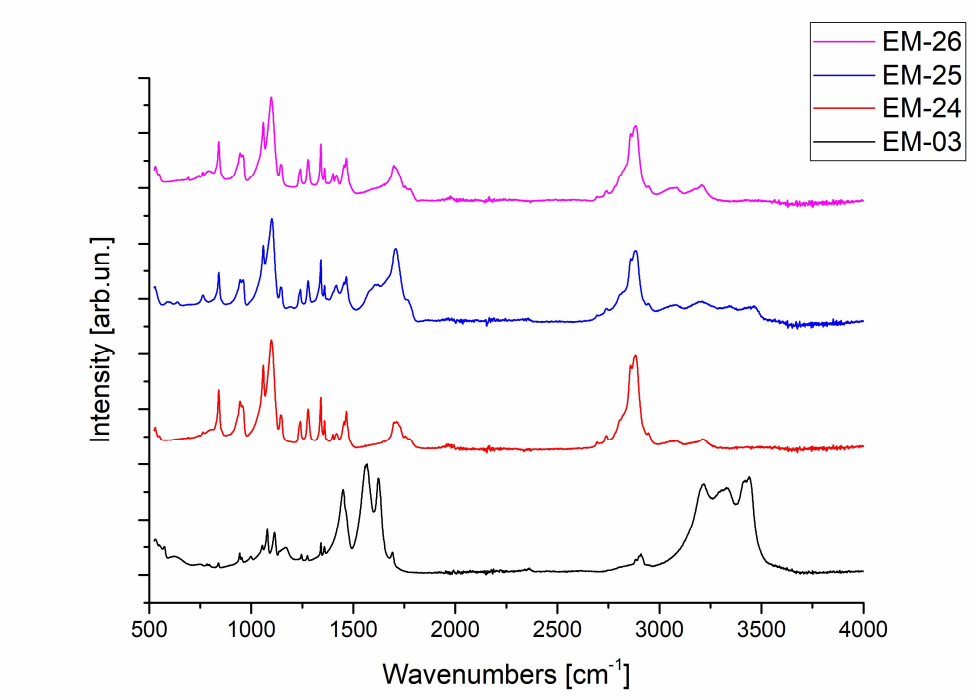

Figure 25 The IR spectra of the products for the syntheses of EM-03 at 550 °C with different reaction times.

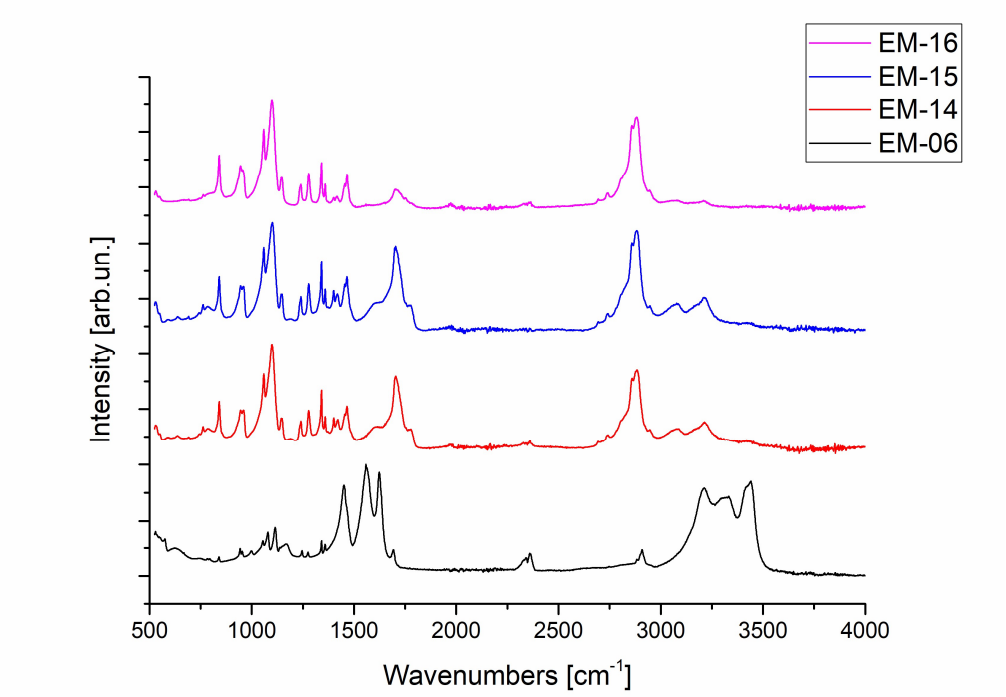

Figure 26 The IR spectra of the products for the syntheses of EM-06 at 550 °C with different reaction times.

In fig(25)(26) is reported a different pattern from the ones seen before. The amides peak disappears completely but in contrast to what we have seen before we also don't see the rising of the triazine peak at 1571 cm^{-1}. This behaviour can be explained by hypothesizing that PEG prevents the formation of perimetric groups, like the carboxylic ones, while promotes the aromatization process in the core of CDs. The rising peak at 2800 cm^{-1} is assigned to C-H stretching, while the peak around 1000 cm^{-1} is assigned to C-O. Both of these compounds come from the PEG structure which is abundant in the precursor of this synthesis. The region of C-H bending also changes in the range between 1300 cm^{-1} and 1450 cm^{-1}. The remaining peaks around 3000 cm^{-1} indicate the progressing aromatization process.

The synthesis for both precursors was also run for 250 °C for 10 minutes and 80 °C overnight but the spectra of these syntheses show that the reagents do not react, for this reason, the spectra are not reported.

The precursor EM-03 has been synthesized for a reaction time of fifteen minutes to compare it to the ten minutes synthesis, but, as previously reported for precursor EM-01 and EM-02 there are not enough differences in the spectra to justify the more time needed. Since it does not provide new information, the spectrum is not reported.

On the basis of the Infrared Spectroscopy analysis, the most promising products are chosen. The products devoid of PEG chosen are EM-18, synthesized at 550 °C for seven minutes, and EM-36 synthesized at 450 °C for seven minutes. The EM-23 is chosen from the samples containing 0.1 g of PEG, and EM-26 from the ones containing 1 g of PEG, both obtained at 550 °C with a reaction time of ten minutes. The yield of the syntheses for these compounds is reported in the tab(6).

	YIELD
EM-18	27.3 %
EM-36	68.2 %
EM-23	2.0 %
EM-26	4.3 %

Table 6 Yield for EM-18, EM-36, EM-23, EM-26.

The promising products mentioned above have undergone other characterization analyses: TGA, XPS and RAMAN.

Subsequently, these products have undergone the loading process.

3.2.2 Thermogravimetric analysis

The carbon dots synthesized at high temperatures, as described above, are analysed with the thermogravimetry analysis to investigates the compounds' thermal stability in order to deduce information about the structure of the dot and get confirmations about the structure hypothesized from the IR spectra.[49]

In fig(27) is reported the TGA analysis for the EM-18 product

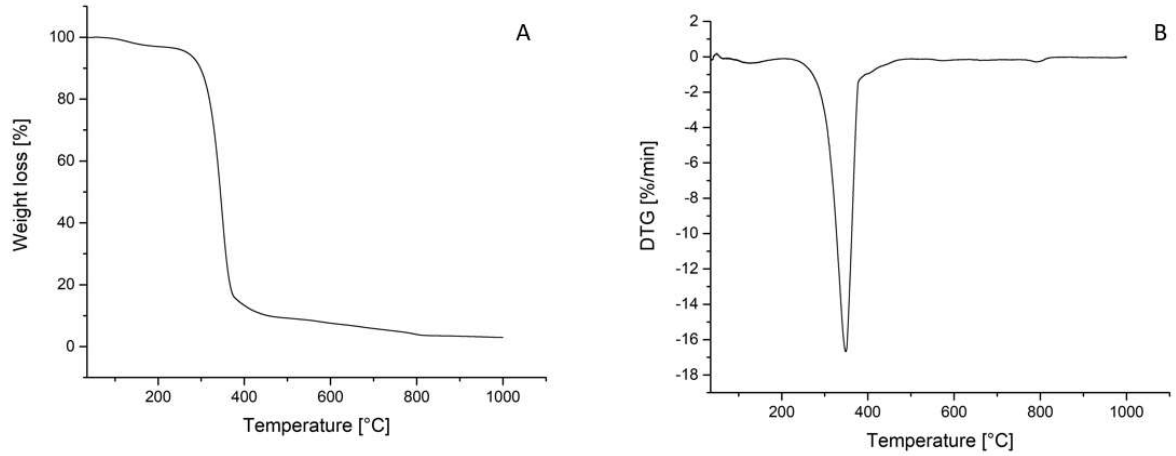

Figure 27 TGA analysis for EM-18: (A) weight loss (B) DTG.

EM-18 does not contain PEG and was produced at 550 °C for 10 minutes. In the first part of the spectrum, we can see a first downward trend at low temperatures caused by the evaporation of the free carboxylic in the sample, which is common to all the spectra in this section. Between 200 °C and 400 °C we can see a sharp trend of the curve assigned to the weight loss which correspond to 5 wt%, this point indicates the starting point of the degradation process.[50] The Differential thermo gravimetry red line helps to observe better the following mechanism. The negative peak in the DTG is caused by the degradation of the non-aromatic compounds, mainly carboxylic groups. The slope after 400 °C is assigned to the degradation of the graphitic core N-doped, which requires higher temperatures to degrade.[51]

EM-36 was produced at 450 °C, with a difference of 100 °C from the synthesis of EM-18, but, as is shown in fig(28), it presents a totally different trend of thermic degradation from the previous one.

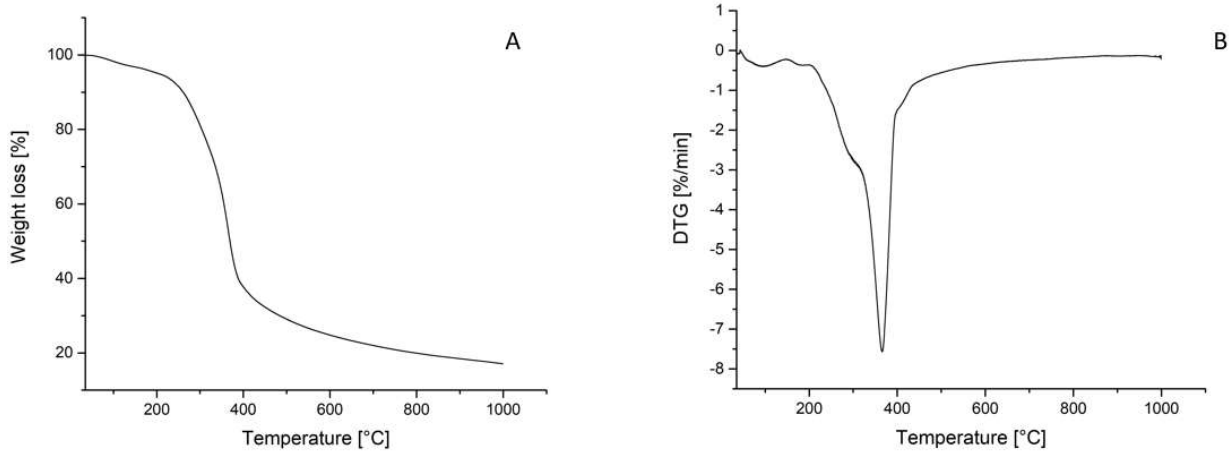

Figure 28 TGA analysis for EM-36: red line for DTG, black line for weight loss.

The trend of the EM-36 displays a structure of a not fully completed process with a large amount of not fully reacted moieties showing fewer aromatics compounds content. Accordingly, we hypothesized that the carbon dot formation is not entirely completed. This is proved by the broad TGA spectrum reported in fig(28), which support, in the temperature range investigated, a further thermic evolution of the structure considered.

Prior to the analysis of the spectra of the PEG-containing compounds, it is worth looking at the PEG spectrum to see at which temperature it degrades, in order to separate the peak of PEG from the other information that the next spectra provide.

In fig(29) is reported the Thermo Gravimetry Analysis of PEG.

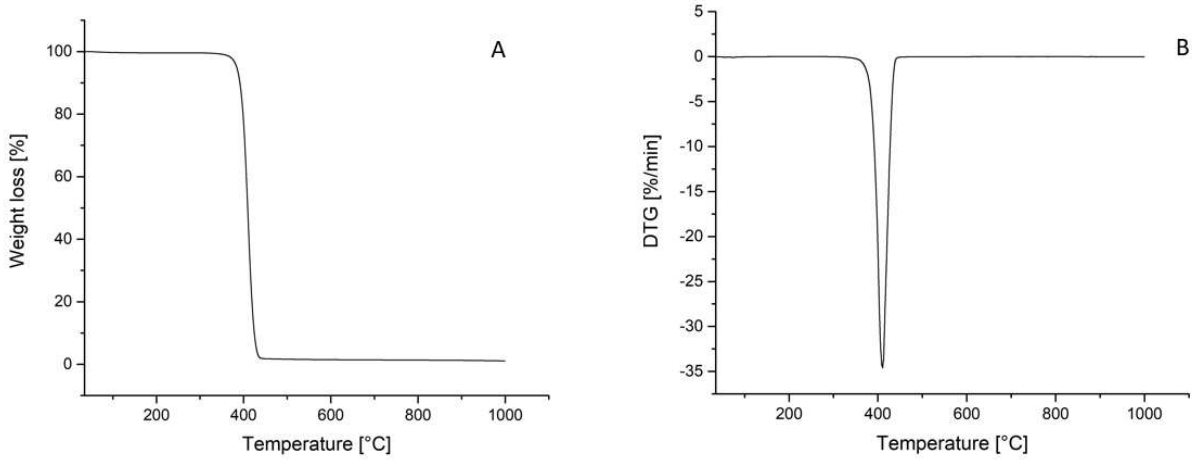

Figure 29 TGA analysis of PEG: (A) weight loss (B) DTG.

The spectrum displays a sharp peak at 400 °C, this is the temperature at which PEG degrades. A likewise deduction can be inferred in the Differential Thermo Gravimetry as it shows the minimum peak. [52]

The products EM-23 and EM-26 are the ones containing PEG, therefore the TGA graph will look different than the ones in fig(27)(28).

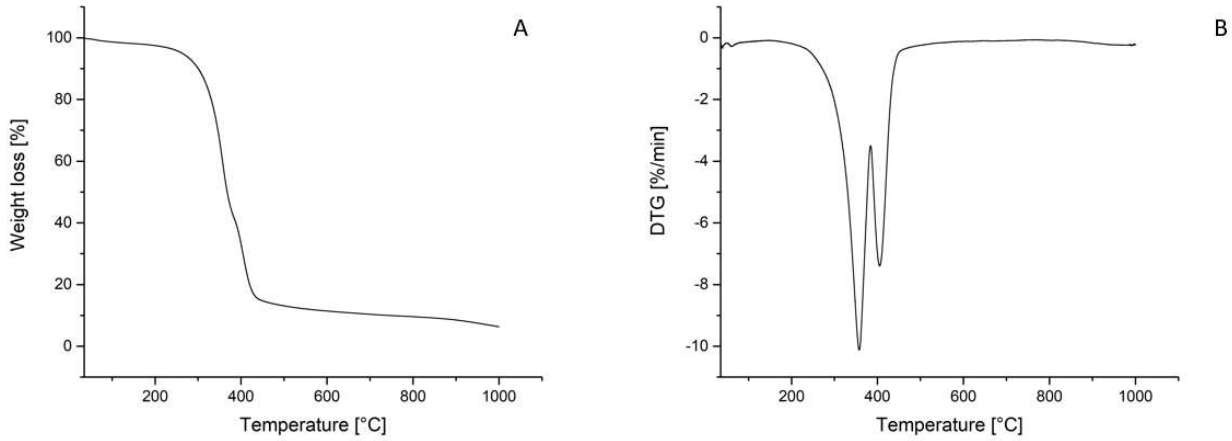

Figure 30 TGA analysis for EM-23: (A) weight loss (B) DTG.

EM-23 is the product from precursor EM-02, therefore it contains 0.1 g of PEG. The presence of PEG is more evident in the DTG (Differential Thermo Gravimetry) at 400 °C whereas it presents a minimum in the derivative. EM-23 has a trend very similar to EM-18 however, it displays several shoulders in the region 200 – 400 °C; this region corresponds to the 5 wt% of weight losses, which indicates the presence of different moieties in the structure but still shows the presence of the aromatic compounds after 400 °C.

EM-26 is obtained from the precursor EM-03, it contains 1 g of PEG, hence ten times more than the previous product. In fig(31) is reported its spectrum.

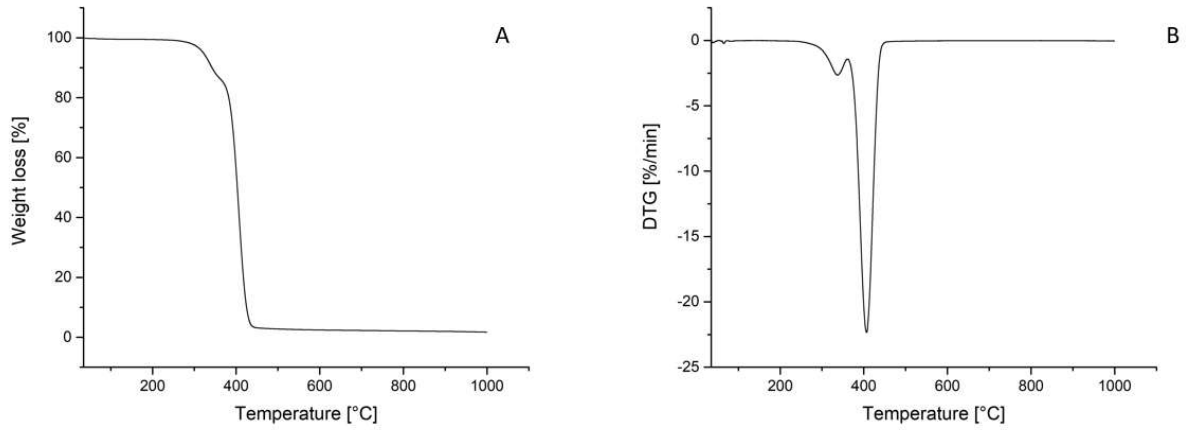

Figure 31 TGA analysis for EM-26: (A) weight loss (B) DTG.

In fig(31), at 335 °C, it can be seen the start of the degradation of the perimetric groups as it shows the DTG with the first minimum. At 400 °C, with the degradation of PEG, all the other structures degrade: first, the simple bonded moieties and then the aromatics compounds that constitute the graphitic core of the Carbon Dot. In the same way that PEG promotes the aromatization process, aromatics compounds degrade with PEG at 400 °C.

3.2.3 X-ray Photoelectron spectroscopy

The characterization of the Carbon dots produced continues with the X-ray photoelectron spectroscopy analysis to determine the elements present on the surface of the dot: carbon, nitrogen, and oxygen.[53] The spectra were elaborated with OriginPro to process the information coming from the XPS analysis: the area under each curve was studied, and the ratio with the total value of the areas was used to calculate the percentage of the compounds present.

Let's start analysing the structures of EM-18 in fig(32).

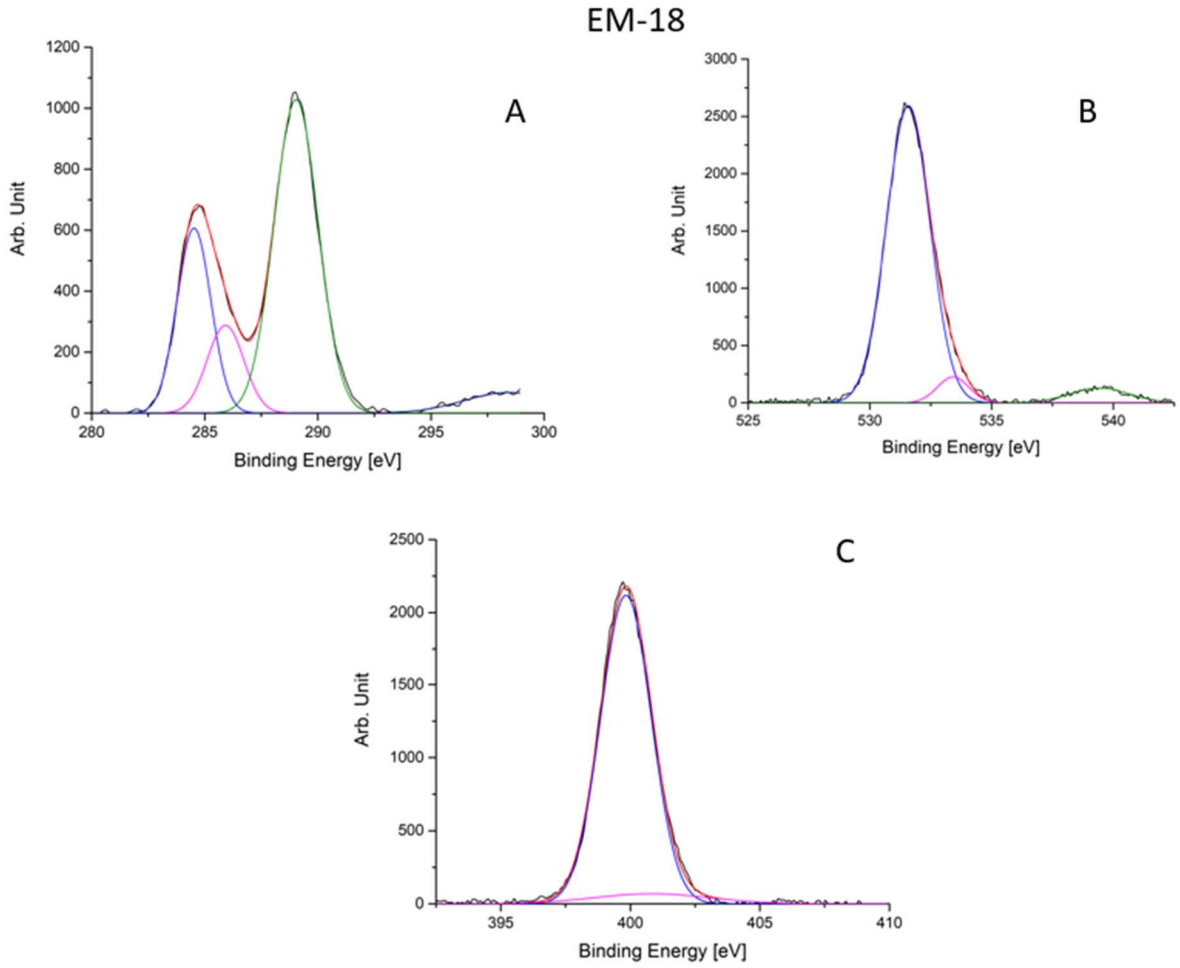

Figure 32 XPS results for EM-18: (A) Carbon, (B) Oxygen, (C) Nitrogen.

In fig(32) (A) the curves indicate how the carbon on the surface is bonded and which groups we can find and in what measure. The carbon hybridized sp^2 is present for 27% of the total, as shown by the blue component peaked at 284.5 eV. The peak at 285 eV is assigned to C-X (X=O,N) moieties, they are just 14%. At this stage, the differentiation between C-O or C-N cannot be explicited since these components peak at similar values. The green component which peaks at 290 eV is assigned to carboxylic groups.[53] It would be expected from the carboxylic compounds to be on the perimeter[54], they represent 59% of the total carbon. This analysis finds correspondence with the IR examined in a previous section: we did find the peak of the carboxylic in the region 3400 – 3500 cm^{-1}, the peak assigned to C-X at 1300 – 1450 cm^{-1}, and the unsaturated bond of carbon at 3200 cm^{-1}.

In fig(32) (B) there is the spectrum related to the oxygen's bonds and groups. In blue there is the component that peaks at 531 eV which is assigned to carboxylic groups. The carboxylic groups are 89% of the total compounds present, which confirms the previous assumptions made for these moieties. The oxygen double and single bonded with carbon are, respectively, in pink and green: they both are 6% of the total oxygen-containing compounds.

Less information comes from the nitrogen-related graph in fig(32)(C) where we can only see the massive presence of the graphitic nitrogen insert in aromatic moieties, 93%, which are the compounds seen in section 3.1.1 fig(11). Only 7% of nitrogen is present as pyrrolic.

In fig(33) the spectra of the XPS analysis for EM-36 are reported.

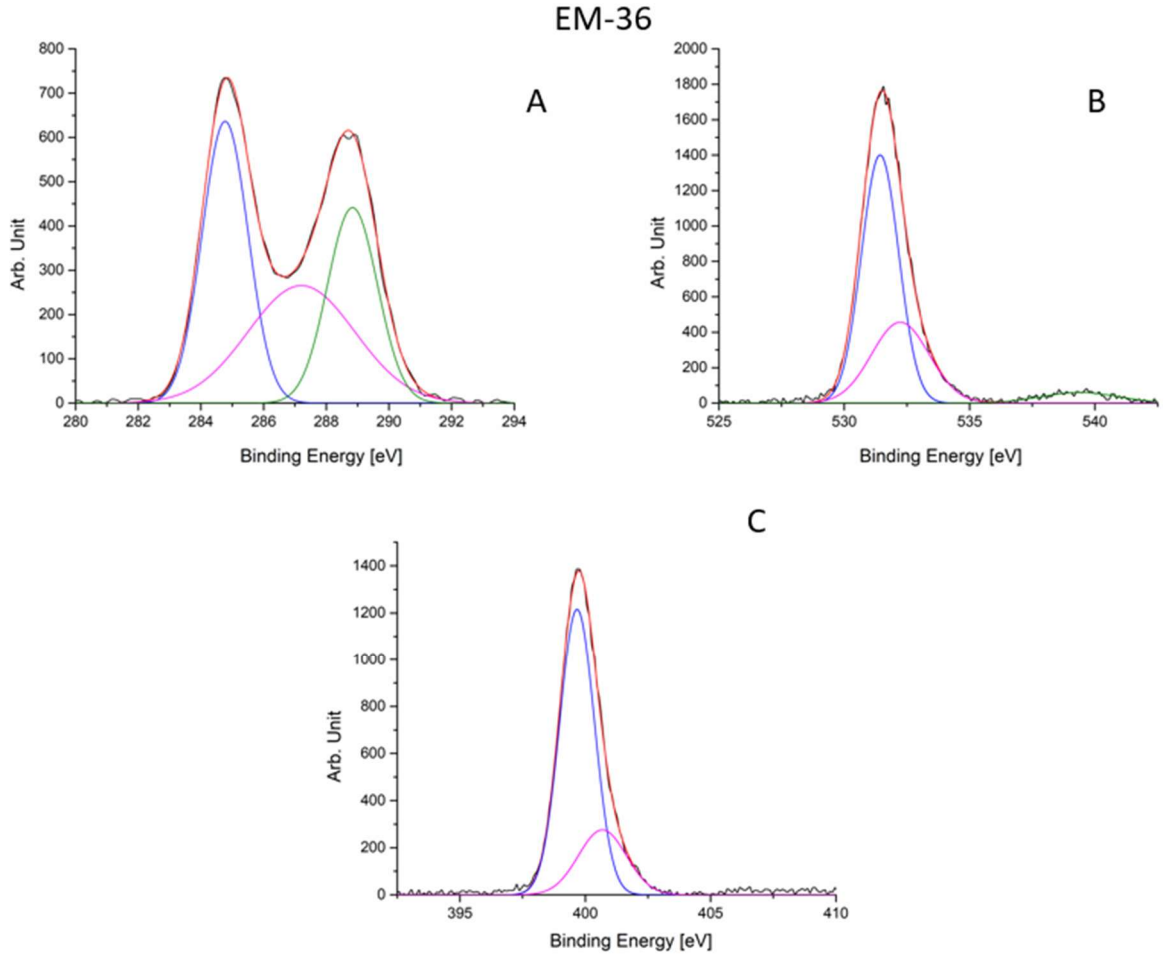

Figure 33 XPS results for EM-36 (A) Carbon, (B) Oxygen, (C) Nitrogen.

In fig(33) (A) there is the spectrum related to the carbon structures present on the carbon dot's surface. The component in blue indicates the presence of carbons hybridized sp3, which peaks at 284.8 eV and represents 37% of the total compounds. The carbonyl groups are 28 % and the component color is pink, while the carboxylic groups are 35% and the curve is green. Furthermore, it is possible to compare the carbon graphs for EM-18 and EM-36. Previously we have seen a massive presence of carboxylic groups and hybridized sp2 carbons in EM-18, while now, in EM-36, their presence is balanced with the single-bonded carbon, indicating how the aromatization process did not progress completely at lower temperatures.

In fig(33) (B) we find a situation very similar to fig(32) (B), in blue, there are the carboxylic groups and their presence was evaluated for 63% of the total oxygen-containing compounds. The oxygen single-bonded to carbon is now more present on the surface than the unsaturated

bonds: in pink C-O is 32% while carbonyl groups are only 6%. In fig(33)(C) reported the graph inherent to nitrogen where now the graphitic compounds are less: 76%. The presence of the pyrrolic compounds is now evaluated to be 24%. Fig(33) provides information that supports both the interpretation of the IR spectra and the conclusion that at 450 °C the graphitic core and aromatization process did not occur properly.

Fig(34) shows the surface components of EM-23.

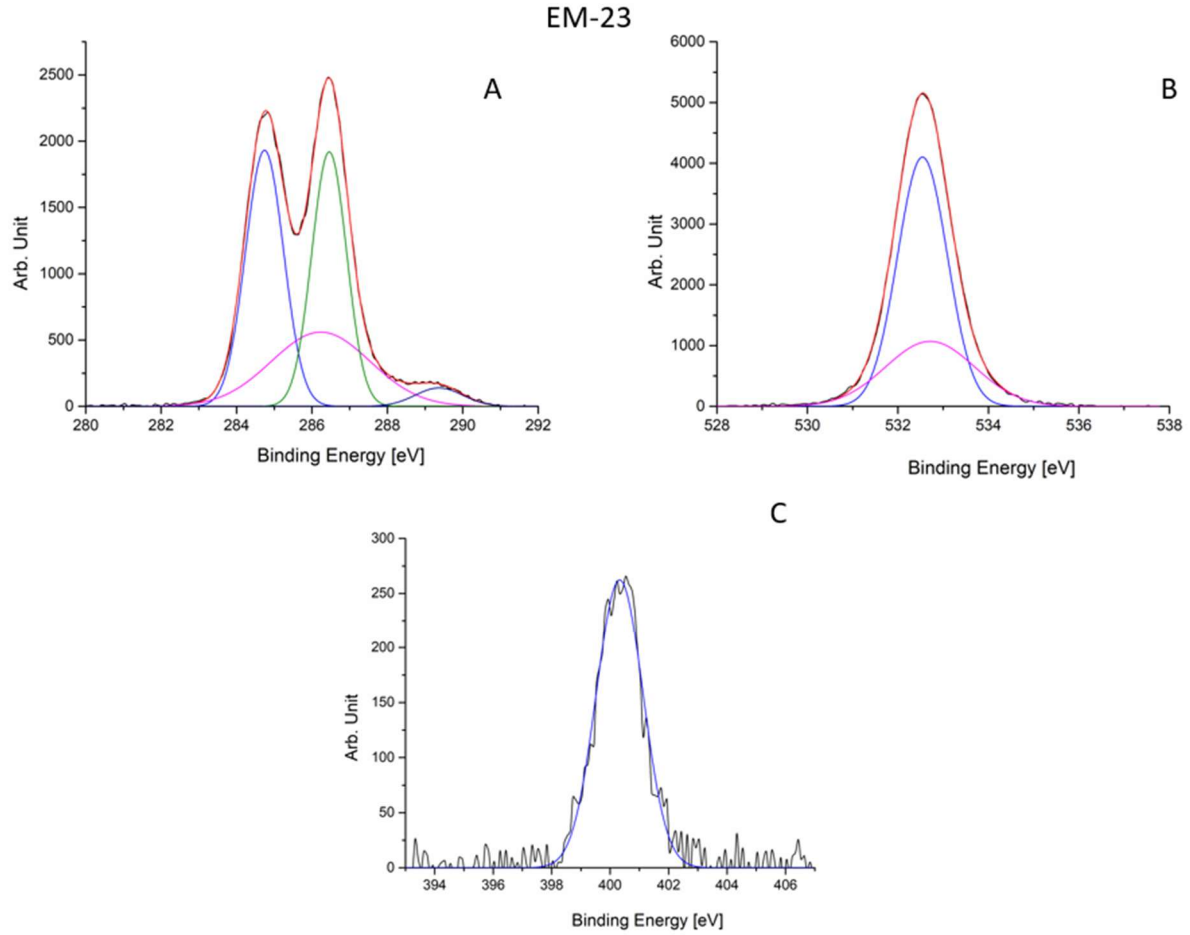

Figure 34 XPS results for EM-23, (A) Carbon, (B) Oxygen, (C) Nitrogen.

In fig(34)(A) are displayed the carbon moieties. The component in blue that peaks at 284 - 284.5 eV is assigned to carbon hybridized sp^2, this component represents 36% of the total carbon moieties. The curve in pink is C-X (X=O,N) with the peak around 286 eV, this type of compounds are 27%. The green spectrum, instead, which peaks at 287 eV, represents the carbonyl groups in a percentage of 33%. The remaining compounds are carboxylic, whose, unlike in the previous spectra (EM-18, EM-36), percentage is lower (4%). This different behaviour can be explained by the presence of PEG. Fig(34)(B) shows the oxygen moieties presence: one peak, in color blue, can be observed at 532 eV, that is assigned to carboxylic compounds; the other peak, at 535 eV and in color pink, indicates moieties containing C-O groups. In fig(34)(C) the spectrum is for one component only, that peaks after 400 eV and is assigned to pyrrolic nitrogen. The dynamic that was previously hypothesized has further confirmation: the presence of PEG promotes the aromatization process and a different rearrangement of the components. To better understand the role of PEG it is necessary to

analyse the spectra of the product EM-26 in fig(35). Please note that EM-26 contains ten times more PEG than EM-23.

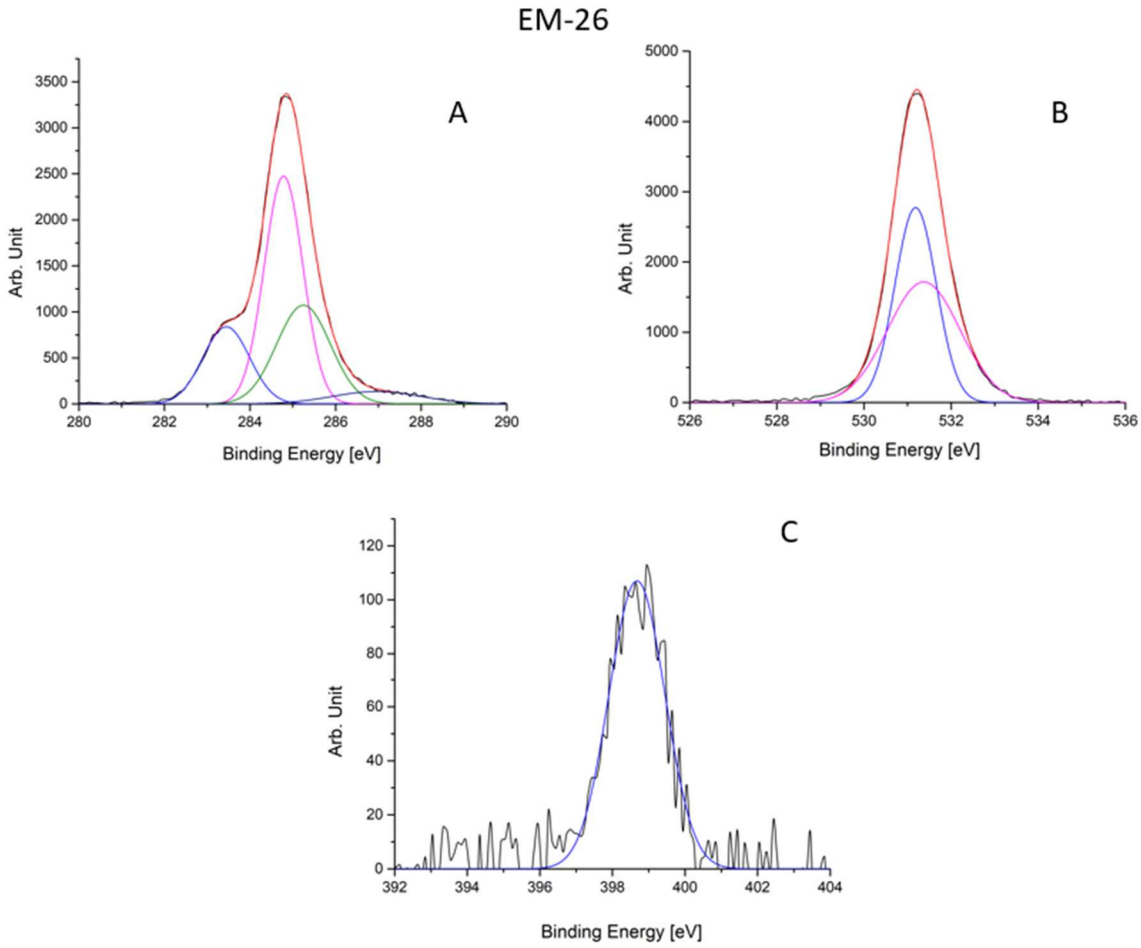

Figure 35 XPS results for EM-26, (A) Carbon, (B) Oxygen, (C) Nitrogen.

In fig(35)(A) is reported the spectra for the carbon moieties: the component in blue peaks at 283.5 eV and is assigned to carbon hybridized sp^2 which is present for 19% of the total carbon compounds. At 285 eV there is the peak assigned to the carbon hybridized sp^3, this component is the more abundant: 47% of the total carbons. These moieties derive from the PEG structure. The green component is assigned to C-N compounds while the last peak is C=O.

Since the presence of PEG in this product is substantial , the dynamics have changed, as it can be observed: the aromatization proceeds and the carboxylic groups' percentage decrease, indicating, that is possible that the PEG takes the place of the hydroxyl's functions which are bonded to the aromatic structures. In fig(35)(B) are reported the oxygen-containing components. The component in blue that peaked at around 531 eV is assigned to the carboxylic groups that are present for 48% of the total. The component in pink is assigned to C-O compounds that are present for the rest of the total, these moieties come directly from the

structure of PEG. The nitrogen-compounds in fig(35)(C) show only one peak before 400 eV which indicates the presence of pyrollic components.

3.2.4 Raman

The results from RAMAN spectroscopy were collected, in order to study the materials' order obtaining information on the structure of the material analysed.[55]

The spectrum of the product EM-22, synthesized at 550 °C for seven minutes, is reported in fig(36) as an example of the spectra collected.

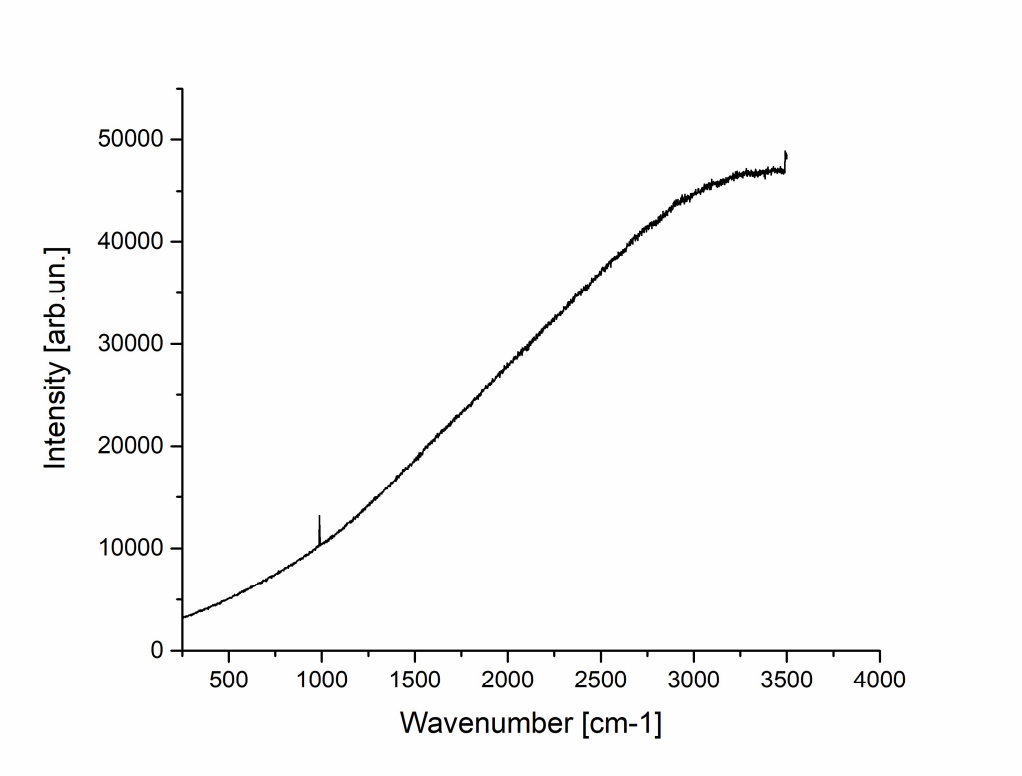

Figure 36 RAMAN spectrum for EM-22.

Due to the high fluorescence of the CDs, the spectrum appears to be dominated by fluorescence and consequently, no peaks are detected. This behaviour can be accounted for by the high functionalization of the CDs that results in extreme fluorescence. The functionalization of EM-22 is exposed in the IR spectrum in fig(22).

3.3 Loading process

The loading process yield is evaluated with a Thermogravimetric Analysis (TGA). Knowing the evaporation temperature for the DAAD compounds is possible to calculate the weight loss percentage relative to the loaded compounds. Subsequently, the yield for every load is calculated and then reported in the tab(7).

Table 7 Loading process yield per type of compound loaded and relative error.

LOAD	YIELD [%]
Thiophene	0,16 ± 0,01
DAAD type X	0,18 ± 0,04
DAAD type A	0,12 ± 0,07
DAAD type B	0,16 ± 0,01

The yield, as reported in tab(7), is always below 0.2%, which means that around one DAAD molecule is adsorbed on one Carbon Dot structure, considering the hypothesized molecular weight. The software's computational limit of one thousand atoms hinders the possibility of simulating a bigger Carbon Dot structure. Therefore, the Carbon Dot simulated will have a molecular weight of 8822 g/mol with at least one molecule of adsorbed DAAD on the surface.

3.4 Approach to biological applications

This synthesis and the following characterization aim to create a library of compounds for biological applications. When it comes to the field of materials' engineering for biological applications two main approaches can be undertaken: The first consist in starting from the study of the target and design a product for said target only. The second approach consists of creating a library from which the best fit can be chosen for the relevant situation. The variables in the creation of a material with diagnostic and therapeutic purposes are multiple, if not countless: an equilibrium between the best possible characteristics of the material has to be found. The perfect material has a good balance in its polarity to reach the cell in its habitat, a high yield in its production, a high yield in the loading process, and it has to penetrate the cellular barrier easily among other things. To satisfy all these criteria, a countless compounds library becomes crucial. This work and characterization intend to produce different products in order to direct future syntheses.

4. Simulations

4.1 Unloaded Carbon Dots

The full characterization of the product, reported in the third section of this work, provides the information needed to understand the material structure in its entirety. Based on these data is possible to simulate the Carbon Dots structure and the mechanisms involved in the loading process. The HyperChem software is employed to simulate the energetic minimum while the structure is laid out with ChemSketch.

To start, fig(37) reports the simulation of the Carbon Dot base structure.

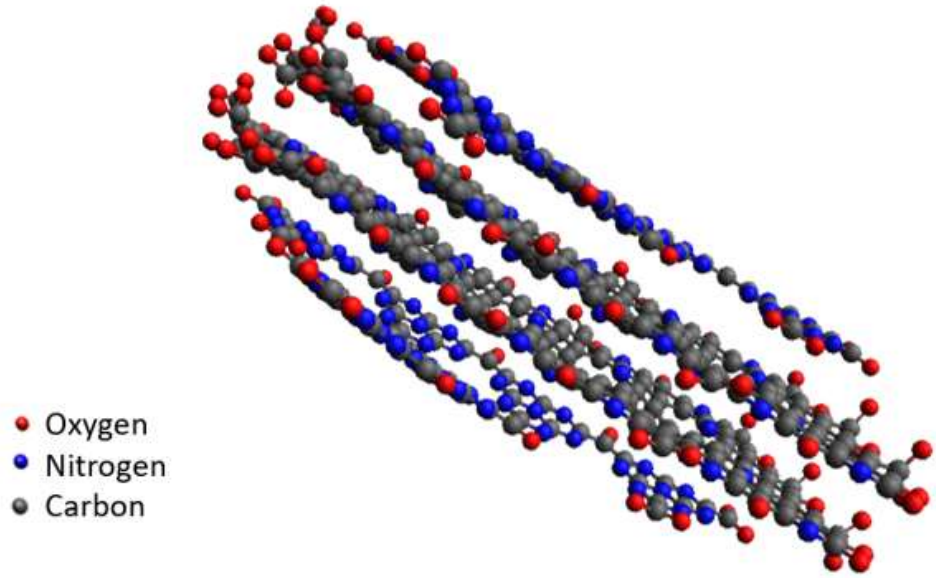

Figure 37 Carbon Dot structure's simulation.

As it can be seen, in fig(37) the core is graphitic and the perimeter presents a high functionalization. Layers one and four are constituted by triazines and hydroxyl groups. The distance between two different layers, for instance, layers three and four, is around 3.5 Å. The covalent bond distance in the entire structure ranges from 1.29 to 1.47 Å. In graphite crystals the interatomic bond is around 1.42 Å, depending on the kind of graphite[56]. Furthermore, the interlayer distance ranges from 3.3 Å to 3.7 Å. The energetic value of this structure is 904.3 kcal/mol, this data, in particular, will be fundamental during the study for the loaded structure.

Fig(38), on the other hand, displays the containing-PEG structure.

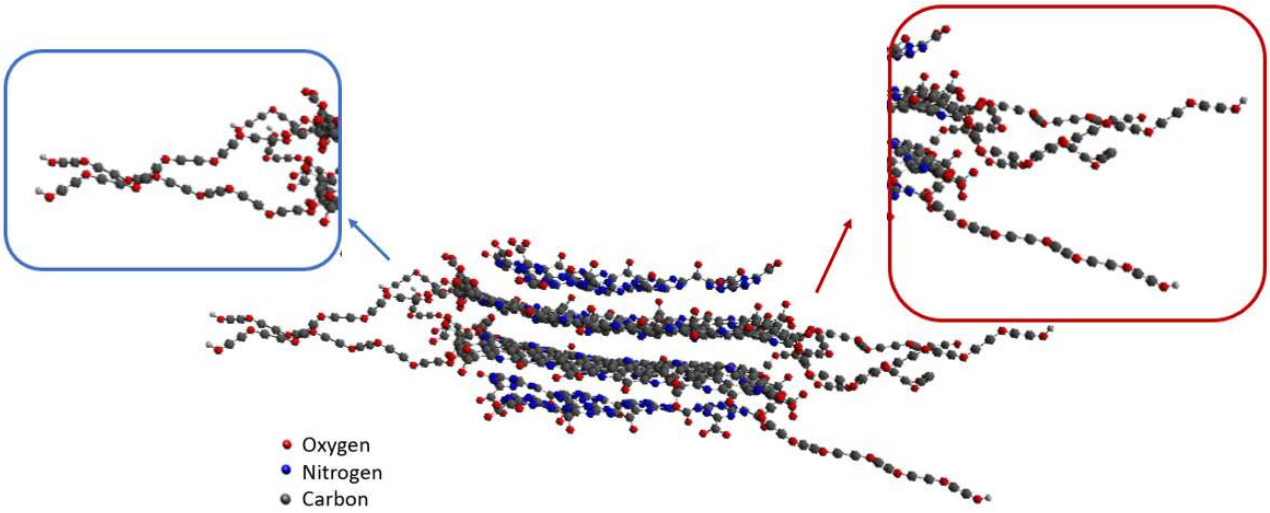

Figure 38 Carbon Dot containing PEG structure's simulation.

Fig(38) illustrates the Carbon Dot optimized structure with the addition of PEG chains. In this case, the energetic value is 862.2 kcal/mol. During the optimization, close PEG chains start twisting, while the detached ones do not. This tendency can be observed in the zoomed part of the figure, framed in red. In the blue box on the left, on the other hand, it can be observed another behavior: PEG chain can arrange itself bordering the carboxylic groups of the graphitic layers.

4.2 Thiophene loaded Carbon Dots

Thiophene is chosen as a model compound for the loading process. Its structural features resemble the Diallyl Disulphur ones. This heterocyclic compound is picked among various unsaturated compounds due to the steric hindrance comparable to the DAAD one. Compounds like sulfones and thiols are not suitable for the scope of the model simulation.

Fig(39) displays the optimal energetic configurations of a thiophene molecule.

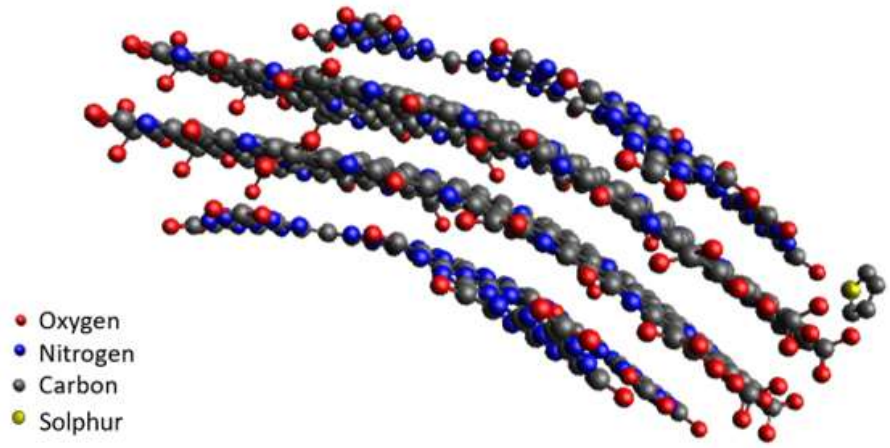

Figure 39 Simulation of a Carbon Dot loaded with one molecule of thiophene.

The tendency of the molecule is to bond with the structure with π-bonds. Thiophene aligns itself with the functional groups on the perimeter. While, the sulphur atom, which has more steric hindrance than the remaining atoms, is located in the opposite direction of the Carbon Dots structure. The carbon atoms' position, orthogonal to the layers, shows the π-bond tendency described above.

The thiophene-loaded structure in fig(39) has an energetic value of 990.5 kcal/mol. Knowing the base structure and thiophene energies is possible to estimate the bond strength: 70.8 kcal/mol. The π-bond between two atoms is usually from 30 to 65 kcal/mol, while, for example, the hydrogen bond is much higher (more than 100 kcal/mol).[57] Accordingly, thiophene Carbon Dots interactions could be ascribed to weak interactions.

The bond length between the closest layer and the molecule is calculated to be 3.5 Å, coherently with the values expected.

A different possible configuration is shown in fig(40).

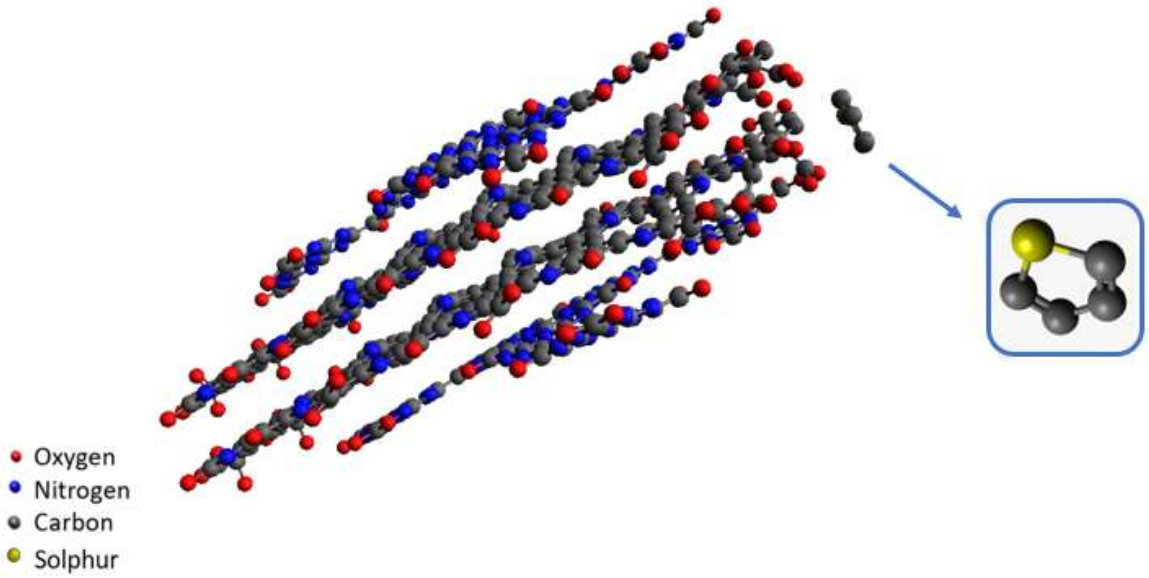

Figure 40 Second possible configuration of a Carbon Dot loaded with one molecule of thiophene.

Fig(40) presents a different spatial arrangement of the hydroxyl functional groups. The perimetric groups align the -OH in order to expose the carbon atoms to the carbons of the thiophene molecule. This behaviour confirms the tendency observed in fig(39). In this case, the bond length is 4.9 Å while the energy has a different nature. The final energetic value is -5.9 kcal/mol which means that the structure is more stable, this indicates that the thiophene molecule induces stability in the structure.

An additional simulation is reported in fig(41).

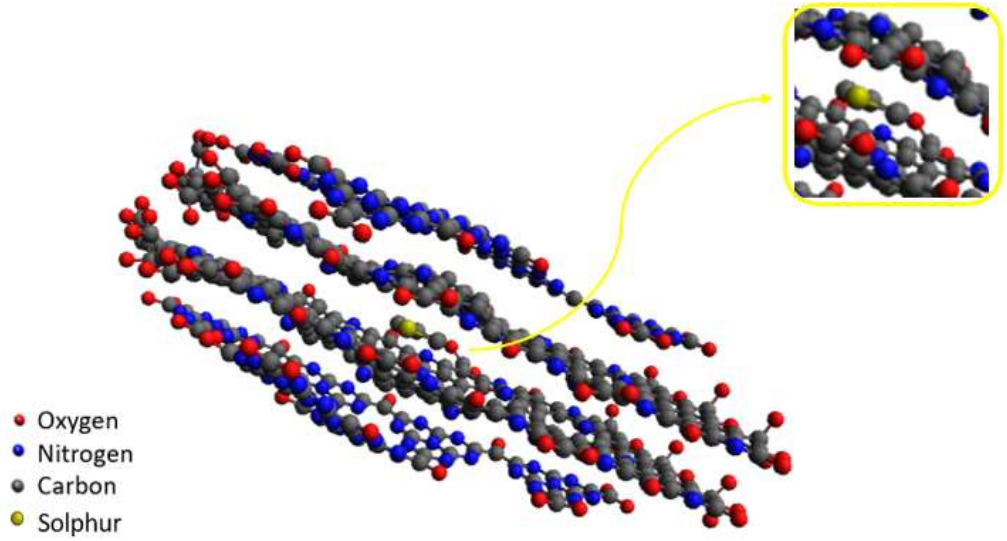

Figure 41 Third possible configuration of a Carbon Dot loaded with one molecule of thiophene.

The situation in fig(41) is improbable. This configuration is hard to achieve due to the steric hindrance and the high energy required to reach the inner core of the Carbon Dot. The corresponding energy is 968.3 kcal/mol which allows the strength bond calculation: 48.6 kcal/mol. Therefore, the bond is weak even in this final configuration. By inserting a thiophene molecule between the Carbon Dot's layers they start deforming. Consequently, the high energy required for this configuration represents a disadvantage for the absorption in that site.

Fig(42) and fig(43) display the structure of a Carbon Dot containing four PEG chains loaded with one molecule of thiophene.

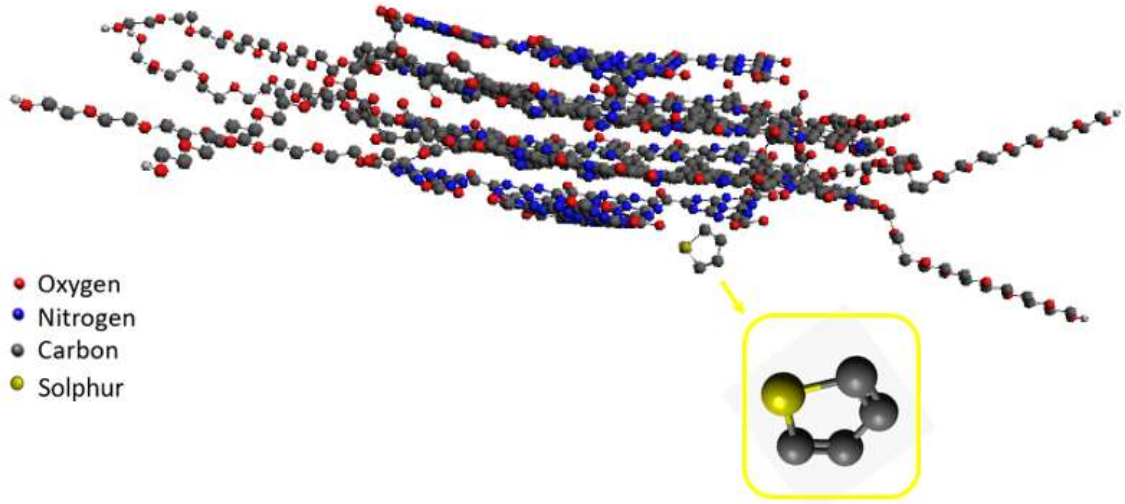

Figure 42 First possible configuration for PEG-containing Carbon Dots loaded with one molecule of thiophene.

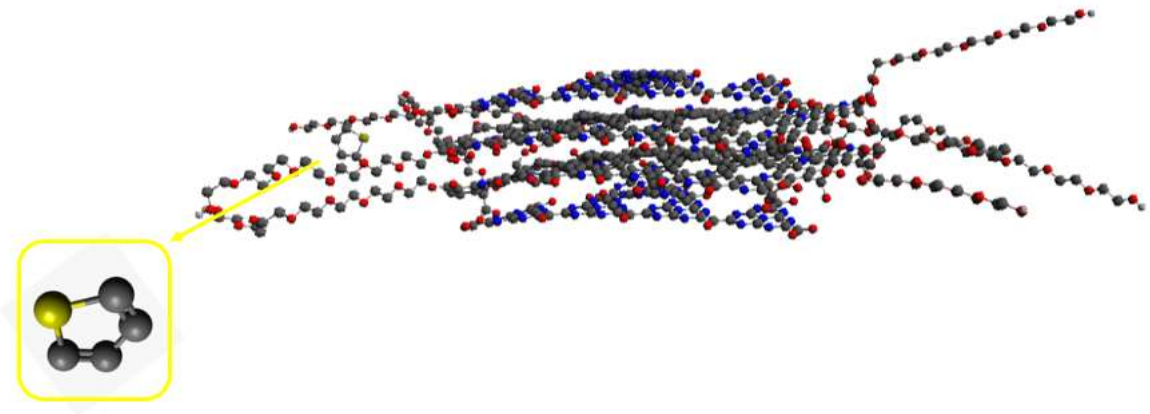

Figure 43 Second possible configuration for PEG-containing Carbon Dots loaded with one molecule of thiophene.

The structure displayed in fig(42) shows how thiophene have a tendency to form π-bonds with the Carbon Dot structure, deforming the triazines layers. Meanwhile, fig(43) presents another possibility: thiophene interacts with the structure, however, prefers to interact with PEG chains. Nonetheless, thiophene still interacts with the outer border of the carbon dots' structure.

4.3 DAADs loaded Carbon Dots

Accordingly, to the model compound simulations, the following section will present the simulations with DAAD molecules.

4.3.1 DAAD A

The unsaturated compound with the external double bonds (DAAD A) has the tendency, as the model compound, of forming π-bonds with the structure, as reported in fig(42).

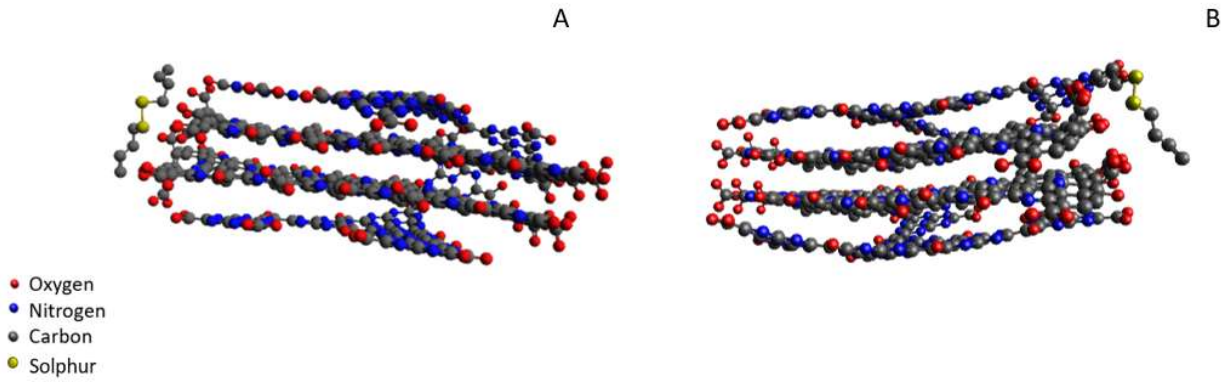

Figure 44 DAAD A loading process simulations starting from different positions of the molecule.

As reported before in fig(39)(40), the tendency of the unsaturated compounds interacting through π-bonds become more appreciable in fig(44). These allow the spatial arrangement of DAAD molecule parallel to C=O bond of border carboxylic groups. The energies of configurations A and B are almost the same: around 928 kcal/mol and the consequent interacting strength is 23 kcal/mol.

The geometry deformation regards the DAAD molecule itself. The interaction with the Carbon Dot structure induces an alteration of the bond length between the sulphur atoms of the compound. The sulphurs' bond strength is weaker than the carbon-carbon one, for this reason, this bond will be the one to be more deformed during the adsorption process, changing from 2.03 Å to 2.04 Å.

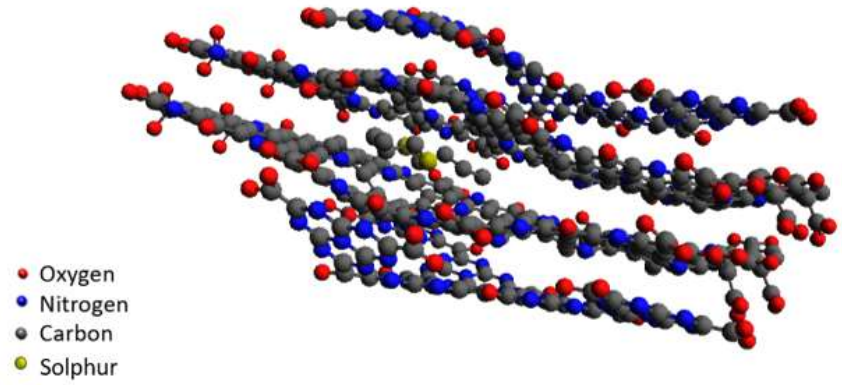

Figure 45 Third possible configuration of a Carbon Dot loaded with one molecule of DAAD A.

The DAAD molecule in fig(45) deforms geometrically the Carbon Dot structure. It generates a pocket-like deformation by curving every layer around the compound. Furthermore, the bond strength of the configuration displayed above is 90 kcal/mol.

4.3.2 DAAD B

Fig(46) reports two configurations very similar to fig(44). The DAAD B compound does not have the external double bond but still behaves as the previous DAAD A.

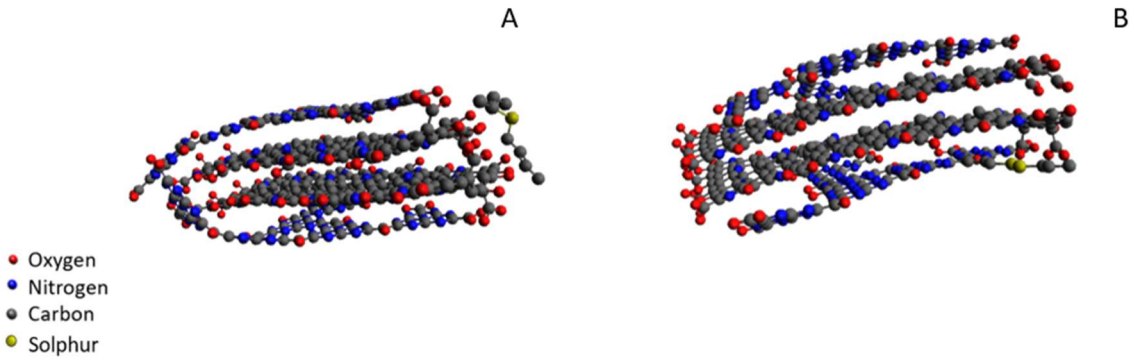

Figure 46 DAAD B loading process simulations starting from different positions of the molecule.

The bond strength is below 20 kcal/mol. The different disposition of the molecule is due to the position of the unsaturated bond: it enables the possibility of a totally different spatial arrangement of the molecule bordering the carboxylic groups. The sulphur atoms bond length change from 2.04 Å in configuration (A) To 2.16 Å in configuration (B).

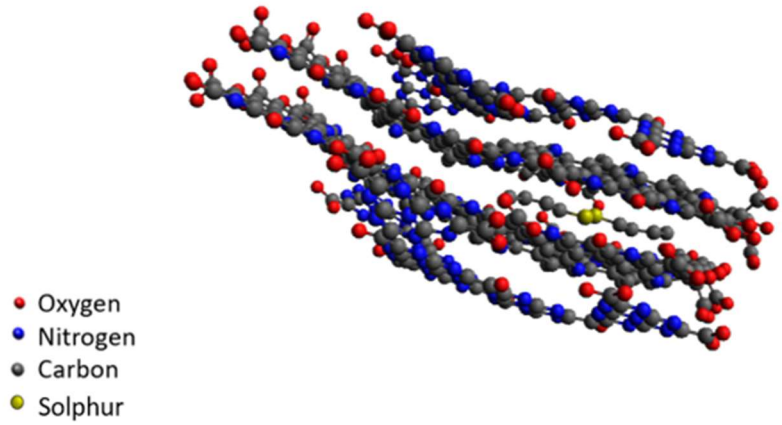

Figure 47 Third possible configuration of a Carbon Dot loaded with one molecule of DAAD B.

The pocket-like structure displayed in fig(45) resembles the one presented above in fig(47). The Dyallil compound has a bond strength -73 kcal/mol, this energy indicates the stability of this structure compared to the one in fig(45). Although, due to the steric hindrance, this disposition is still improbable. The internal carbon-carbon double bond freezes the structure reducing the mobility of alkyl chains. This enables the minimization of the interplanar deformation, this was the reason for the low interaction energy observed for the config in fig(47).

4.3.3 DAAD X

The natural Dyallil compound X is shorter than the A and B type. It has only six carbon atoms in its structure and the unsaturated bond is external. To observe the different behaviours that these variables promote, fig(48) is reported.

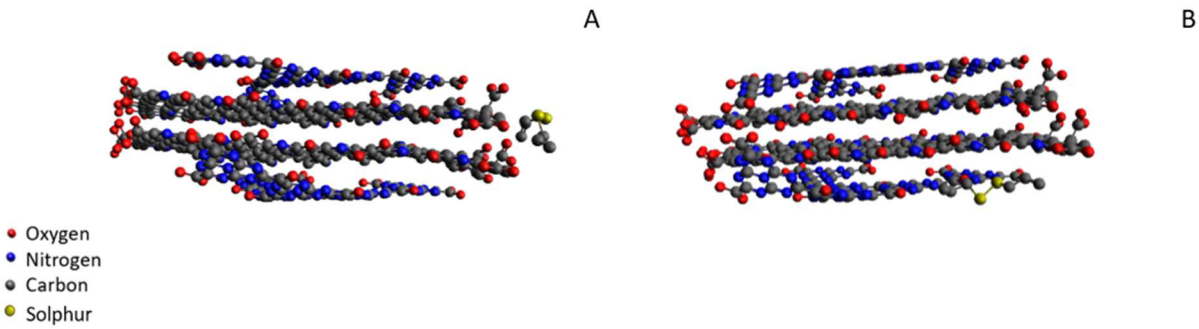

Figure 48 DAAD X loading process simulations starting from different positions of the molecule.

In fig(48)(A) the DAAD molecule borders the carboxylic groups, aiming to create π-bonds with the structure. The molecule geometrical deformation is more evident here: the distance between the sulphur atoms is 2.03 Å. In fig(48)(B) the diallyl compound interacting with the triazine layers does not massively modify the geometrical conformation of the inner layers. This was due to its low steric hindrance compared with DAAD A and B that allows interaction with Carbon Dots without appreciable deformation. The bond strength is, respectively, 37 kcal/mol and 31 kcal/mol.

Simulating an initial arrangement of DAAD X inside the internal layer, can be observed the configuration reported in fig(49).

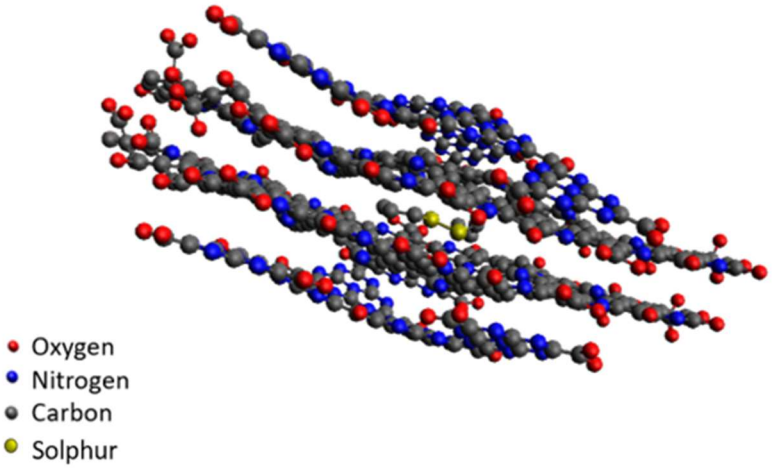

Figure 49 Third possible configuration of a Carbon Dot loaded with one molecule of DAAD X.

As already displayed for the other unsaturated compounds, in fig(45) and fig(47), the deformation induced by the molecule adsorbed, creates a pocket also in this case. The energy bond is in this case over 100 kcal/mol. The higher energy indicates the inferior stability of the compound due to the smaller dimensions of the molecule. The smaller dimension of the Diallyl compound hinders the possibility of a geometrical deformation adjustment.

4.3.4 DAADs loaded on PEG-containing Carbon Dots

The PEG-containing Carbon Dot simulations are reported in fig(50) and fig(51).

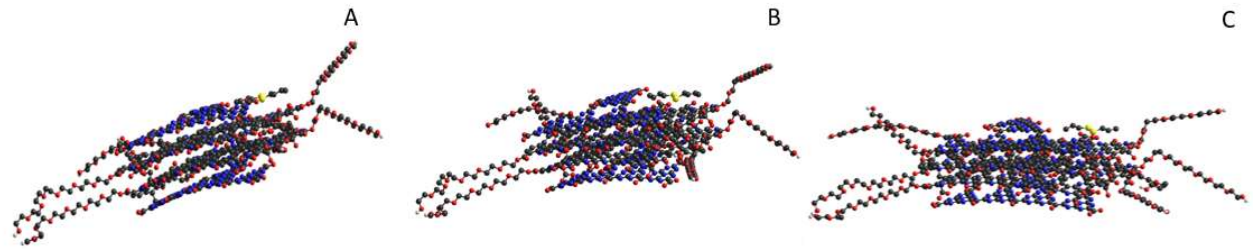

Figure 50 First possible configuration of PEG-containing Carbon Dot loaded with (A) DAAD A (B) DAAD B (C) DAAD X.

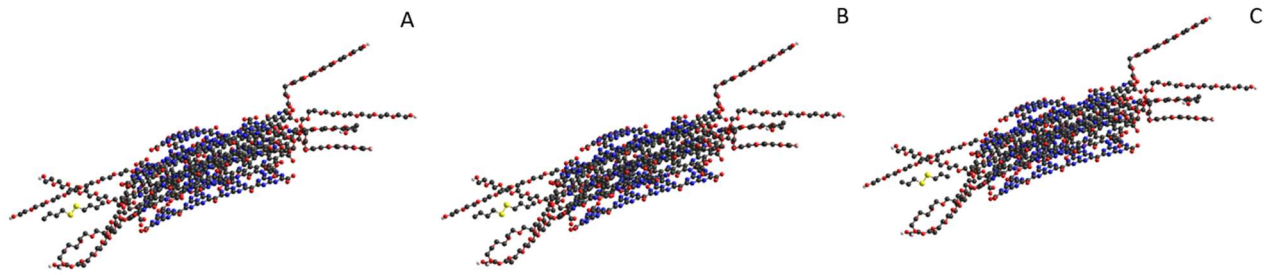

Figure 51 Second possible configuration of PEG-containing Carbon Dot loaded with (A) DAAD A (B) DAAD B (C) DAAD X.

The simulations report a behaviour very similar to the model compound thiophene. Fig(50) displays how every Diallyl molecule have a tendency to deform the triazine layer forming π-bonds with the structure. The configurations do not report evident differences between the behaviour of the various compounds.

Fig(51) exhibit a different possible configuration. The polarity of the PEG chains and the apolarity of the structure induce the Dyallil molecule to orientate as reported in figure. The compound loaded will preferentially interact with PEG chains. Nonetheless, DAAD interfaces

with the Carbon Dot core structure. The configurations (A), (B), and (C) are very similar for every DAAD type.

5. Conclusions

This work aimed to synthesize a specific class of Carbon Dot with thermal syntheses run under different conditions. A consequently full characterization of the products provides the information to properly choose the Carbon Dot suitable for the DAADs loading process. Afterward, a structural study performed through HyperChem software provides an insight into their chemical configurations and arrangements.

The experimental procedure starts with the preparation of the precursors for the thermal syntheses. All the precursors are prepared with Citric Acid and Urea in a ratio of 1:10, while the amount of Polyethylene Glycol (PEG) is varied to investigate precisely its role in assisting the synthesis and in enhancing its photoluminescence. Besides, the precursors are stirred with mechanical agitation or with ultrasonication. The synthesis parameters are the temperature, which is varied in a range from 250°C to 550 °C, and the reaction time, which spans from 5 minutes to 15 minutes. Furthermore, the purification process is conducted in water with ultrasonication. The Carbon Dots thus produced and purified are, then, characterized. The characterization provides for analyses with Infrared Spectroscopy, Thermogravimetric analysis, X-ray photoelectron spectroscopy, and Raman spectroscopy. The IR spectroscopy investigates the evolution of the compounds occurring during the synthesis and drives the choice of the most promising Carbon Dots for the loading process. The precursors' IR spectra show the stirring process's role in enhancing the reaction start. Meanwhile, the purified products IR spectra demonstrate how the subsequent syntheses promote the triazine moieties formation and the aromatization processes. The formation of aromatics compounds is more extensive in PEG-containing Carbon Dots where PEG promotes aromatization while hinders the formation of perimetric groups. Based on the IR data the Carbon Dots chosen are the ones produced at 550 °C for seven and ten minutes with different concentrations of PEG. Nevertheless, a compound synthesized at 450 °C is chosen between the ones devoided of PEG. Then, a further comprehensive characterization follows on the small set of Carbon Dots chosen for the loading process. The thermogravimetry analysis investigates the compounds' thermal stability to deduce information about the structure of the Dot while the X-ray photoelectron spectroscopy analysis determines the elemental composition on the product surface. The results of the sequent characterization confirms the disappearance of the amines with the formation of triazines and carboxyl perimetric groups. The Raman spectroscopy provides data on the material structure and bulk order. The loading process is performed on the limited series of fully characterized carbon dots acting as shuttle platforms for the Dyallil Disulfide. The loading process involves four different loads: thiophene, DAAD type X, A, and B where the compounds vary the carbon chain length and the double bond position. This work aims to combine these resourceful disulphides with Carbon Dots to integrate the diagnostic capability of fluorescent carbon dots with the therapeutic activity of these specific allicin by-products. The solutions for the adsorption process are made in petroleum ether and then undergo a mechanical agitation overnight. Afterward, they are filtered under vacuum by using a Buckner and a paper filter. The material obtained subsequently the absorption and filtration is analysed through TGA in a range from 35 °C to 120 °C, this analysis allows to calculate the adsorption yield. The yield is always approximately 0.2%, which means that around one DAAD molecule is adsorbed on one Carbon Dot structure, considering a hypothesized molecular weight based on previous researches.[58]

The full characterization of the product provides the information needed to understand the material structure in its entirety and based on these data, is possible to simulate the Carbon Dots

structure and the mechanisms involved in the loading process. The HyperChem software is employed to simulate the energetic minimum while the structure is laid out with ChemSketch. The simulation shows the tendency, recurrent in all the unsaturated compounds, to border the Carbon Dot structure to form π-bonds with the perimetric groups, carboxylic for instance. The PEG-containing Carbon Dots present alternatively propensity where the polarity of PEG chains and apolarity of the structure orient the molecule adsorbed.

This work and characterization intend to produce different products in order to direct future syntheses where the central role of Carbon Dots in diagnostic applications can be paired efficiently with therapeutic compounds as, for instance, allicin by-products, as investigated in this thesis.

Acknowledgements

I wish to acknowledge prof. Alberto Tagliaferro for hosting me in his research group. Thanks for the kindness and continuous support in this hard period.

I would also like to thank Dr. Mattia Bartoli for having supported and above all endured me during these months of work. Thank you for gifting me with the passion for your work.

My heartfelt gratitude goes to my family.

To my Mom, Patrizia Venesia, and my Dad, Leonardo Marras, for always believe in me and encourage me during this growth path. This one goes to you more than to anyone else. You hold on this even when I was not.

To my sister Teto, Stefania Marras, which have, for no reason, the highest consideration of me. Thank you for never doubting me, for being my shoulder, arm, leg and the best friend I could ask for. And to quote something we both know: this one goes to my reason to get up in the morning.

I hope I made you proud today even half as much as you make me proud every day.

And to all the Marras. I love you.

I would also like to thank all the people who have supported me and stand by me during this journey.

Alessandra Cerato, for all the phone calls at 8 in the morning before an exam, for the days spent together studying, but especially for all the trust and support all the way since 1999. It meant the world to me.

Roger Pagliarin, I thank you for all the support and the affection you show me everyday. You always make me laugh no matter what. You helped me more than you think.

Enrico Degani, my old-time friend, I cherish the laughs, the beers and the sage. You were not the wisest back in the day but you sure are now.

Linda Zaccaria, I thank you for your precious friendship during these decades, for the encouragement and for being the first one to call me Ing. Writing this thesis remembered me why you are the English-one and I am the math-one.

Antonio Bucci, for being a great friend and the best and funniest classmate. Without you, I would be still studying for Calcolo Numerico.

Luca massolo and Livio Marenco for being the best companions and to not mention all the productive afternoons.

And I want to thank Federica Marongiu, you are the proof that distance doesn’t matter in friendship.

And I wish to acknowledge all the people that supported me during these challenging years.

References

[1] S. Sagbas, N. Sahiner, Carbon dots: preparation, properties, and application, in: Nanocarbon and its Composites, Elsevier, 2019, pp. 651-676.
[2] H. Luo, Q. Guo, P.Á. Szilágyi, A.B. Jorge, M.-M. Titirici, Carbon dots in solar-to-hydrogen conversion, Trends in Chemistry, (2020).
[3] A.L. Himaja, P.S. Karthik, B. Sreedhar, S.P. Singh, Synthesis of carbon dots from kitchen waste: conversion of waste to value added product, Journal of fluorescence, 24 (2014) 1767-1773.
[4] A. Cayuela, M.L. Soriano, C. Carrillo-Carrión, M. Valcárcel, Semiconductor and carbon-based fluorescent nanodots: the need for consistency, Chemical Communications, 52 (2016) 1311-1326.
[5] A. Kasouni, T. Chatzimitakos, C. Stalikas, Bioimaging applications of carbon nanodots: a review, C—Journal of Carbon Research, 5 (2019) 19.
[6] F. Catania, E. Marras, M. Giorcelli, P. Jagdale, L. Lavagna, A. Tagliaferro, M. Bartoli, A Review on Recent Advancements of Graphene and Graphene-Related Materials in Biological Applications, Applied Sciences, 11 (2021) 614.
[7] M.L. Liu, B.B. Chen, C.M. Li, C.Z. Huang, Carbon dots: synthesis, formation mechanism, fluorescence origin and sensing applications, Green chemistry, 21 (2019) 449-471.
[8] I. Khan, K. Saeed, I. Khan, Nanoparticles: Properties, applications and toxicities, Arabian journal of chemistry, 12 (2019) 908-931.
[9] Z. Li, L. Wang, Y. Li, Y. Feng, W. Feng, Frontiers in carbon dots: design, properties and applications, Materials Chemistry Frontiers, 3 (2019) 2571-2601.
[10] D. Pan, J. Zhang, Z. Li, Z. Zhang, L. Guo, M. Wu, Blue fluorescent carbon thin films fabricated from dodecylamine-capped carbon nanoparticles, Journal of Materials Chemistry, 21 (2011) 3565-3567.
[11] B. Yao, H. Huang, Y. Liu, Z. Kang, Carbon dots: A small conundrum, Trends in Chemistry, 1 (2019) 235-246.
[12] X.T. Zheng, A. Ananthanarayanan, K.Q. Luo, P. Chen, Glowing graphene quantum dots and carbon dots: properties, syntheses, and biological applications, small, 11 (2015) 1620-1636.
[13] C.A. Munson, J.L. Gottfried, F.C. De Lucia Jr, K.L. McNesby, A.W. Miziolek, Laser-based detection methods of explosives, in: Counterterrorist Detection Techniques of Explosives, Elsevier, 2007, pp. 279-321.
[14] K.N. Shinde, S.J. Dhoble, H.C. Swart, K. Park, Phosphate phosphors for solid-state lighting, Springer Science & Business Media, 2012.
[15] C.-L. Shen, Q. Lou, K.-K. Liu, L. Dong, C.-X. Shan, Chemiluminescent carbon dots: Synthesis, properties, and applications, Nano Today, 35 (2020) 100954.
[16] S. Tao, S. Lu, Y. Geng, S. Zhu, S.A.T. Redfern, Y. Song, T. Feng, W. Xu, B. Yang, Design of metal-free polymer carbon dots: a new class of room-temperature phosphorescent materials, Angewandte Chemie International Edition, 57 (2018) 2393-2398.
[17] A. Zhao, C. Zhao, M. Li, J. Ren, X. Qu, Ionic liquids as precursors for highly luminescent, surface-different nitrogen-doped carbon dots used for label-free detection of Cu2+/Fe3+ and cell imaging, Analytica chimica acta, 809 (2014) 128-133.
[18] S.-T. Yang, X. Wang, H. Wang, F. Lu, P.G. Luo, L. Cao, M.J. Meziani, J.-H. Liu, Y. Liu, M. Chen, Carbon dots as nontoxic and high-performance fluorescence imaging agents, The Journal of Physical Chemistry C, 113 (2009) 18110-18114.

[19] J. Du, N. Xu, J. Fan, W. Sun, X. Peng, Carbon dots for in vivo bioimaging and theranostics, Small, 15 (2019) 1805087.
[20] G. Várady, J. Cserepes, A. Németh, E. Szabó, B. Sarkadi, Cell surface membrane proteins as personalized biomarkers: where we stand and where we are headed, Biomarkers in medicine, 7 (2013) 803-819.
[21] S.-T. Yang, L. Cao, P.G. Luo, F. Lu, X. Wang, H. Wang, M.J. Meziani, Y. Liu, G. Qi, Y.-P. Sun, Carbon dots for optical imaging in vivo, Journal of the American Chemical Society, 131 (2009) 11308-11309.
[22] H. Eskalen, S. Uruş, S. Cömertpay, A.H. Kurt, Ş. Özgan, Microwave-assisted ultra-fast synthesis of carbon quantum dots from linter: Fluorescence cancer imaging and human cell growth inhibition properties, Industrial Crops and Products, 147 (2020) 112209.
[23] C. Ding, Z. Deng, J. Chen, Y. Jin, One-step microwave synthesis of N, S co-doped carbon dots from 1, 6-hexanediamine dihydrochloride for cell imaging and ion detection, Colloids and Surfaces B: Biointerfaces, 189 (2020) 110838.
[24] C. Fang, M. Zhang, Nanoparticle-based theragnostics: Integrating diagnostic and therapeutic potentials in nanomedicine, Journal of controlled release: official journal of the Controlled Release Society, 146 (2010) 2.
[25] M. Ashrafizadeh, R. Mohammadinejad, S.K. Kailasa, Z. Ahmadi, E.G. Afshar, A. Pardakhty, Carbon dots as versatile nanoarchitectures for the treatment of neurological disorders and their theranostic applications: A review, Advances in colloid and interface science, 278 (2020) 102123.
[26] P.Y. Liyanage, R.M. Graham, R.R. Pandey, C.C. Chusuei, K.J. Mintz, Y. Zhou, J.K. Harper, W. Wu, A.H. Wikramanayake, S. Vanni, Carbon nitride dots: A selective bioimaging nanomaterial, Bioconjugate chemistry, 30 (2018) 111-123.
[27] V. Mishra, A. Patil, S. Thakur, P. Kesharwani, Carbon dots: emerging theranostic nanoarchitectures, Drug discovery today, 23 (2018) 1219-1232.
[28] V.P. Londhe, Role of garlic (Allium sativum) in various diseases: An overview, angiogenesis, 12 (2011) 13.
[29] M.M. Donma, O. Donma, The effects of allium sativum on immunity within the scope of COVID-19 infection, Medical hypotheses, 144 (2020) 109934.
[30] M. Moutia, N. Habti, A. Badou, In Vitro and In Vivo Immunomodulator Activities of Allium sativum L, Evidence-Based Complementary and Alternative Medicine, 2018 (2018).
[31] M.L. Gioia, Synthesis and preliminary evaluation of the anti-cancer activity on A549 lung cancer cells of a series of unsaturated disulfides, MedChemComm, 10 (2019) 116-119.
[32] T. Seki, T. Hosono, S. Suda, K. Kimura, T. Ariga, Anticancer Property of Allyl Sulfides Derived from Garlic (Allium sativum L.), Journal of Food & Drug Analysis, 20 (2012).
[33] J. Javanmardi, C. Kubota, Variation of lycopene, antioxidant activity, total soluble solids and weight loss of tomato during postharvest storage, Postharvest biology and technology, 41 (2006) 151-155.
[34] H. Shaikh, S. Shaikh, Phytochemistry And Neuroprotective Effect Of Alium Sativum: An Exhaustive Review, World Journal of Advanced Scientific Research, 3 (2020) 155-168.
[35] R.K. Winn, J.M. Harlan, The role of endothelial cell apoptosis in inflammatory and immune diseases, Journal of Thrombosis and Haemostasis, 3 (2005) 1815-1824.

[36] A. Sachdev, I. Matai, S.U. Kumar, B. Bhushan, P. Dubey, P. Gopinath, A novel one-step synthesis of PEG passivated multicolour fluorescent carbon dots for potential biolabeling application, Rsc Advances, 3 (2013) 16958-16961.
[37] K.J. Mintz, M. Bartoli, M. Rovere, Y. Zhou, S.D. Hettiarachchi, S. Paudyal, J. Chen, J.B. Domena, P.Y. Liyanage, R. Sampson, A deep investigation into the structure of carbon dots, Carbon, 173 (2021) 433-447.
[38] M. Răcuciu, D.E. Creangă, A. Airinei, Citric-acid-coated magnetite nanoparticles for biological applications, The European Physical Journal E, 21 (2006) 117-121.
[39] R. Keuleers, H.O. Desseyn, B. Rousseau, C. Van Alsenoy, Vibrational analysis of urea, The Journal of Physical Chemistry A, 103 (1999) 4621-4630.
[40] Y. Ji, X. Yang, Z. Ji, L. Zhu, N. Ma, D. Chen, X. Jia, J. Tang, Y. Cao, DFT-calculated IR spectrum amide I, II, and III band contributions of N-methylacetamide fine components, ACS omega, 5 (2020) 8572-8578.
[41] W. Geng, T. Nakajima, H. Takanashi, A. Ohki, Analysis of carboxyl group in coal and coal aromaticity by Fourier transform infrared (FT-IR) spectrometry, Fuel, 88 (2009) 139-144.
[42] P.J. Larkin, M.P. Makowski, N.B. Colthup, The form of the normal modes of s-triazine: infrared and Raman spectral analysis and ab initio force field calculations, Spectrochimica Acta Part A: Molecular and Biomolecular Spectroscopy, 55 (1999) 1011-1020.
[43] T. Kondo, The assignment of IR absorption bands due to free hydroxyl groups in cellulose, Cellulose, 4 (1997) 281-292.
[44] O. Asvany, P. Kumar, B. Redlich, I. Hegemann, S. Schlemmer, D. Marx, Understanding the infrared spectrum of bare CH5+, Science, 309 (2005) 1219-1222.
[45] Y. Huang, L. Wang, Y. Chao, D.S. Nawawi, T. Akiyama, T. Yokoyama, Y. Matsumoto, Analysis of lignin aromatic structure in wood based on the IR spectrum, Journal of wood chemistry and technology, 32 (2012) 294-303.
[46] M. Zaib, A. Akhtar, F. Maqsood, T. Shahzadi, Green Synthesis of Carbon Dots and Their Application as Photocatalyst in Dye Degradation Studies, Arabian Journal for Science and Engineering, (2020) 1-10.
[47] K.J. Zhu, L. Xiangzhou, Y. Shilin, Preparation, characterization, and properties of polylactide (PLA)–poly (ethylene glycol)(PEG) copolymers: A potential drug carrier, Journal of applied polymer science, 39 (1990) 1-9.
[48] J. Zhang, B. Han, M. Liu, D. Liu, Z. Dong, J. Liu, D. Li, J. Wang, B. Dong, H. Zhao, Ultrasonication-induced formation of silver nanofibers in reverse micelles and small-angle X-ray scattering studies, The Journal of Physical Chemistry B, 107 (2003) 3679-3683.
[49] N.E. Zafeiropoulos, Interface engineering of natural fibre composites for maximum performance, Elsevier, 2011.
[50] A. Hardy, K. Van Werde, G. Vanhoyland, M.K. Van Bael, J. Mullens, L.C. Van Poucke, Study of the decomposition of an aqueous metal–chelate gel precursor for (Bi, La) 4Ti3O12 by means of TGA–FTIR, TGA–MS and HT-DRIFT, Thermochimica acta, 397 (2003) 143-153.
[51] H.-K. Jeong, Y.P. Lee, M.H. Jin, E.S. Kim, J.J. Bae, Y.H. Lee, Thermal stability of graphite oxide, Chemical physics letters, 470 (2009) 255-258.
[52] D. Cheng, Y. Wen, L. Wang, X. An, X. Zhu, Y. Ni, Adsorption of polyethylene glycol (PEG) onto cellulose nano-crystals to improve its dispersity, Carbohydrate polymers, 123 (2015) 157-163.
[53] J.F. Watts, J. Wolstenholme, An introduction to surface analysis by XPS and AES, (2003).

[54] A. Lerf, H. He, T. Riedl, M. Forster, J. Klinowski, 13C and 1H MAS NMR studies of graphite oxide and its chemically modified derivatives, Solid State Ionics, 101 (1997) 857-862.
[55] D.A. Long, Raman spectroscopy, New York, (1977) 1-12.
[56] F. Tuinstra, J.L. Koenig, Raman spectrum of graphite, The Journal of chemical physics, 53 (1970) 1126-1130.
[57] D.J. Grant, D.A. Dixon, σ-and π-bond strengths in main group 3− 5 compounds, The Journal of Physical Chemistry A, 110 (2006) 12955-12962.
[58] K.J. Mintz, G. Mercado, Y. Zhou, Y. Ji, S.D. Hettiarachchi, P.Y. Liyanage, R.R. Pandey, C.C. Chusuei, J. Dallman, R.M. Leblanc, Tryptophan carbon dots and their ability to cross the blood-brain barrier, Colloids and Surfaces B: Biointerfaces, 176 (2019) 488-493.